MECHANISTIC AND THERAPEUTIC INSIGHTS FOR
EPIGENETIC REGULATION IN CANCER DEVELOPMENT

APPROVED BY SUPERVISORY COMMITTEE

First Name Last Name, credentials
Lu Q. Le, M.D., Ph.D.
Rolf A. Brekken, Ph.D.
Rene L. Galindo, M.D., Ph.D.
Elisabeth D. Martinez, Ph.D.

DEDICATION

To my parents Minaxi and Jayanti, thank you providing a roof over my head as I grew up, and for love & support in my all my endeavors. To Sandip, my brother, I am always grateful for your words of wisdom and perspective. To my friends (Nimesh, Siddarth, Imad, Moushumi) for supporting my goals/aspirations in scientific research, and believing in me. To Linda Brzustowicz for giving me my first opportunity in a lab during my undergraduate years, and supporting me all the way through even today. To Marco Azaro for taking me under his wing, and showing me the ropes when I was an undergraduate student in the lab. To Eric Thomas for inspiring motivation in my last year of graduate studies; your words have really helped me put things in perspective, and realize how much is possible with discipline, sacrifice, and perseverance. To Dr. Martinez, Dr. Brekken, and Dr. Galindo for advice, guidance, and perspective. Much appreciation to Dr. Lu Le, the greatest mentor thus far in my career. Thank you for the quality of training, guidance, advice, support, trust, and patience during my graduate studies; I always knew from the beginning you would be a great mentor, and you proved me right.

MECHANISTC AND THERAPEUTIC INSIGHTS FOR EPIGENETIC REGULATION IN CANCER DEVELOPMENT

by

AMISH JAYANTIBHAI PATEL

DISSERTATION / THESIS

Presented to the Faculty of the Graduate School of Biomedical Sciences

The University of Texas Southwestern Medical Center at Dallas

In Partial Fulfillment of the Requirements

For the Degree of

DOCTOR OF PHILOSOPHY

The University of Texas Southwestern Medical Center at Dallas

Dallas, Texas

December, 2014

MECHANISTIC AND THERAPEUTIC INSIGHTS FOR

EPIGENETIC REGULATION IN CANCER DEVELOPMENT

Publication No. 3

Amish Jayantibhai Patel, B.A.

The University of Texas Southwestern Medical Center at Dallas, 2014

Supervising Professor: Lu Quang Le, M.D., Ph.D.

Malignant Peripheral Nerve Sheath Tumors (MPNSTs) are highly aggressive sarcomas that develop sporadically or in patients with Neurofibromatosis type 1 (NF1). Effective treatment options are lacking, and MPNSTs are typically fatal. To gain insights into MPNST pathogenesis, we utilized a novel MPNST mouse model that allowed us to study the evolution of these tumors at the transcriptome level. Strikingly, we found that progression to MPNST and loss of MPNST relevant tumor suppressors is associated with increased levels of chromatin regulator/BET bromodomain protein BRD4, and paradoxically, sensitivity and resistance to BET bromodomain inhibition with small molecule inhibitor JQ1. Indeed, genetic and pharmacological inhibition of BRD4 profoundly suppresses both growth and

tumorigenesis of MPNSTs. Mechanistically, we uncovered that BET bromodomain inhibition leads to engagement of the ER stress/UPR pathway, and apoptosis through induction of pro-apoptotic effector molecule BIM and suppression of anti-apoptotic BCL-2 in MPNSTs. Moreover, we find that suppressed transcription of Cyclin D1 oncogene upon BRD4 inhibition correlates with reduced proliferation of MPNSTs. All together, this dual restraint on proliferation (via Cyclin D1 downregulation) and survival (via BIM induction) may indicate how BRD4 inhibition is exquisitely effective against MPNSTs and may represent a paradigm shift in therapy for MPNST patients. Moreover, these findings indicate an epigenetic mechanism underlying the balance of anti-/pro-apoptotic molecules, which suggests that BET bromodomain inhibition can shift this balance in favor of cancer cell death. Collectively, these studies provide new insights for developing strategies to overcome resistance to BET bromodomain inhibitor therapy for subverting cancer cell survival.

TABLE OF CONTENTS

PRIOR PUBLICATIONS

Patel, A.J., Liao, C.P., Chen, Z., Liu, C., Wang, Y., Le, L.Q. (2013). BET Bromodomain Inhibition Triggers Apoptosis of NF1-associated Malignant Peripheral Nerve Sheath Tumors through Bim Induction. ***Cell Reports***. 6, 81-92.

Mo, W., Chen, J., **Patel, A.**, Zhang, L., Chau, V., Li, Y, Cho, W., Lim, K., McKay, R., Lev, D., Le, L.Q. and Parada, L. (2013). CXCR4 mediates autocrine cell cycle progression in NF1-associated malignant peripheral nerve sheath tumors. ***Cell***. 152(5): 1077-1090.

Chau, V., Lim, S.K., Mo, W., Liu, C., **Patel, A.J.**, McKay, R.M., Wei, S., Posner, B.A., De Brabander, J.K., Williams, N.S., Parada, L.F., Le, L.Q. (2013). Preclinical therapeutic efficacy of a novel pharmacological inducer of apoptosis in malignant peripheral nerve sheath tumors. ***Cancer Research***. 74(2): 1–12

LIST OF FIGURES

LIST OF APPENDICES

LIST OF DEFINITIONS

NF1 – Neurofibromatosis Type I

MPNST – Malignant Peripheral Nerve Sheath Tumor

Nf1 – designation for “neurofibromin 1” gene

P53 – designation for “tumor protein p53” gene

BET – Bromodomain with extra-terminal domain

Brd2 – designation for “bromodomain containing 2” gene

Brd3 – designation for “bromodomain containing 3” gene

Brd4 – designation for “bromodomain containing 4” gene

Brdt – designation for “bromodomain, testis-specific” gene

BRD2 – designation for “bromodomain containing 2” protein

BRD3 – designation for “bromodomain containing 3” protein

BRD4 – designation for “bromodomain containing 4” protein

GEMM – Genetically Engineered Mouse Models

SKP – Skin deriver precursor or skin derived progenitor cell

ChIP-seq – Chromatin Immunoprecipitation-sequencing

CHAPTER ONE
Introduction

1.1 – Neurofibromatosis Type I

Neurofibromatosis type I (NF1) is the most common human genetic disorder of the nervous system, and affects one in 3,500 individuals around the world regardless of ethnicity and gender (Wallace et al., 1990). Clinically, NF1 patients are predisposed to a wide spectrum of symptoms including developmental, neurological, dermatological, cardiovascular defects and tumor development (Figure 1) (Le and Parada, 2007; Martin et al., 1990). NF1 manifests through inheritance or sporadic mutation of the *Nf1* tumor suppressor gene (encodes the 2839 amino acid containing protein Neurofibromin), a negative regulator of oncogenic p21-RAS (Figure 2). Neurofibromin contains a GAP domain (GTPase activating domain) that stimulates GTPase activity of RAS to hydrolyze its GTP to GDP, thus switching RAS from active (GTP-bound) state to inactive (GDP-bound) state (Ballester et al., 1990; Martin et al., 1990; Xu et al., 1990a; Xu et al., 1990b). Thus *Nf1* deficient cells tend to have over-active RAS/RAF/MAPK signaling, which is believed to participate in the pathogenesis of clinical

Skin	*Neurologic*
Café au lait macules	UBO on MRI
Axillary and inguinal freckling	Learning disabilities
Dermal neurofibroma	Seizure
Plexiform neurofibroma	Mental retardation
Juvenile xanthogranuloma	Aqueduct sternosis
Neoplasia	*Skeletal*
Optic glioma	Macrocephaly
MPNST	Sphenoid wing dysplasia
Pheochromocytoma	Scoliosis
Juvenile chronic myelogenous leukemia	Spinal bifida
Other CNS tumors (astrocytoma)	Pseudoarthrosis
Rhabdomyosarcoma	Thinning of long bone cortex
Duodenal carcinoid	Absence of patella
Somatostatinoma	Vertebral disc dysplasia
Parathyroid adenoma	Short stature
Cardiovascular	*Eyes*
Hypertension	Lisch nodules
Pulmonic sternosis	Hyperterrorism
Renal artery sternosis	Glaucoma
Gastrointestinal	*Psychiatric*
Constipation	Heavy psychosocial burden

Abbreviations: CNS, central nervous system; MPNST; malignant peripheral nerve sheath tumor; UBO: unidentified bright object.

Figure 1. Clinical symptoms observed in NF1 patients [from (Le and Parada, 2007)]

features in NF1 patients. Consistent with this idea, mouse models of *Nf1* deficiency or hyper-active RAS signaling exhibit neurological symptoms including learning and memory impairments, which can be alleviated or rescued by inhibiting RAS signaling through either farnesyltransferase or MEK inhibitors (Cui et al., 2008; Li et al., 2005; Wang et al., 2012).

However, in diverse human cancer tissues or cells, mutations/deletions/insertions in the *Nf1* coding sequence is widely distributed, and not always found in the GAP domain (Figure 3). Furthermore, the exact function(s) of other regions of the Neurofibromin protein sequence (excluding the GAP domain and others that relate to its function) remain uncharacterized. Therefore, much remains unknown about the role of mutations in those uncharacterized regions of *Nf1*, and how they may participate in the pathogenesis of NF1. In support of this idea, *Nf1*$^{-/-}$ mice are embryonic lethal, but can be rescued via expression of Nf1-GRD (GAP-related domain), yet these mice still develop neural crest related defects and perish shortly after in the neonatal period, which suggests

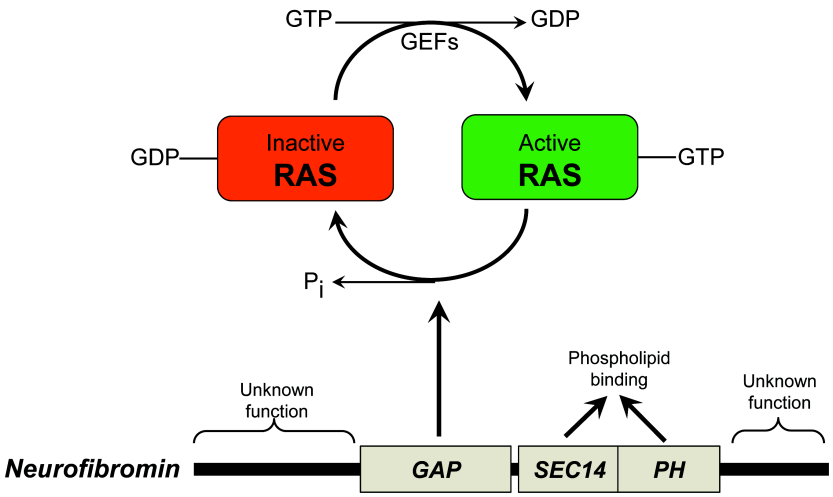

Figure 2. *Nf1* encodes Neurofibromin, a GAP domain containing protein that stimulates RAS inactivation.
The GAP (GTPase activating) domain of Neurofibromin stimulates GTPase activity of RAS to catalyze hydrolysis of GTP to GDP, therefore switching RAS to the inactive GDP-bound state. Adapted from (Le and Parada, 2007).

new biology regarding non-GAP related function of *Nf1* in development and NF1 yet to be discovered (Ismat et al., 2006). The enormity of the genomic sequence and cDNA for *Nf1* has posed a barrier to dissecting *Nf1* gene function to a greater extent. However, recent developments that facilitate more rapid genome engineering may provide a pipeline for systematically dissecting the role of the wide-spectrum of *Nf1* mutations in development and NF1. Nevertheless, mouse models whereby *Nf1* knockout is induced in a tissue specific

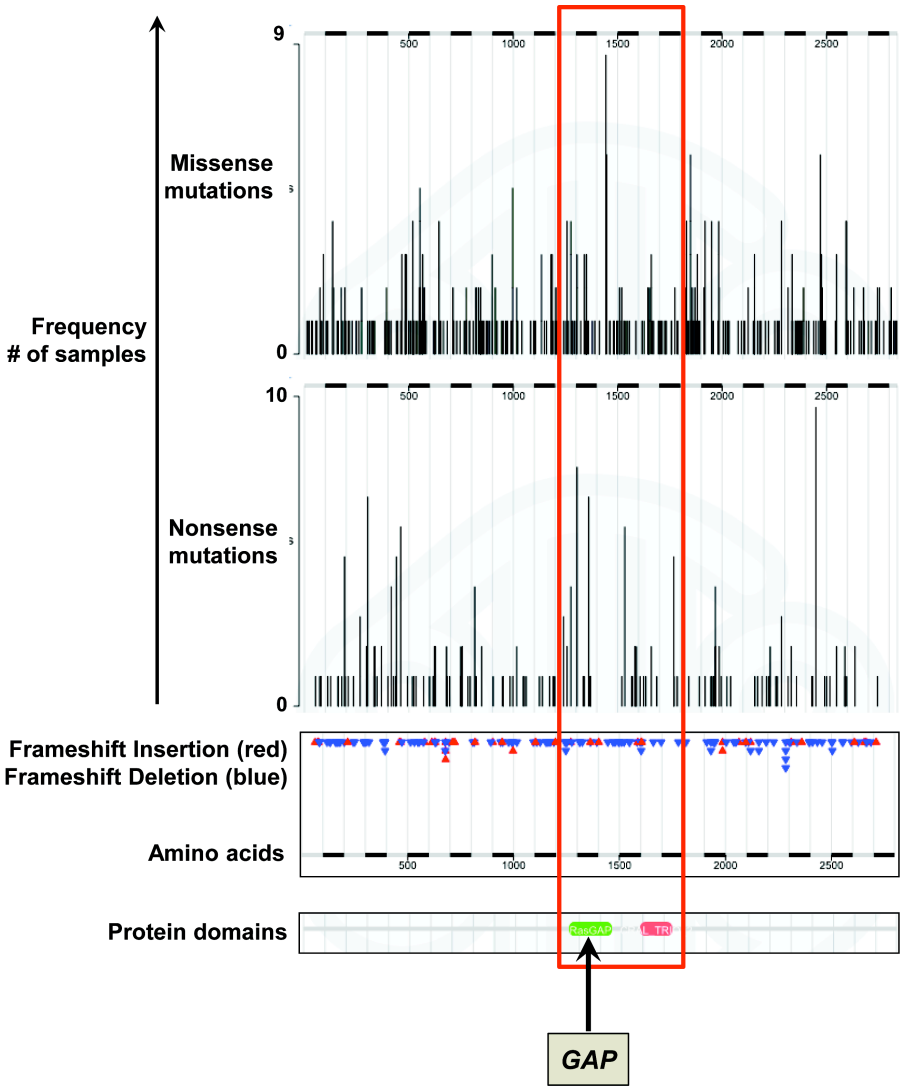

Figure 3. Distribution of somatic mutations found in the coding sequence of Neurofibromin in diverse human tumors
Data acquired by mining the COSMIC (Catalogue of Somatic Mutations in Cancer) database. Data represents mutation analysis from approximately 896 samples (tumor tissue or cells) from a wide range of tissue types (including *Nf1*-associated neurofibromas/MPNSTs and non-NF1 derived neoplasms.

manner have been invaluable tools for understanding and developing therapies for *Nf1*-associated neoplastic/tumor development and neurological deficits.

1.2 – Benign neurofibromas and their progression to MPNST

While NF1 patients are susceptible to developing various neoplasms (juvenile myelomonocytic leukemia, optic glioma, astrocytoma, rhabdomyosarcoma), the most common occurring are benign neurofibromas, which can be stratified into 2 subgroups: plexiform and dermal (Albers and Gutmann, 2009; Bajenaru et al., 2003; Le and Parada, 2007; Shannon et al., 1992). Plexiform neurofibromas can progress to malignant sarcomas known as malignant peripheral nerve sheath tumors (MPNSTs), which account for 10% of all soft tissue sarcomas (Figure 4) (King et al., 2000). They are highly aggressive, incurable

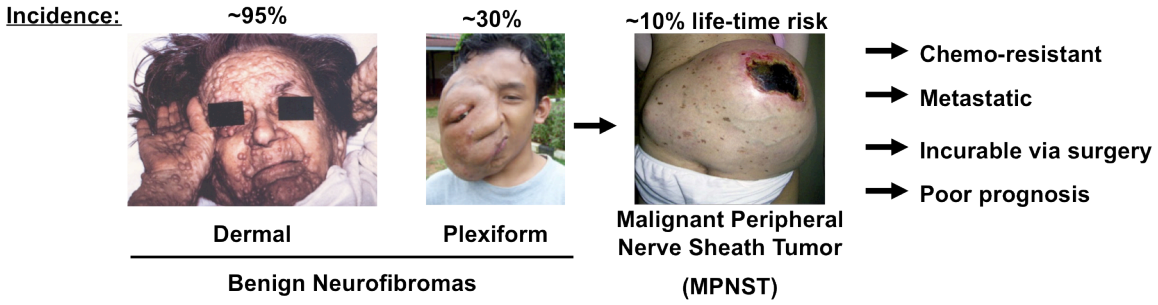

Figure 4. NF1-associated neurofibromas and MPNSTs
Figures adapted from (Ferner et al., 2007; Spitz, 2005).

through conventional chemotherapy or surgical resection, and a leading cause of mortality in the NF1 patient population (Duong et al., 2011). Although significant progress in understanding NF1 tumor development has been made, surgery remains the standard of care for MPNST patients, and prognosis remains bleak (Zou et al., 2009).

Development of neurofibromas is thought to be a complex process as these tumors contain multiple cell types including mast cells, endothelial cells, neurons, fibroblasts, and Schwann-like cells (Lakkis and Tennekoon, 2000). Although many questions regarding this process remains unknown, we know that human neurofibromas frequently contain Schwann-

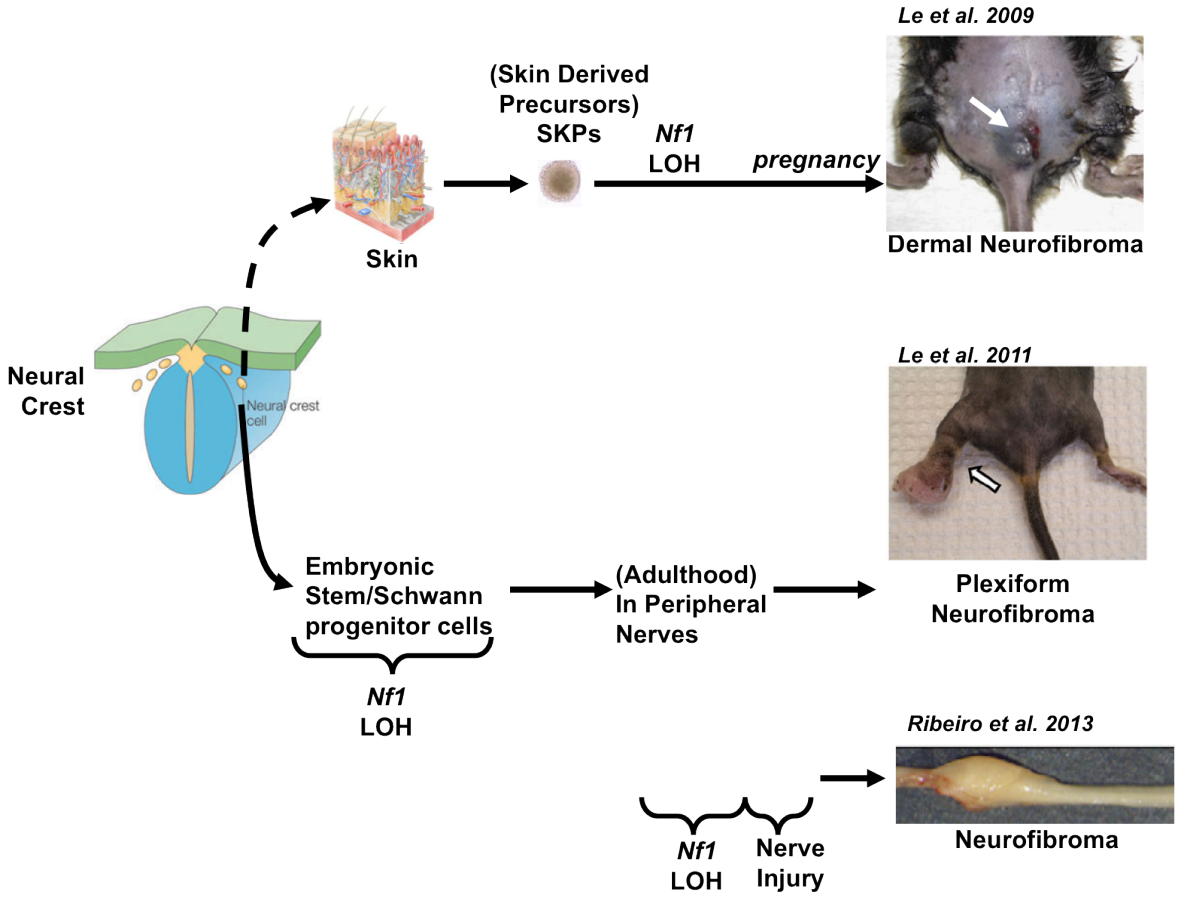

Figure 5. Distinct cells of origin and non-cell autonomous mechanisms in *Nf1*-associated neurofibroma development.
References: (Jessen and Mirsky, 2005; Joseph et al., 2008; Le et al., 2011; Le et al., 2009; Mayes et al., 2011; Ribeiro et al., 2013; Zheng et al., 2008; Zhu et al., 2002)

like cells with loss of heterozygosity for *Nf1*, which suggests that the cells of origin for these complex tumors may originate from the Schwann cell lineage (De Raedt et al., 2006; Upadhyaya et al., 2004). In support of this idea, research studies from diverse groups have

identified various stages of Schwann cell development in which *Nf1* loss leads to plexiform neurofibroma development (Joseph et al., 2008; Le et al., 2011; Mayes et al., 2011; Wu et al., 2008; Zheng et al., 2008; Zhu et al., 2002). In general, dermal neurofibromas typically did not develop in mice from those studies. This suggests that perhaps a different cell of origin, other genetic/epigenetic changes, or a certain microenvironment context is distinctly required for dermal rather than plexiform neurofibroma development. Indeed, Le and colleagues identified neural crest-related stem/progenitors called SKPs (Skin Derived Precursors) as a cell of origin for dermal neurofibroma under the right microenvironmental context (Figure 5).

Neurofibroma progression to MPNST in NF1 patients is associated with additional genetic changes including amplification/over-expression of oncogenic receptor tyrosine kinases (i.e. EGFR, PDGFR, MET) or growth factors (i.e. neuregulin-1, hepatocyte growth factor) and loss of tumor suppressors *Ink4a, Pten*, or *P53* (the latter being the most common) (Cichowski et al., 1999; Endo et al., 2011; Gregorian et al., 2009; Huijbregts et al., 2003; Joseph et al., 2008; Keng et al., 2012; Ling et al., 2005; Perrone et al., 2009; PERRY et al., 2002; Torres et al., 2011; Vogel et al., 1999).

1.3 – From human MPNST biology to novel mouse models

Consistent with clinical observations, work from the lab of Luis Parada and Tyler Jacks led to development of the very first mouse models of NF1-associated MPNST. They demonstrated that single hit mutations engineered in *Nf1* and *P53* tumor suppressor genes in

cis on mouse chromosome 11 (*Nf1*$^{+/-}$ *P53*$^{+/-}$ mice) led to robust tumor development (Cichowski et al., 1999; Vogel et al., 1999). Most of the tumors were primarily sarcomas (77%), whereas lymphomas (8%), neuroblastomas were less frequent. Of the tumors characterized, approximately half of these tumors were diagnosed as MPNSTs, while the remainder were MTTs (malignant triton tumors), leiomyosarcomas, or rhabdomyosarcomas. Interestingly, early passage cell lines derived from more than 70 tumors derived from cis *Nf1*$^{+/-}$ *P53*$^{+/-}$ mice had loss of heterozygosity for their remaining wildtype *Nf1* and *P53* alleles (Cichowski et al., 1999; Vogel et al., 1999). These observations had suggested that loss of *P53* was important for development of malignant tumors in NF1 as these groups observed that *Nf1*$^{+/-}$ did not develop malignant tumors.

1.4 – Is loss of tumor suppressors *Nf1* and *P53* sufficient for MPNST development?

On the other hand, these models suggested but did not prove that loss of heterozygosity for both *Nf1* and *P53* is required for the development of malignant tumors. This could not be addressed at that time because *Nf1*$^{-/-}$ mice were embryonic lethal, and thus *Nf1*$^{-/-}$ *P53*$^{-/-}$ mice were the same due to developmental defects (Brannan et al., 1994; Cichowski et al., 1999; Jacks et al., 1994; Vogel et al., 1999). Moreover, neither a conditional loxP allele for *Nf1* was available nor was the precise cell of origin known. However, in those early studies, molecular analysis of tumor cell lines did reveal expression of neural crest and Schwann cell markers, which alluded to a potential cell of origin (Cichowski et al., 1999; Vogel et al., 1999). Indeed, the development of a conditional loxP allele for *Nf1* coupled with tissue-specific Cre drivers in mice revealed that the Schwann cell

lineage contained the cell of origin for NF1-associated neurofibromas (Joseph et al., 2008; Le et al., 2011; Mayes et al., 2011; Wu et al., 2008; Zheng et al., 2008; Zhu et al., 2002). More recently, unpublished data from our lab demonstrates that tamoxifen inducible knockout of both *Nf1* and *P53* in Schwann cell lineage of PLP-CreERT2::*Nf1*$^{F/F}$ *P53*$^{F/F}$ mice led to the development of MPNSTs. These data suggested that complete loss of both of these tumor suppressors could initiate MPNST development in mice. Yet, it was unclear whether those genetic events were completely sufficient for this process as we observed that those mice developed few tumors despite loss of both *Nf1* and *P53* in many cells. Hence, it was unknown as to whether additional cell intrinsic (genetic or epigenetic changes, cancer stem cells) or extrinsic factors (tumor microenvironment) were required for MPNST initiation, maintenance, and progression after loss of both *Nf1* and *P53*.

Nonetheless, MPNST mouse models in which *Nf1* loss is coupled with human MPNST genetic events (loss of either *P53*, *Ink4a*/*Arf*, or *Pten*) confirm their contributions to MPNST pathogenesis and afford us with pre-clinical models to test and develop targeted molecular therapies. Indeed, these tumor models have been invaluable for validation of pre-clinical therapeutic targets regulating the cell cycle, thus allowing for inhibition of proliferation, but eventual resistance or tumor burden are likely to hinder the efficacy of such agents (Albritton et al., 2006; Jessen et al., 2013; Johannessen et al., 2008; Mo et al., 2013; Patel et al., 2012; Wu et al., 2013a). Selective inhibition of both proliferation and survival may offer MPNST patients a better prognosis. However, identification of molecular targets for therapy by use of these genetically defined models remains a challenge given that the precise location and isolation of tumor initiating cells hampers our ability to molecularly

profile and dissect the events dictating initiation and progression to MPNST. Similarly, our limited capability to culture human MPNSTs for genome-wide analysis or functional interrogation of MPNSTs has hindered the elucidation of survival dependencies in MPNSTs. Thus new mouse models, reagents, and paradigms will be essential for rapidly identifying the most promising therapeutic targets for MPNSTs.

Recently, our lab identified skin-derived precursors (SKPs) with *Nf1* deficiency to be a cell of origin for dermal neurofibromas (Le et al., 2009). Serendipitously, we found that *Nf1*-deficient SKPs are also capable of giving rise to plexiform neurofibromas when transplanted into a nerve, and further loss of *P53* readily allows for malignant transformation into MPNSTs with histological and molecular features consistent with human MPNSTs (Figure 6) (Chau et al., 2013a; Mo et al., 2013).

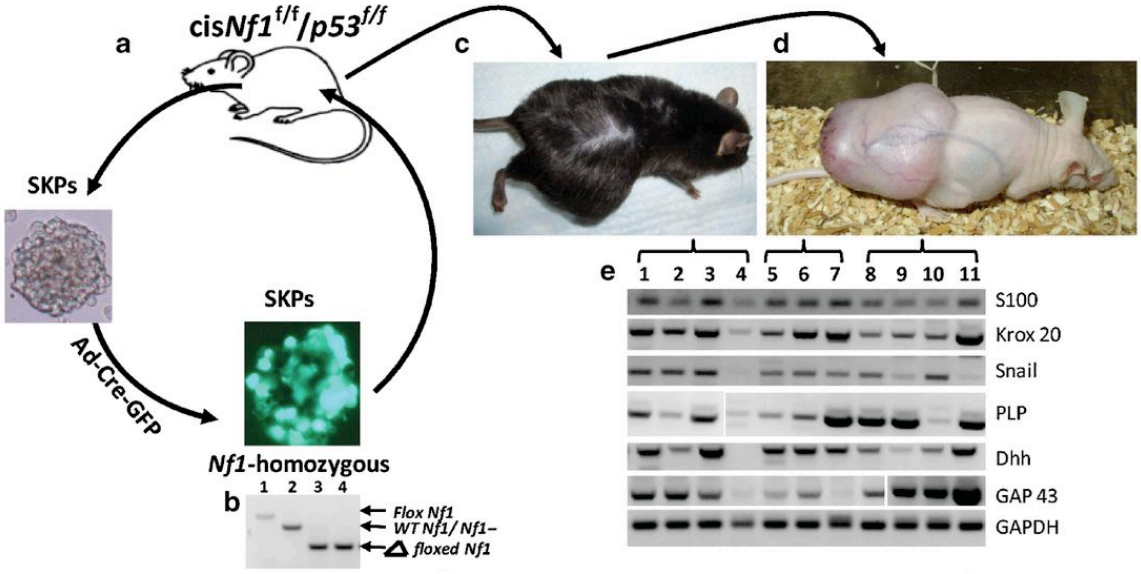

Figure 6. SKPs with loss of tumor suppressors *Nf1* and *P53* can undergo malignant progression to MPNSTs in *in vivo*. (Adapted from Figure 1 in (Chau et al., 2013b))
(A) Diagram for generating *Nf1*/*P53* double knockout SKPs

(B) Validation of *Nf1* knockout in *Nf1*$^{F/F}$ *P53*$^{F/F}$ SKPs infected with Ad-Cre-GFP by PCR genotyping of cell DNA. Lane 1 = *Nf1*$^{F/F}$ control. Lane 2 = Wildtype *Nf1*$^{+/+}$ control. Lane 3 = *Nf1*$^{-/-}$ SKP control. Lane 4 = *Nf1*$^{F/F}$ *P53*$^{F/F}$ SKPs infected with Ad-Cre-GFP.
(C) sMPNST tumors arising in mouse in which *Nf1*$^{F/F}$ *P53*$^{F/F}$ SKPs were autologously injected to original mouse.
(D) Secondary sMPNST tumors arising in nude mice transplanted with tumor tissue fragment from primary sMPNST in figure 6C.
(E) RT-PCR analysis of Schwann cell markers in MPNSTs derived from cis-*Nf1*$^{+/-}$ *P53*$^{+/-}$ mice (lanes 1-4), PLP-CreERT:: *Nf1*$^{F/F}$ *P53*$^{F/F}$ mice (lanes 5-7), sMPNSTs (lanes 8-11).

1.5 – SKPs as a novel platform for dissecting progression to MPNST

This novel MPNST mouse model for the first time affords us the opportunity to monitor the evolution of these tumors from stem cell to benign neurofibroma to MPNST (Figure 7D). In this regard, we first observed that SKP-derived MPNSTs (sMPNSTs) retain robust tumorigenic potential when either transplanted as tumor fragments or as few as 10,000 cells, whereas at least 100,000 pre-tumorigenic *Nf1*$^{-/-}$ *P53*$^{-/-}$ SKPs (NP-SKPs) were required and longer time *in vivo* for sMPNST tumors to arise. These observations suggested that other factors in addition to *Nf1*/*P53* loss regulate the initiation of MPNST development. Indeed, we have previously observed that dual loss of *Nf1* and *P53* in the early Schwann cell lineage of mice with a tissue-specific inducible Cre recombinase (PLP-Cre^{ERT2}) required several months for tumor initiation, and relatively few tumors developed despite loss both tumor suppressors in a large population of cells *in vivo*. Given these observations, we hypothesized that loss of tumor suppressors *Nf1* and *P53* is required but not sufficient for initiation and progression to MPNSTs. We envision a role for additional events including but not limited to further genetic or epigenetic alterations, the tumor microenvironment, and cells of origin that influence progression to MPNST. To elucidate these additional events, SKPs may serve as novel platform for identifying novel cell-intrinsic and –extrinsic factors underlying

MPNST initiation, maintenance, and progression (Figure 7A and 7D), whereas it would be difficult to do so with traditional GEMMS of MPNST (Figure 7A-C).

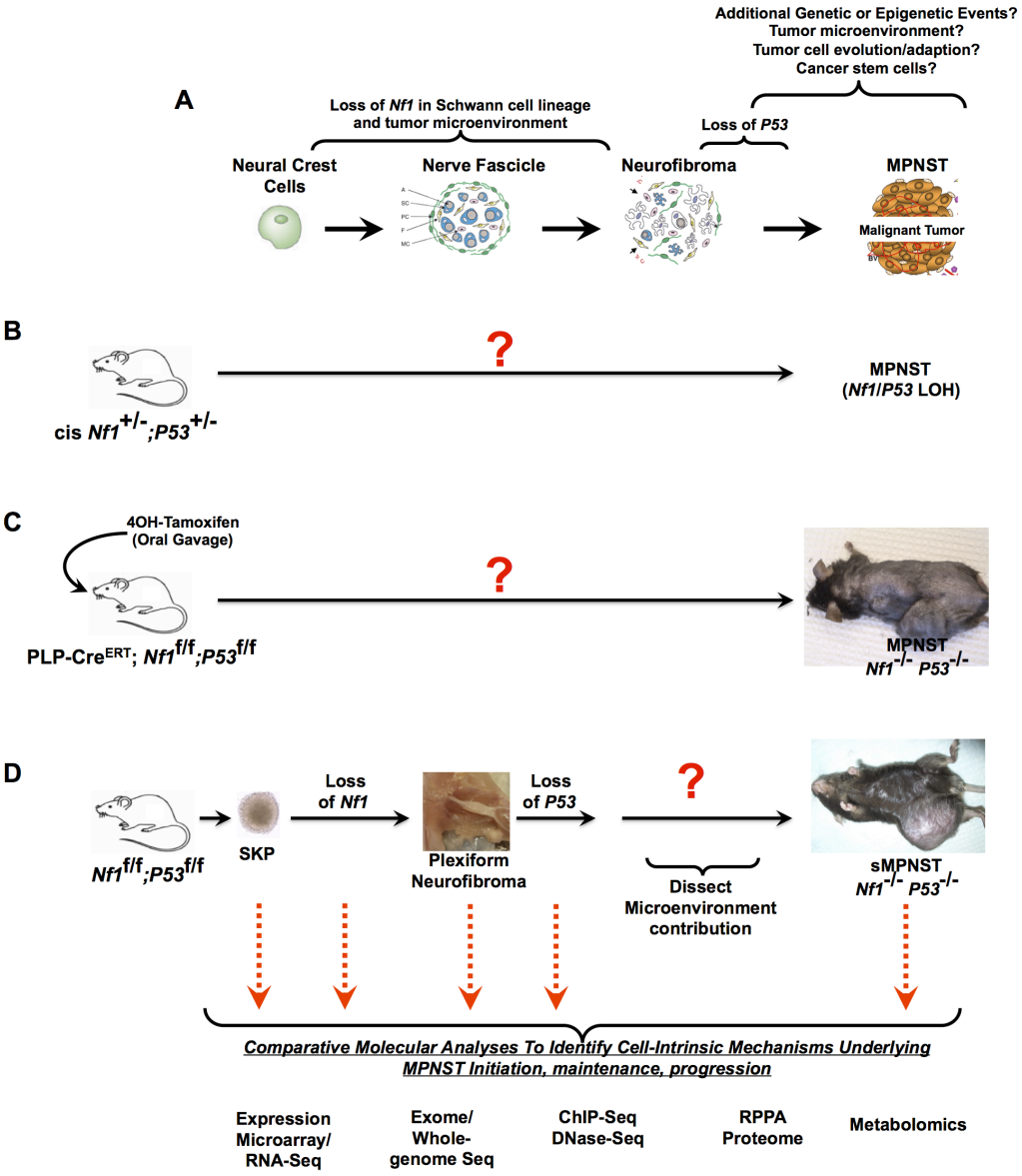

Figure 7. SKPs as a novel platform for identifying cell-intrinsic and –extrinsic factors underlying MPNST initiation, maintenance, and progression.

(A) Diagram illustrating the importance of *Nf1* loss and microenvironment in benign neurofibroma development and *P53* loss in progression to MPNST while highlighting areas of unknown biology in MPNST development waiting to be discovered with the right tools/models, and potential for identifying new therapeutic strategies for MPNST. [Reference: (McLaughlin and Jacks, 2002)]

(B and C) cisNP and PLP models of MPNST as powerful pre-clinical tools, but limited ability to dissect additional cell-intrinsic factors in MPNST development. [References: (Cichowski et al., 1999; Vogel et al., 1999)]
(D) SKPs as novel/ex-vivo platform for identifying cell-intrinsic and –extrinsic factors in MPNST development. [References: (Le et al., 2009; Mo et al., 2013)]

In support of this idea, we first tested the role of the microenvironment in dictating tumor initiating capacity of NP-SKPs. Previously, our lab observed that *Nf1*$^{-/-}$ SKPs could more easily give rise to plexiform neurofibroma when implanted into the sciatic nerve of mice, whereas it was rare when *Nf1*$^{-/-}$ SKPs were implanted subcutaneously in mice (with exception of dermal neurofibroma development in female mice undergoing pregnancy). These observations suggest that the microenvironment is important for tumorigenesis of *Nf1*$^{-/-}$ SKPs. Therefore, we compared tumor-initiating capacity of

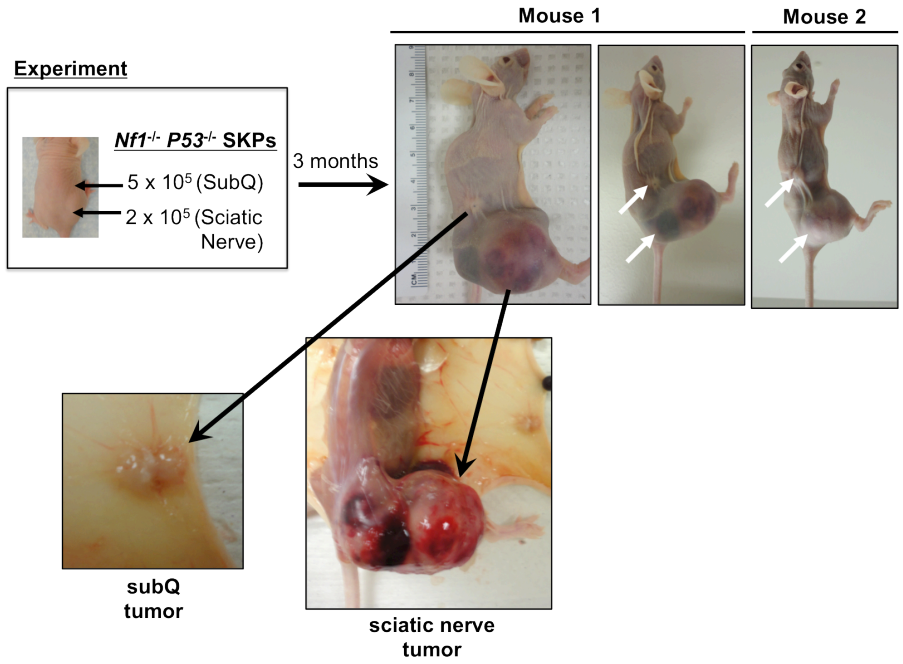

Figure 8. Nerve microenvironment robustly supports malignant transformation of *Nf1*$^{-/-}$ *P53*$^{-/-}$ SKPs compared to subcutaneous microenvironment.
SKPs were isolated from *Nf1*$^{F/F}$ *P53*$^{F/F}$ newborn mice (post-natal day 2), cultured less than 2 weeks prior to addition of adenovirus-Cre-GFP to induce knockout of both *Nf1* and *P53*, which was confirmed by PCR genotyping of DNA from cells. These NP-SKPs were cultured 4 passages before injection to nude mice as shown in upper-left diagram in this figure.

NP(*Nf1*$^{-/-}$ *P53*$^{-/-}$) SKPs when implanted to sciatic nerve compared to subcutaneous (subQ) (Figure 8). To account for differences between mice, we injected to both locations in the same nude mice (n=4). Furthermore, if the microenvironment of the sciatic nerve is more supportive of NP-SKP tumorigenesis, then injection of fewer NP-SKPs to sciatic nerve compared to subQ should be sufficient to allow robust tumor initiation. We injected 500,000 cells to subQ and 200,000 cells to sciatic nerve. After 3months, we observed that each nude mouse had a severely enlarged right leg due to robust/malignant expansion of NP-SKPs in sciatic nerve while subQ tumors were relatively smaller, and confined in their environment (Figure 8). Sciatic nerve tumors tended to be more highly vascular than subQ tumors. These observations suggest that the microenvironment plays a pivotal role in supporting or suppressing tumor initiation/progression of NP-SKPs to sMPNSTs in vivo. From a different perspective, one might argue that these observations parallel how different microenvironments may be non-fertile barriers in the process of metastasis whereby tumor cells from their tissue of origin have limited ability to spread to other tissues, and be able to survive/thrive long enough to initiate a tumor. Nonetheless, the fact remains that NP-SKPs had to be injected at higher cell numbers in the sciatic nerve to form a tumor in at least 2 months, whereas from previous experiences, we know that as little as 10,000 sMPNST cells can robustly form tumors in less than a month. Thus, in light of this new experiment, we hypothesize that there must be cell-autonomous mechanisms that still govern the pace of tumor initiation in addition to extrinsic factors such as the microenvironment. To address this, we reasoned that the underlying perturbation of the transcriptome as pre-tumorigenic NP-SKPs progress to sMPNST would reveal molecular insights that we could functionally

dissect through use of our MPNST mouse models. Thus, in Chapter 2, we utlize our novel SKP derived MPNST model as a platform to study the evolution of these tumors by comparative transcriptome analysis of SKP-derived MPNSTs (sMPNSTs) and their pre-tumorigenic ancestors (NP-SKPs).

CHAPTER TWO

Transcriptome analysis identifies genetic and epigenetic factors underlying SKP progression to MPNST

2.1 – Introduction

Cells of origin for neurofibroma

Benign neurofibromas are composed of diverse cell types ranging from Schwann cells, fibroblasts, mast cells, perineurial cells, and neurons (Le and Parada, 2007). Through mouse modeling efforts from several groups, it is evident that the cells of origin for plexiform neurofibroma arise from the Schwann cell lineage, while $Nf1^{+/-}$ cells of tumor microenvironment are suggested to play an important role in supporting neurofibroma development (Le et al., 2011; Mayes et al., 2011; Zhu et al., 2002). Schwann cells arise from Schwann cell progenitors, which were originally derived from the neural crest (Jessen and Mirsky, 2005). Although dermal neurofibromas contain Schwann-like cells, neither the dermis nor skin was known to contain precursors to those cells.

Neural crest related-SKPs a cell of origin for dermal neurofibroma

More recently, multi-potent skin-derived precursor (SKP) cells residing in dermis of skin with ability to give rise/differentiate into neural crest derivatives (e.g. Schwann cell, neuron, adipocyte) suggested a pool of stem cells residing in skin with ability to give rise o Schwann cells, thus perhaps a cell of origin for dermal neurofibroma (Biernaskie et al., 2007; Fernandes et al., 2004). Indeed, $Nf1^{-/-}$ SKPs could give rise to dermal neurofibromas contingent on microenvironment conditions. Remarkably, these cells could also give rise to

plexiform neurofibromas when implanted into the sciatic nerve, thus suggesting a role for the microenvironment in dictating tumor type (Le et al., 2009).

SKP as a platform for dissecting progression to MPNST

Given the remarkable flexibility to recapitulate benign neurofibromas through this ex-vivo/transplantation system, we reasoned that this new mouse model would allow us for the first time to characterize the molecular events underlying NF1-realted tumorigenesis from a stem cell to benign neurofibroma, and allow us to ask what other mutations are necessary for malignant progression to MPNST. Human MPNSTs frequently have loss of heterozygosity in the second *Nf1* allele as well as *P53* loss. Based on these clinical findings, we tested whether additional loss of *P53* could permit malignant transformation of $Nf1^{-/-}$ SKPs. Indeed, we observed that $Nf1^{-/-}$ $P53^{-/-}$ SKPs could form tumors that molecularly and histopathologically resemble human MPNSTs (Chau et al., 2013b; Mo et al., 2013). We termed those tumors as sMPNSTs (SKP-derived MPNSTs). Upon analysis of NP-SKP versus sMPNST tumorigenic potential, we observed that as few as 10,000 sMPNST cells could rapidly form subcutaneous tumors in athymic nude mice while as few as 100,000 NP-SKPs could form tumors in athymic nude mice at slower rate than sMPNST cells. These observations suggest that loss of tumor suppressors *Nf1* and *P53* is required but not sufficient for progression of NP-SKP to sMPNSTs.

<u>Hypothesis</u>: We hypothesize that further genetic or epigenetic events after loss of both Nf1 and P53 are required for progression to MPNST. To address this hypothesis, we utilized SKPs as novel platform to dissect what happens after acute loss of both Nf1 and P53 in SKPs and progression to sMPNST tumors in vivo by transcriptome analysis (Figure 7D).

2.2 – Experimental Procedures

Isolation of SKPs, and derivation of sMPNSTs

SKPs were isolated from postnatal day 1 mice with genotype *Nf1*$^{flox/flox}$ *P53*$^{flox/flox}$ Rosa26-*LacZ* using standard protocol as described previously (Biernaskie et al., 2007; Chau et al., 2013b; Patel et al., 2014). See Appendix A for SKP growth media formulation. SKPs were transiently infected overnight with adenovirus-Cre-GFP to allow Cre-mediated recombination of *Nf1* and *P53* flox alleles to generate NP-SKPs. Adenovirus-GFP was used as a control. Approximately 10^6 NP-SKPs (passage 5, 3 passages after adenovirus-Cre-GFP infection) were subcutaneously injected to lower ventral side of athymic nude mice. One to two months later, mice developed tumors. Tissues from each tumor were harvested for DNA, RNA, protein, histology, and derivation of tumor cell lines. Tumors were termed as sMPNSTs after histopathological analysis of tumor tissue sections. After 3 passages of tumor cells in vitro, cells were validated to be more than 95% derived from NP-SKPs as determined by X-gal staining for β-galactosidase enzymatic activity per cell (Chau et al., 2013b).

PCR genotyping for Nf1 and P53 knockout

To determine recombination of *Nf1* and *P53* flox alleles in NP-SKPs and sMPNST tumors, specific oligonucleotide primers were used for PCR based analysis of DNA from samples as described previously (Chau et al., 2013b). See Figure 10 for primers sequences, and validation data.

Histopathological validation of NP-SKP tumors as sMPNSTs

Tumor tissue sample preparation, immunohistochemistry, and data quantification were performed as described previously (Mo et al., 2013). Tumors that stained predominantly positive for S100β and GAP43, while also containing cells with high nuclear/cytoplasmic ratio, mitotic cells, and high cellularity/density were termed as sMPNST tumors. See Appendix G for detailed protocol.

Quality control analysis of total RNA samples for expression microarray analysis

Total RNA was isolated from sMPNST tumors and NP-SKPs from which those tumors were derived from (3 biological replicates were prepared for both groups). RNA quality was assessed using Bioanalyzer chips (Agilent) by the UT Southwestern Microarray core facility. All samples used for microarrays had an RNA integrity number between 9 and 10 (where 10 represents the highest RNA integrity/quality).

Expression microarray and data analysis

Microarray experiments were conducted using Mouse Genome 430 2.0 microarrays (Affymetrix) by the UT Southwestern Microarray core facility. Data was analyzed with GeneSpring GX software (Agilent Technologies).

qRT(quantitative, reverse transcription)-PCR and Western blot

RNEasy mini kit (Qiagen) was used to isolate total RNA from cells, followed by cDNA synthesis with iScript Select cDNA synthesis kit (Bio-Rad), and then qRT-PCR using iTaq Universal SYBR Green Supermix (Bio-Rad) on the CFX Connect Real-Time PCR platform (Bio-Rad). Data was quantified by ΔCt method, and normalized relative to *Gapdh*. See Appendix E for list of oligonucleotide primers used.

Protein isolation, and subsequent Western blot analysis was performed as described previously (Mo et al., 2013). Antibodies Used: BRD4 (Bethyl Labs), SETD7 (Cell Signaling), Gapdh (Santa Cruz Biotechnology). See Appendix F for protocol and list of antibodies used.

2.3 – Results

Isolation and validation of NP-SKPs and sMPNSTs

To address our hypothesis, we utilized the SKP-derived MPNST mouse model, which allowed for the first time to monitor evolution towards MPNST after loss of tumor suppressors *Nf1* and *P53* by comparative transcriptome analysis. We first began by isolating SKP from post-natal mice (P0-3) with genotype $Nf1^{F/F}$ $P53^{F/F}$ $Rosa26^{lox\text{-}stop\text{-}lox\text{-}LacZ}$ (Figure 9A). Next, after 2 passages, SKPs were infected with an adenovirus expressing either Cre-GFP or GFP (control) to allow for Cre-mediated recombination of *Nf1* and *P53* flox alleles, which result in their knockout, which we validated by PCR genotyping after two additional passages (Figure 9A-C and Figure 10). Approximately 1 passage later, we isolated total RNA from ($Nf1^{-/-}$ $P53^{-/-}$) NP-SKPs, and injected remaining (1-2 x 10^6) cells to athymic nude mice. About 1-2 months later, these mice developed tumors at the site of injection (Figure 9A). We

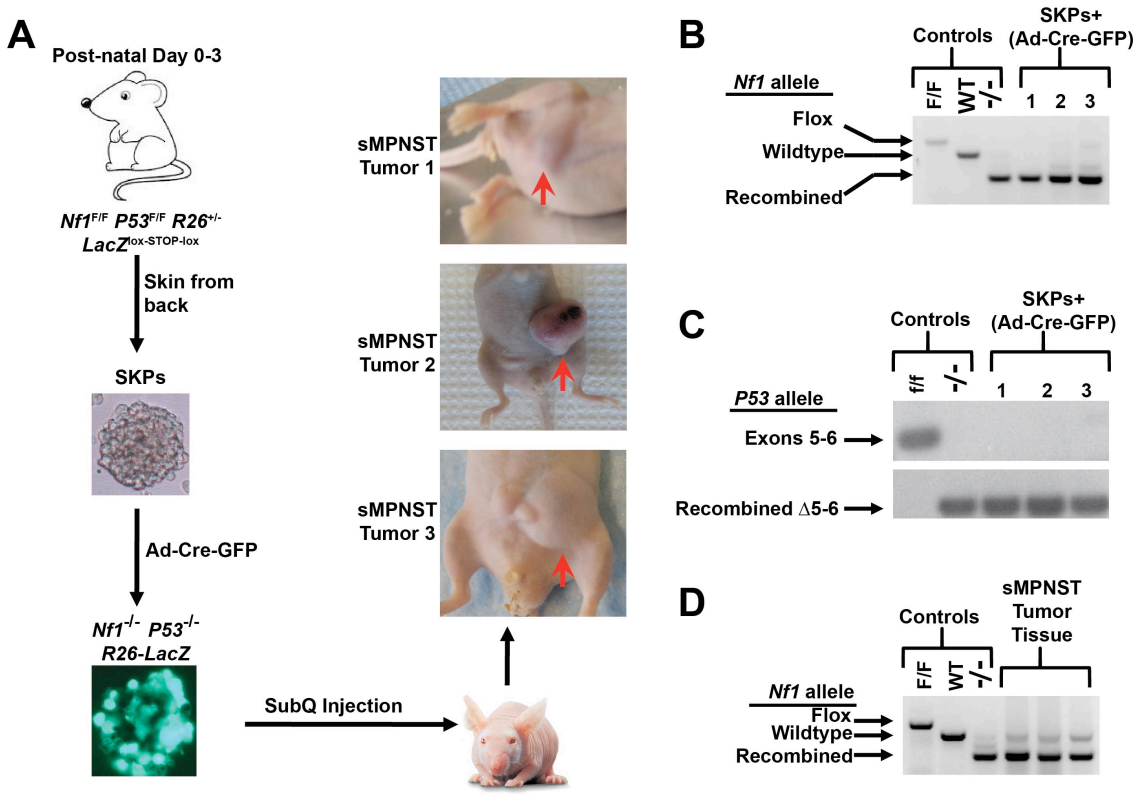

Figure 9.Isolation, derivation, and validation of NP-SKPs and sMPNSTs
(A) Flowchart diagram for isolating SKPs, generating NP-SKPs, and sMPNSTs (3 biological sets where each set consists of 1 batch of NP-SKPs and 1 batch of sMPNSTs derived from those NP-SKPs).
(B) PCR validation of *Nf1* knockout via adenovirus Cre-mediated recombination in NP-SKPs.
(C) PCR validation of *P53* knockout by adenovirus Cre-mediated recombination in NP-SKPs
(D) PCR analysis of *Nf1* knockout cells in sMPNST tumors to evaluate derivation from NP-SKPs.

isolated total RNA from these fresh tumors, and confirmed that these tumors are derived from NP-SKPs as indicated by predominant presence of *Nf1* recombined allele, and positive for X-gal staining (Figure 9C, and data not shown). Analysis of sections of these tumors after hematoxylin and eosin (H&E) staining revealed tumors with high/uniform cellularity, presence of mitotic cells, and high nuclear/cytoplasmic ratio, which collectively indicated

that these tumors were indeed malignant, while presence of spindle-shaped cells suggested

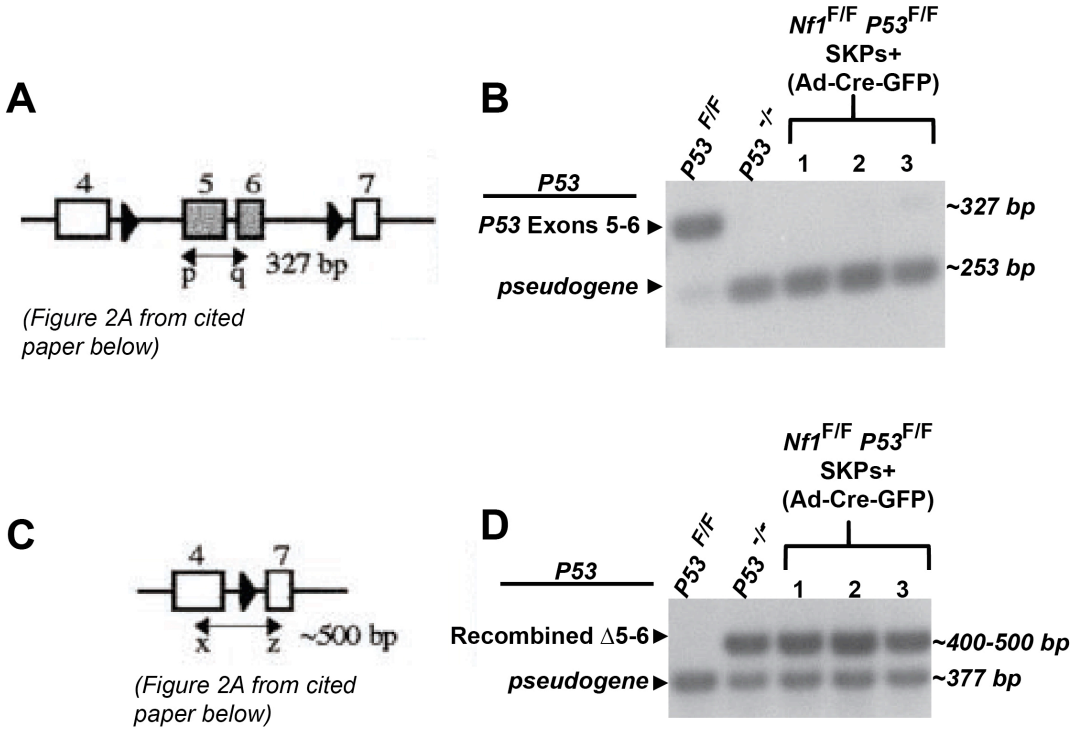

PCR w/ primers (p+q)
p: 5'-TACTCTCCTCCCCTCAATAAGCTAT-3'
q: 5'-GTCTTCCAGATACTCGGGATACAAA-3'

PCR w/ primers (x+z)
x: 5'-TGGGACAGCCAAGTCTGTTA-3'
z: 5'-CATGCAGGAGCTATTACACA-3'

PCR primers and exon figures adapted from Lin,S.-C. J., K.-F.Lee et al. (2004) Somatic Mutation of p53 Leads to Estrogen Receptor alpha-positive and negative-mouse mammary tumors with high frequency of metastasis. Cancer Research 64(10):3525-3532

Figure 10. PCR validation of *P53* knockout via Cre-mediated recombination. Related to Figure 9
(A) Diagram indicating relative location of PCR primers to detect exons 5 and 6 of mouse *P53*
(B) PCR validation of *P53* knockout
(C) Diagram indicating relative location of PCR primers to detect deletion of exons 5 and 6 of mouse *P53*
(D) PCR validation of *P53* knockout

Schwann-like cells (Figure 11). To classify these tumors as MPNSTs, we stained for expression of S100β and GAP43, which are markers commonly used to identify human

MPNSTs. Indeed, these tumors stained positive for both markers, and thus we termed these tumors as sMPNSTs, and therefore proceeded with comparative transcriptome analysis (Figure 11).

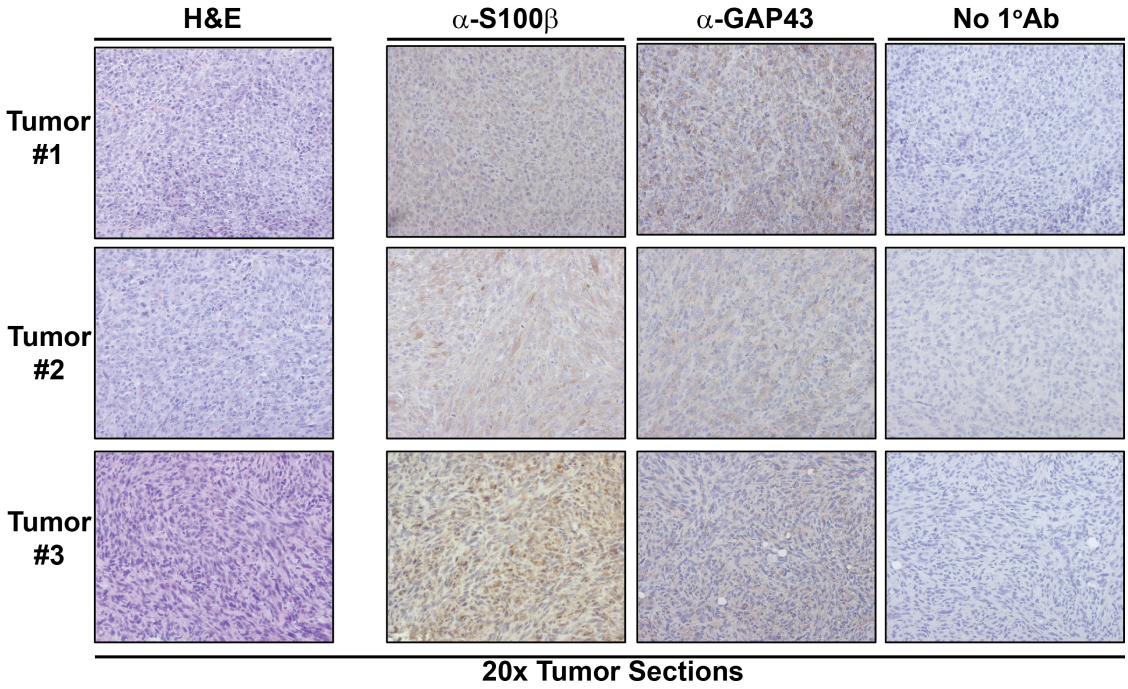

Figure 11. Histopathological analysis of NP-SKP derived tumors prior to expression microarray analysis.

Comparative transcriptome analysis identifies increased gene expression associated with upregulation of chromatin regulators in the tumorigenic state of sMPNSTs

To identify the molecular events underlying NP-SKP progression to sMNPSTs, we utilized total RNA samples we had collected above to compare the gene expression profiles of sMPNST tumors to their pre-tumorigenic ancestors (NP-SKPs) via microarray analysis (Figure 12A). As anticipated, comparative microarray analysis indicates that sMPNST tumors had numerous genes up- and down-regulated when compared to NP-SKPs (Figure 12B). However, we found substantially more genes upregulated, and with greater magnitude

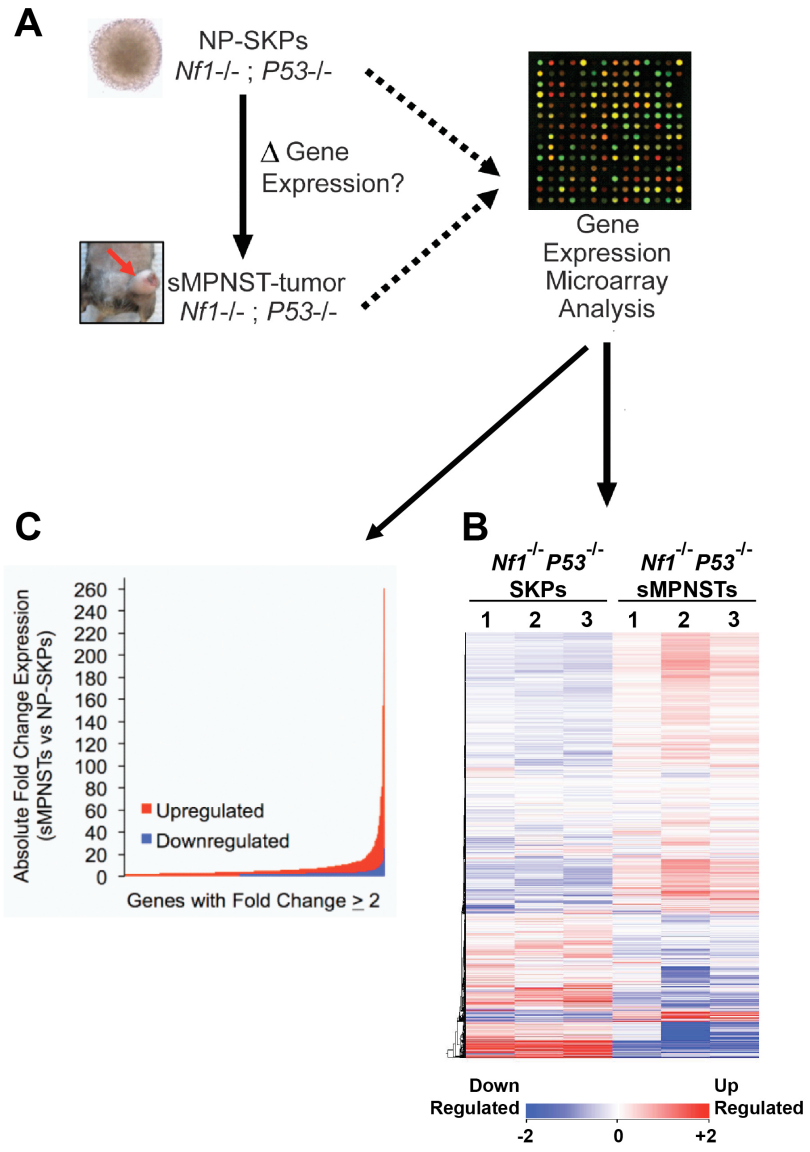

Figure 12.Transcriptome analysis of NP-SKP progression to sMPNSTs *in vivo*.
(A) Diagram for gene expression microarray analysis experiment.
(B) Global analysis of gene expression differences/fold changes (≥2) in heatmap format for each sample from microarray experiment.
(C) Global analysis of absolute fold change (≥2) in gene expression from sMPNSTs compared to NP-SKPs in bar graph format.

of fold change expression (Figure 12C), which was associated with upregulation of RNA polymerase II (RNAP II) regulator *Brd4* in addition to numerous epigenetic regulators that may potentially regulate global transcriptional output (Figure 13A).

Given the observation that upregulation of epigenetic regulators are associated increased gene expression in the tumorigenic state (sMPNSTs) compared to the pre-tumorigenic state (NP-SKPs), we wished to explore this connection by first validating these findings on a broader array of samples. By quantitative RT-PCR and

and Western blot analyses, we indeed confirmed our microarray data, and observed high levels of epigenetic regulators in MPNSTs compared to pre-tumorigenic cells (Figures 13B-

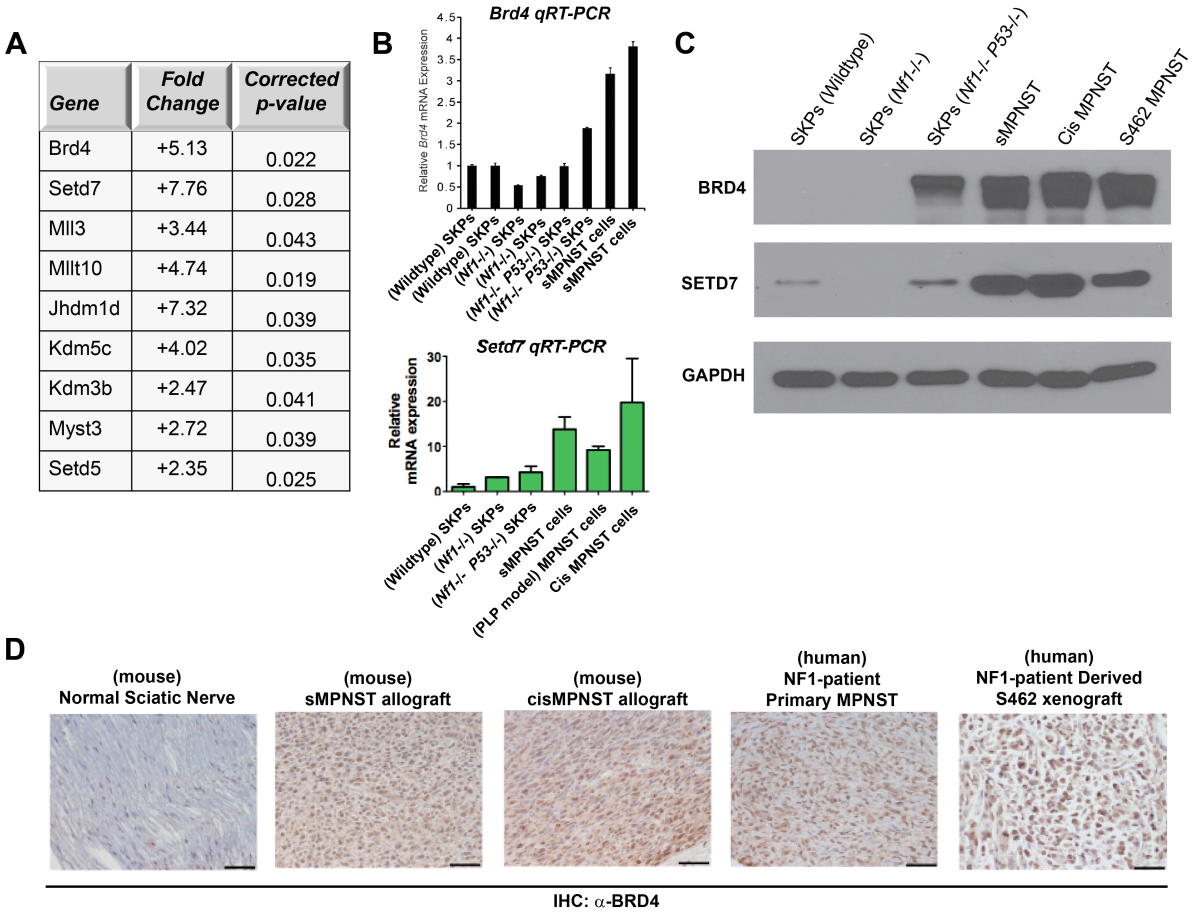

Figure 13.Epigenetic regulators upregulated during NP-SKP progression to sMPNSTs. (A) Epigenetic regulators found by microarray analysis to be upregulated in sMPNST compared to NP-SKPs.
(B) Primary validation of select epigenetic regulators by qRT-PCR.
(C) Secondary validation of select epigenetic regulators by Western blot analysis.
(D) Immunohistochemistry (IHC) for BRD4 in panel of tissues above indicates predominant/wide-spread expression of BRD4 in both mouse and human MPNSTs.
[Figure 13B, 13C, and 13D adapted from (Patel et al., 2014)

C). Consistent with these data, we also observed abundant expression of BRD4 in human MPNST primary tissue and xenograft (Figure 13D) (SETD7 could not be evaluated by immunohistochemistry given that reliable antibodies are not available for that specific application). All together, these results suggest that epigenetic regulators may underlie MPNST development, and warrant further investigation through functional studies, which are presented in Chapter 3.

2.4 – Discussion

Our comparative analysis of transcriptome data between sMPNST tumors and NP-SKPs suggest that there may be globally increased transcription in sMPNST tumors compared to NP-SKPs. In support of this idea, we found increased expression of numerous epigenetic regulators that may participate in this process of transcriptional regulation on a global scale (Figure 12B-C). However, sMPNST tumors are likely to contain some amount of host mouse cells (not derived from NP-SKP) such immune cells or fibroblasts, which may affect the interpretation of transcriptome data from sMPNST tumors. In hindsight, as an alternative approach, we could have used NP-SKP (Rosa26-GFP) or stably infected NP-SKPs with a GFP virus, then used these cells to generated sMPNST tumors from which GFP-positive cells could be isolated by flow cytometry, or other methods such as TRAP (translating ribosome affinity purification) (Zhang et al., 2013). Nevertheless, at that time, we chose to use sMPNST tumors because it was unclear to us whether culturing sMPNST tumor cells *in vitro* might change their intrinsic gene expression program, and we desired to capture the gene expression signature of primary tumors *in vivo* to better understand what dictates MPNST development in the *in vivo* context. Moreover, by PCR analysis of the *Nf1*

allele in the sMPNST tumors, we observed only minor amounts of wildtype *Nf1* allele (from host mouse cells/not NP-SKP derived), which suggested that these tumors were relatively homogenous, thus we felt confident the transcriptome data from those samples would be informative (Figure 9D). And of course, every microarray experiment requires secondary validation, which I did using primary sMPNST tumor cell lines, and as well as other mouse and human MPNSTs (Figure 13B-D). As a result, we identified higher levels of 2 epigenetic regulators (*Brd4*, *Setd7*) in MPNSTs compared to pre-tumorigenic cells (Figure 13B-C), and have worked on defining the role those two genes in MPNST development.

SETD7 is a lysine methyltransferase identified by the laboratories of Danny Reinberg and Yi Zhang. Both groups found that SETD7 has mono-methyltransferase activity upon histone 3 at lysine residue 4 (H3K4), thus indicating role in facilitating H3K4me1 deposition (Nishioka et al., 2002; Wang et al., 2001). Subsequent studies by their group and others indicate non-histone substrates (e.g. P53, RB1, YAP1) for SETD7 (Chuikov et al., 2004; Kurash et al., 2008; Munro et al., 2010; Oudhoff et al.). Shortly after we identified SETD7 in our transcriptome analysis, two independent research groups generated *Setd7* knockout mice, and found that global H3K4me1 levels were unaffected, and that SETD7 remains primarily in the cytoplasm (Campaner et al., 2011; Lehnertz et al., 2011). Indeed, with collaboration from Zhiguo Chen in the Le lab, we found that SETD7 is exclusively found in the cytoplasm of mouse MPNST and Schwannoma cells (assayed by nuclear/cytoplasmic fractionation followed by Western blot) (data not shown). These findings suggest that this protein does not have methyltransferase activity *in vivo* in living cells upon histone 3, but may have activity against other substrates in MPNST. Thus, the role of SETD7 remains

elusive, but our observation of SETD7 being highly upregulated in MPNSTs brings an opportunity to clarify the role of this protein in tumorigenesis.

BRD4 along with Mediator and pTEFb are all implicated in promoting RNA polymerase II (RNAP II) dependent transcriptional elongation (Donner et al., 2010; Jang et al., 2005; Wu and Chiang, 2007). BRD4 has been previously implicated in cancer biology (Dawson et al., 2011; Delmore et al., 2011; Filippakopoulos et al., 2010; Firestein et al., 2008; Lovén et al., 2013; Zuber et al., 2011), and is currently amenable to pharmacological inhibition through small molecule bromodomain inhibitor JQ1 (Filippakopoulos et al., 2010), which may present a novel therapeutic modality for treating NF1-associated MPNSTs. For the purpose of clarity and linearity, we focus on *Brd4* in the remainder of this thesis since it has become a major focus of this project.

CHAPTER THREE

Effect of Genetic and Pharmacological Inhibition of BRD4 in MPNST

3.1 – Introduction

Bromodomain containing proteins

BRD4 is one of several proteins that contain a highly conserved 110 amino acid motif known as bromodomain (Belkina and Denis, 2012). The name bromodomain originates from the founding member in Drosophila Melanogaster (Marmorstein and Berger, 2001). The protein Brahma in D. Melanogaster, when characterized initially, was found to contain a protein domain sequence that was conserved in a diverse array of proteins in higher organisms (Tamkun et al., 1992). Thus, this domain was given the name "bromodomain," in which "bromo" is derived from the Drosophila protein Brahma (Belkina and Denis, 2012). Bromodomains permit bromodomain-containing proteins to read or allow binding to acetyl-lysine post-translation chromatin modifications found on histones, which is suggested to allow these proteins to facilitate transcriptional activation or repression (Wu and Chiang, 2007). It has been approximated that 42 proteins in humans contain a bromodomain. Most bromodomain containing proteins contain a single bromodomain, and include SWI/SNF proteins (SMARCA2 and SMARCA4) and chromatin remodelers such as histone acetyltranferases (CBP and TAF1) (Belkina and Denis, 2012).

BET proteins

In contrast, BRD4 contains two bromodomains in tandem. BRD4 is one of 4 proteins (BRD2, BRD3, BRD4, BRDT) that have twin bromodomains in addition to also carrying

carboxy-terminal extra-terminal (ET) domain for protein-protein interactions (Belkina et al., 2013). Together, these proteins are broadly termed as BET (Bromodomain with Extra-terminal domain) proteins (Belkina et al., 2013). In terms of homology, there is about 80% amino acid conservation in the bromodomains of BRD2 and BRD4 (Belkina and Denis, 2012). Also, BRD2, BRD3, BRD4, and BRDT all share similar domain organization and size, with exception of the long form (Isoform A) of BRD4, which contains additional ~600 amino acid sequence (proline-rich) at tis carboxy-terminus (Wu and Chiang, 2007). All 4 BET proteins are expressed in most tissues with exception of BRDT, which expressed in testis (Filippakopoulos et al., 2010; Matzuk et al., 2012).

Functionally, BRD2, BRD3, and BRD4 have been found to physically interact via proteomic approaches (Rahman et al., 2011). This has been further supported by ChIP-seq analysis of their genome-wide occupancy, which indicates some overlap in occupancy; nonetheless, unique sites of genomic occupancy exist (Anders et al., 2014; Asangani et al., 2014). Thus suggesting some functional redundancy, but also unique functions. Indeed, *Brd2*$^{-/-}$ or *Brd4*$^{-/-}$ mice are unviable due to embryonic lethality (Belkina and Denis, 2012). In contrast, mice with a *Brd2* hyomorphic allele become severely obese without exhibiting type II diabetes, and have reduced inflammatory response (Belkina et al., 2013; Wang et al., 2009). *Brd4* heterozygous mice have post-natal phenotypes (reduced subcutaneous adipose, thickening of epidermis of skin, necrotic hepatocytes), and most of these mice die by 20 days after birth (Houzelstein et al., 2002). However, little is known about the *in vivo* physiological role of *Brd3* since mutant mice have never been generated. Thus, BET

proteins may have diverse biological functions. Notably, BRD4 has been the most well studied BET protein.

Brd4 isoforms and function

Since the discovery of *Brd4* more than a decade ago, it is has been known for quite a few years that *Brd4* mRNA also exists in alternatively spliced isoforms (Figure 14) (Shi and Vakoc, 2014). The first isoform to be discovered and studied was the long form (Isoform A), the second was the short form (Isoform C), and more recently Isoform B (Belkina and Denis, 2012; Dey et al., 2003; Floyd et al., 2013; Wu and Chiang, 2007). All isoforms are very

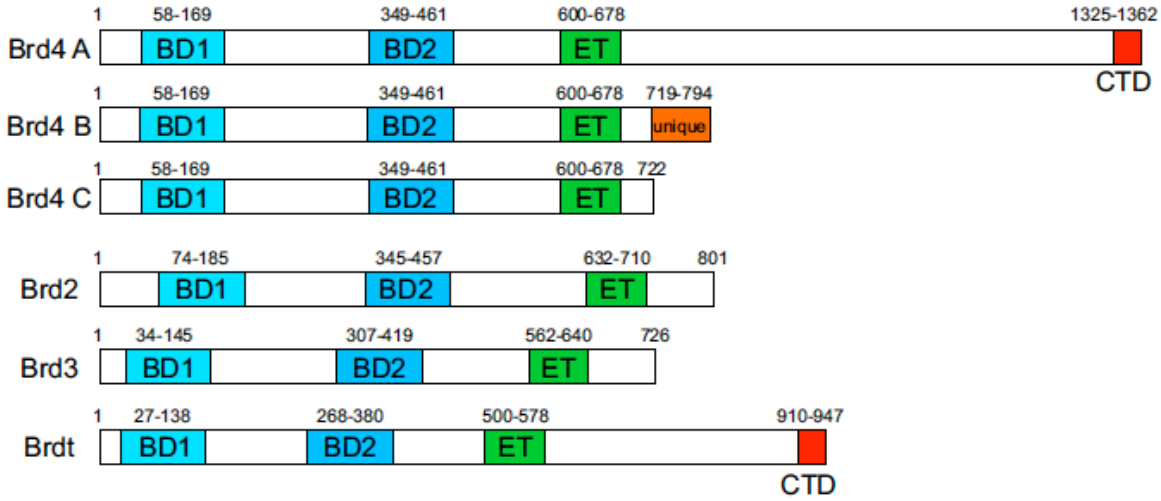

Figure 14. BET bromodomain proteins and isoforms.
BET proteins their shared and divergent domains aligned relative to amino acid length. BD1 = bromodomain 1, BD2 = bromodomain 2, ET = extra-terminal domain, CTD = carboxy-terminal domain. Adapted from Figure 1 in (Shi and Vakoc, 2014).

similar in terms of structure and identity with conservation of the twin bromodomains, ET, and SEED domains. However Isoform B contains a C-terminal exon not found in the other isoforms (Floyd et al., 2013). Isoform C does not contain the proline-rich region nor the C-

terminal domain (known to interact with p-TEFb (Jang et al., 2005; Yang et al., 2008; Yang et al., 2005)). Functionally, Isoform B has been shown to be an inhibitor of DNA damage response by insulating chromatin (Floyd et al., 2013). The role of Isoform C has been linked to various proteins it interacts with (including SIPA1, RRP1B) and as pro-metastatic protein in breast cancer, but its precise/ definitive role has remained elusive (Alsarraj et al., 2013; Alsarraj et al., 2011; Farina et al., 2004). On the other hand, Isoform A has been well characterized, most notably as positive co-regulator of transcription elongation through recognition/binding to acetylated histones followed by recruitment of pTEFb or other transcriptional regulators to activate RNA polymerase II for elongation (Mochizuki et al., 2008; Patel et al., 2013; Rahman et al., 2011; Wu and Chiang, 2007; Yang et al., 2008; Yang et al., 2005). More recently, Isoform A was discovered to be accumulated at double strand DNA breaks induced by immunoglobulin class switching to help recruit proteins essential for repair by the nonhomologous end-joining pathway (Stanlie et al., 2014). Of the 3 isoforms of BRD4, isoform A has been the most well studied, particularly in the context of cancer.

BRD4 as a therapeutic target to disable oncogenic c-Myc in cancer

Although *Brd4* was first discovered more than a decade ago, its role in normal development and disease remained elusive up until 2005 when it was first reported by two groups that BRD4 binds to chromatin to recruit p-TEFb to stimulate RNA polymerase II dependent transcription elongation (Jang et al., 2005; Yang et al., 2005). Then in 2008, it was found that found that BRD4 activates the expression of genes (including *Cyclin D1*, *Jun*, and *c-Myc*) for cell cycle progression from G_1 to S phase (Mochizuki et al., 2008). In the

following two years, 2 independent groups discovered and developed selective inhibitors of BET bromodomain proteins (BRD2/3/4 and BRDT), and demonstrated their clinical utility for suppressing inflammatory gene expression and inhibiting the BRD4-NUT fusion onco-protein in nut-midline carcinoma (NMC) (Filippakopoulos et al., 2010; Nicodeme et al., 2010). With selective inhibitors available, several groups corroborated the role of BRD4 in maintaining transcription of oncogenic c-Myc, and provided compelling rationale for inhibiting BET bromodomains to therapeutically target c-Myc selectively in genetically diverse mouse and human leukemia, multiple myeloma, and T cell leukemia cells (Dawson et al., 2011; Delmore et al., 2011; King et al., 2013; Zuber et al., 2011).

Novel mechanisms of transcriptional regulation through BRD4 at super-enhancers

However, the mechanism by which BRD4 inhibition reduced c-Myc in leukemia but not normal cells *in vitro* and *in vivo* remained a mystery. The lab of Richard Young at that time had been studying genome-wide-localization of chromatin regulators (including BRD4) by ChIP-seq, and had observed that BRD4 was abnormally occupied at high levels across long-stretches of DNA either near or far (>1 megabase) from the vicinity of genes known to be highly expressed in Myc-dependent myelomas, but not in normal cells (Delmore et al., 2011). They experimentally found that these long-stretches were not regular enhancers, but what they termed as super-enhancers, which are capable of promoting high levels of transcriptional elongation when BRD4 is present at sufficiently high levels (Lovén et al., 2013). Thus, upon BRD4 inhibition, super-enhancer regulated genes bound by BRD4 have a marked collapse in transcriptional elongation while genes with typical enhancers were

relatively less affected. This novel mechanism of transcriptional enhancement led to the discovery that super-enhancers play important roles in maintaining transcriptional programs necessary for cellular identity, and that these super-enhancers are frequently mutated in a variety human diseases (most prominently in non-coding DNA that has been implicated in genome-wide association studies) (Hnisz et al., 2013; Parker et al., 2013; Whyte et al., 2013). All together, these findings have significantly advanced our knowledge of BET proteins, cancer, and transcriptional regulation in such a brief period; much of this may not be possible without the development and advancement of pharmacological BET bromodomain inhibitors.

Pharmacological inhibitors of BET proteins

BET bromodomain inhibitors were first developed by two groups independently, and published simultaneously in 2010. The first group screened for BET protein inhibitors through an ApoA1 reporter system to identify potential lead compounds, one of them being a benzodiazepine that was found to bind specifically to both bromodomains of each BET protein (BRD2, BRD3, BRD4), and later modified to more potent inhibitor called "I-BET" also known as GSK525762 (Nicodeme et al., 2010). The second group recognized that Mitsubishi Pharmaceuticals had a patent on thienodiazepines that bind to BRD4, and therefore, they synthesized their own novel derivative, which was named "JQ1" that binds to both bromodomains of each BET protein (Filippakopoulos et al., 2010). Both of these inhibitors will bind to both bromodomains in a competitive manner, and thus displace BET proteins from their acetyl-lysine targets (Filippakopoulos et al., 2010; Nicodeme et al., 2010). Hereafter, I-BET and JQ1, followed by additional BET bromodomain inhibitors developed

by other companies including Constellation Pharmaceuticals, OncoEthix, and Resverlogix, are in clinical phase of development (Filippakopoulos and Knapp, 2014).

Therapeutic utility of BET bromodomain inhibitors for non-cancer indications

While BET protein inhibitors have received wide attention in the fields of oncology and inflammation, new indications have been described more recently. The first being the use of JQ1 as a reversible male contraceptive via inhibition of BET protein BRDT and associated reduction in spermatozoa (Matzuk et al., 2012). The second being in heart disease whereby BET proteins mediate the transcription program activated by heart stress to induced cardiac remodeling which can eventually result in heart failure; therefore, BET protein inhibition with pharmacological inhibitors was shown to block hypertrophy and failure of the heart in mouse models of cardiac stress (Anand et al., 2013; Spiltoir et al., 2013). Third, BET protein inhibition has been found to reactivate HIV dependent transcription, thus suggesting a strategy to reactivate latent or silent HIV for eradication with current antiretroviral drugs (Li et al., 2013; Zhu et al., 2012). Together, these new findings suggest broad clinical benefit in the clinic, but also raise concerns as to how inhibition of BET proteins may affect physiological transcription programs. In many of the initial studies of BET inhibitors *in vivo* in rodent models, broad tolerability was observed for wide range of tissues and overall health. However, in those studies, these inhibitors were used typically for a short duration (up to 1 month), and these drugs were first-generation compounds that have a half-life of less than 24 hours. As second generation derivatives are being evaluated in the clinic, safety concerns are likely to be addressed in the near future. Meanwhile, current and

future basic research into the fundamental biology of BET proteins will likely reveal the broad spectrum of mechanisms underlying therapeutic effects and potential side-effects of BET bromodomain inhibitors.

Therapeutic action of BET bromodomain inhibitors: Mechanistic association versus causation

BET bromodomain inhibitors have received wide attention in oncology research, yet the basis for their mechanism of action has been generally through association, but with exceptions. For example, given that BET proteins generally facilitate transcription elongation, many studies have evaluated the downstream consequences of BET inhibitors either by ChIP-sequencing (for BET protein occupancy at gene promoters) and/or expression microarray analysis. These studies reveal that BET inhibitors regulate expression of wide range of genes regulating cellular growth or survival (e.g. *c-Myc*, *p21*, *Bcl2*), but their re-expression is not always sufficient to rescue effects of BET bromodomain inhibition (Asangani et al., 2014; Cheng et al., 2013; King et al., 2013; Mertz et al., 2011; Zuber et al., 2011). For example, re-expression of *c-Myc* in in acute myeloid leukemia (AML) was reported to rescue proliferation defects when Brd4 was inhibited either genetically or pharmacologically, but was insufficient to rescue AML from cell death. In human glioblastoma and prostate cancer, JQ1 was found to reduce *c-Myc* expression, but re-expression of *c-Myc* was unable to restore proliferation of those cells (Asangani et al., 2014; Cheng et al., 2013). These examples suggest that not all events downstream of BET bromodomain inhibition are functional drivers of anti-neoplastic effects of BET inhibitors, and that perhaps many of them represent passenger events. Additionally, they suggest that

inhibition of *c-Myc* or other genes via these inhibitors may not serve as effective predictors or biomarkers for which tumors or diseases respond to BET bromodomain inhibitors. Thus, comprehensive identification and dissection of functional drivers downstream of BET bromodomain inhibitors in diverse disease contexts will be required to devise predictive biomarkers of therapeutic usage and efficacy. Lastly, while BET inhibitors exert broad therapeutic efficacy, tumors can maintain growth and survival. Thus, it will be necessary to develop combination therapies with BET bromodomain inhibitors as a starting platform while also determining whether tumors develop or harbor mechanisms to resist these inhibitors. In the following section and chapters, our studies shed further insights into the mechanisms underlying therapeutic efficacy, sensitivity, and resistance to BET bromodomain inhibitors.

3.2 – Experimental Procedures

Animal Studies

All mice were housed in the animal facility at the University of Texas Southwestern Medical Center at Dallas (UTSW). Animal care and use were in compliance with regulations of the Institutional Animal Care and Research Advisory Committee at UTSW. Athymic nude mice were used for tumor studies. For shRNA induction in sMPNST-pTripz tumors in vivo, mice were given water containing 1 mg/mL doxycycline (Sigma-Aldrich) in 5% sucrose. For daily drug administration, a single dose of vehicle or 50 mg/kg JQ1 (Cayman Chemical) were prepared as described (Filippakopoulos et al., 2010; Zuber et al., 2011). Tumor volume was calculated as described in (Mo et al., 2013) using the following formula: (0.5) x L x W^2,

where *L*=longest tumor length and *W*=shortest tumor width. 50 mg/kg D-Luciferin was administered by intraperitoneal injection followed by bioluminescent imaging of mice 10 minutes later with IVIS Spectrum system (Caliper Life Sciences).

Lentiviral Constructs

Mouse *Brd4* shRNAs were generated by synthesizing 22mer sequences corresponding to *Brd4* shRNAs described previously (Zuber et al., 2011) for PCR cloning into pTripz lentiviral vector. For lentivirus production, psPAX2 and pMD2.g (Addgene plasmids 12260 and 12259) packaging vectors were used. See Appendix B for plasmids. See Appendix C for virus packaging protocol. See Appendix D for virus infection protocol.

In Vitro Growth Assays

ATP CellTiter Glo assay (Promega – Catalog# G7572) was performed as per manufacturer's instructions. The FLUOstar OPTIMA 96-well plate reader (BMG Labtech) was used for luminescence measurements.

qRT(quantitative, reverse transcription)-PCR

RNEasy mini kit (Qiagen) was used to isolate total RNA from cells, followed by cDNA synthesis with iScript Select cDNA synthesis kit (Bio-Rad), and then qRT-PCR using iTaq Universal SYBR Green Supermix (Bio-Rad) on the CFX Connect Real-Time PCR platform (Bio-Rad). Data was quantified by ΔCt method, and normalized relative to Gapdh. See Appendix E for list of oligonucleotide primers used.

Western Blot

Protein isolation, and subsequent Western blot analysis was performed as described previously (Mo et al., 2013). Antibodies Used: BRD4 (Epitomics, Bethyl Labs). See Appendix F for detailed protocol.

Immunohistochemistry

Tumor tissue sample preparation, immunohistochemistry, and data quantification were performed as described previously (Mo et al., 2013). Antibodies Used: and BrdU (Dako). See Appendix G for detailed protocol.

3.3 – Results

Brd4 is Critical for Growth & Tumorigenic Capacity of MPNSTs

We sought to dissect the function of BRD4 in MPNSTs by employing a doxycycline (Dox) inducible shRNA system to acutely knockdown *Brd4* mRNA levels. sMPNST cells were transduced with lentivirus harboring either scrambled shRNA (pTripz-shCONTROL) or *Brd4* shRNAs (pTripz-shBrd4.523 or pTripz-shBrd4.552), and then treated with puromycin to select for stably infected cells (Figure 15A). Treatment of these cells with doxycycline to induce shRNA expression reveals >80% reduction of *Brd4* mRNA levels via *Brd4* shRNAs compared to scrambled shRNA (shCONTROL) induction, which is consistent with protein levels (Figures 15B and 15C). To evaluate the effect of acute depletion of *Brd4* on sMPNST cellular growth, we evaluated ATP levels as a surrogate for cell numbers before and after

acute knockdown of *Brd4*, and observed significantly reduced growth upon *Brd4* shRNA induction with doxycycline (Figure 15D).

To study the influence of BRD4 on the tumorigenic capacity of MPNST cells, we subcutaneously injected pTripz-shCONTROL and pTripz-shBrd4.552 sMPNST cells

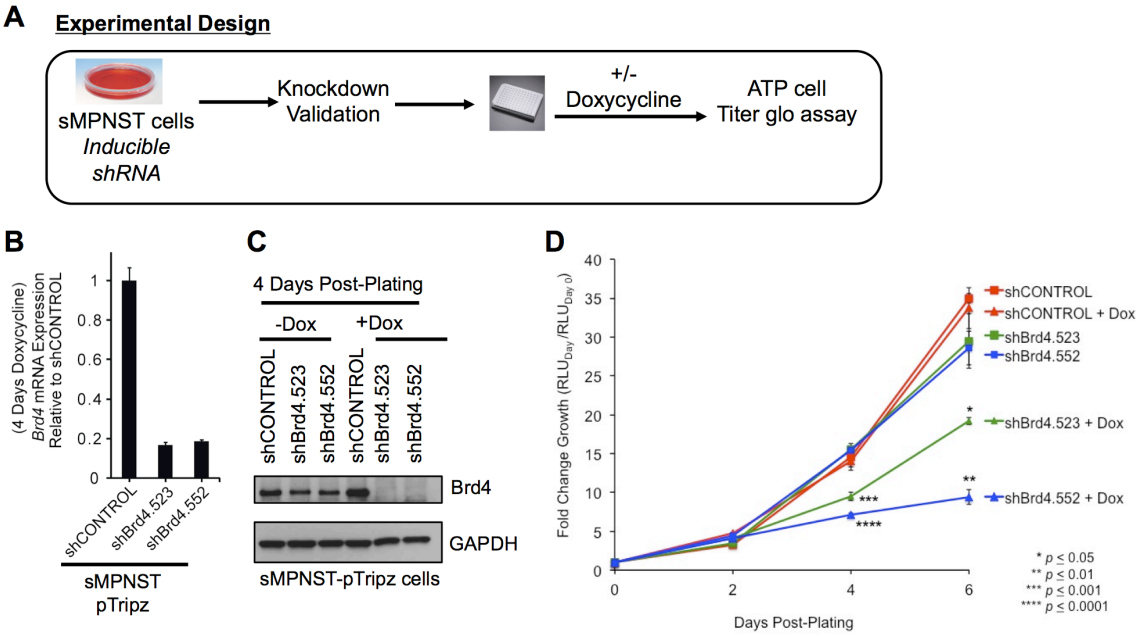

Figure 15. Effect of *Brd4* knockdown on MPNST cells in vitro
(A) Diagram of experimental design and flow for Figures 15B-D.
(B and C) qRT-PCR and western blot analysis for Brd4 knockdown in sMPNST-pTripz cells with or without doxycycline (Dox).
(D) Effect of Brd4 shRNA induction on MPNST cell growth/viability using ATP CellTiter Glo assay.[Adapted from (Patel et al., 2014)]

(Luciferase tagged) into nude mice. Two days later, both scrambled and *Brd4* shRNAs were turned on in sMPNST-allografts by administration of doxycycline (1mg/mL) through drinking water of the mice. By 30 days of shRNA induction in vivo, we found that *Brd4* shRNA-sMPNST cells had significantly delayed tumor burden/progression compared to

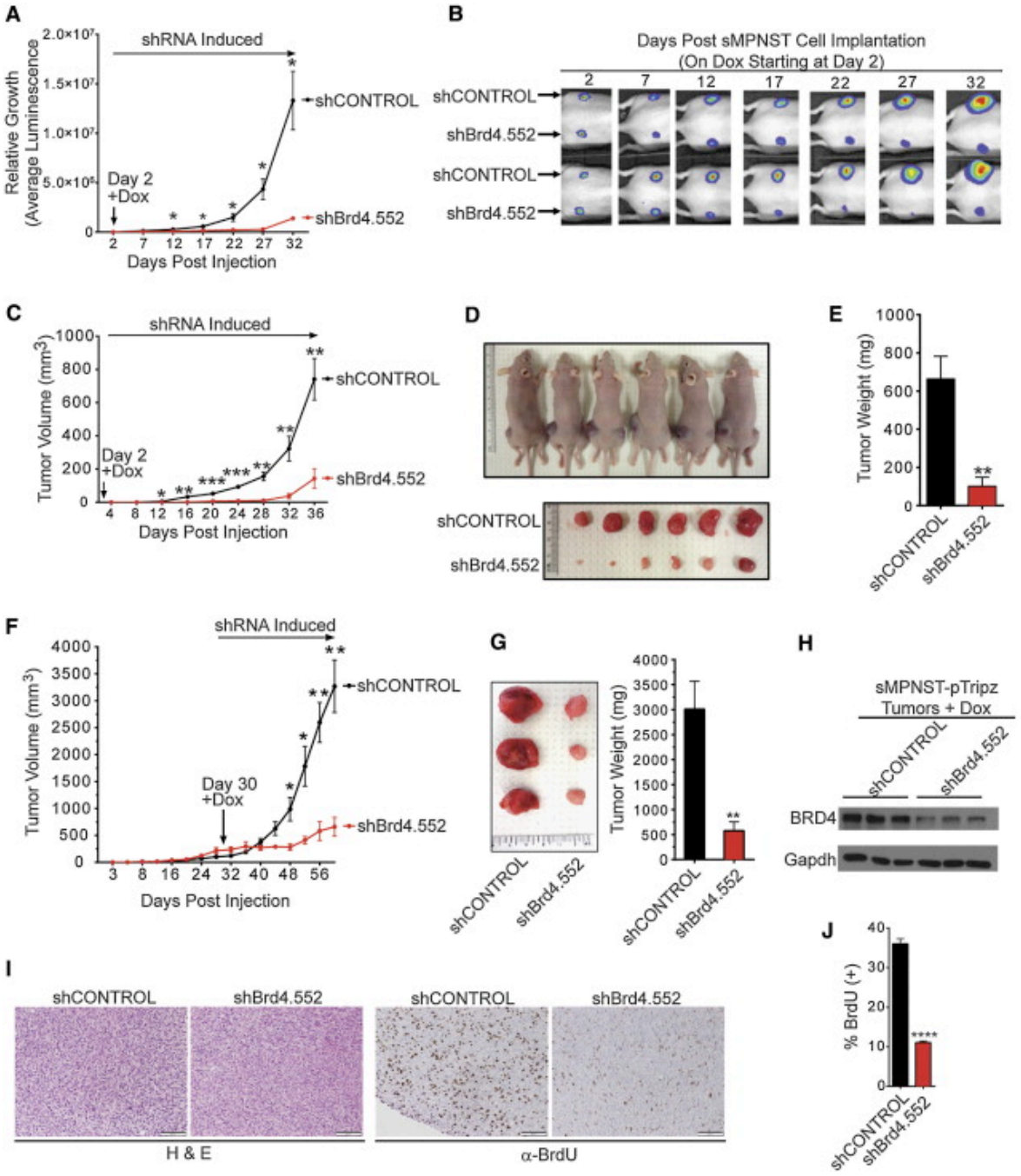

Figure 16. BRD4 Maintains Tumorigenic Capacity of MPNSTs *In Vivo*.
(A) Growth of shCONTROL and shBrd4.552 sMPNST tumors relative to "Day 2" value. Values represent luminescence counts (tumor bioluminescence imaging, n = 6 tumors per group).
(B) Representative pictures of sMPNST tumor bioluminescence in mice over time, which indicate that acute *Brd4* knockdown suppresses MPNST tumorigenesis *in vivo*. Mice were

started on doxycycline water on day 2, and kept on this treatment until the end of the experiment.
(C) sMPNST tumor volume measurements (each data point represents the average measurement from 6 different tumors per group).
(D) Top panel: Mice at 36 days post-subcutaneous implantation of sMPNST tumor cells (shCONTROL on left flank and shBrd4.552 on right flank). Bottom panel: Tumors excised from mice in "Top panel".
(E) Average weight of excised tumors from bottom panel of Figure 3D.
(F) Tumor volume of shCONTROL and shBrd4.552 sMPNST-pTripz tumors in mice. At day 30, when tumors were established (200-400 mm^3), mice were started on doxycycline water.
(G) Representative picture and average weight of excised sMPNST tumors from end of experiment in Figure 3F.
(H) Western blot analysis of BRD4 protein levels in shCONTROL and shBrd4.552 sMPNST tumors in mice given doxycycline water.
(I) Representative images of sMPNST tumor sections stained with either hematoxylin and eosin (H&E) or BrdU antibody.
(J) Quantification of the percentage of BrdU(+) cells from sMPNST tumor sections (scale bars represent 100 mm).
All statistics are represented as the mean +/- SEM (*$p \leq 0.05$, **$p \leq 0.01$, ***$p \leq 0.001$, ***$p \leq 0.0001$). [Adapted from (Patel et al., 2014)]

control as indicated by periodic measurements of tumor bioluminescence and volume, and final weight of excised tumors (Figures 16A, 16B, 16C, 16D, and 16E). Remarkably, induction of *Brd4* shRNA expression in established tumors (30 days after subcutaneous implantation) halted sMPNST tumor progression/growth when compared to shCONTROL sMPNST tumors (Figures 16F and 16G). Western blot analysis of these tumors indicates that these findings are consistent with reduced BRD4 protein levels in shBrd4.552+Dox tumors (Figure 16H). Through molecular analysis of tumor proliferation, we found that shBrd4.552 tumors had significantly fewer BrdU-positive cells than shCONTROL tumors (Figures 16I and 16J). All together, these data indicate an important role for BRD4 in maintaining tumorigenic capacity of MPNSTs *in vivo*.

Pharmacological Inhibition of Brd4 Suppresses MPNST Growth and Tumorigenesis

The remarkable inhibition of MPNST tumorigenesis through *Brd4* knockdown prompted us to evaluate the effect of inhibiting BRD4 with small molecule BET bromodomain inhibitor JQ1 (Filippakopoulos et al., 2010). We tested the effect of JQ1 on pre-tumorigenic NP-SKPs, sMPNST cells, and cis MPNST cells (derived from spontaneous MPNST arising in cis $Nf1^{+/-}$ $P53^{+/-}$ mice) (Mo et al., 2013; Vogel et al., 1999). All MPNST cells and NP-SKPs had decreased cellular viability/growth in a JQ1 dose dependent manner with IC_{50} values less than 400 nM, whereas SKPs (both wildtype and *Nf1*-null) were relatively unaffected (Figure 17A). These data may suggest a role for BRD4 in maintaining *in vitro* growth and survival signaling propagated by loss of both *Nf1* and *P53* in MPNSTs and their pre-tumorigenic precursors (NP-SKPs). Collectively, these promising findings suggest that JQ1 may have important therapeutic value in the treatment of MPNSTs.

In that regard, to investigate the therapeutic efficacy of JQ1 on MPNST tumor progression, we generated palpable (50 mm^3 average) sMPNST-allografts (luciferase expressing) in 14 nude mice (2 tumors per mouse). Prior to drug administration, we measured tumor volume and bioluminescence to separate tumor-bearing mice into 2 groups (14 tumors per group), in which tumor size, mouse gender/weight are equally represented (Figure 17B). Mice were treated with either vehicle or JQ1 for 15 days, and then sacrificed. During this treatment period, we found that growth of all JQ1 treated tumors (n = 14) had been severely blunted compared to vehicle treated tumors (n=14) as indicated by delayed progression of tumor bioluminescence and volume (Figures 17C and 17D).

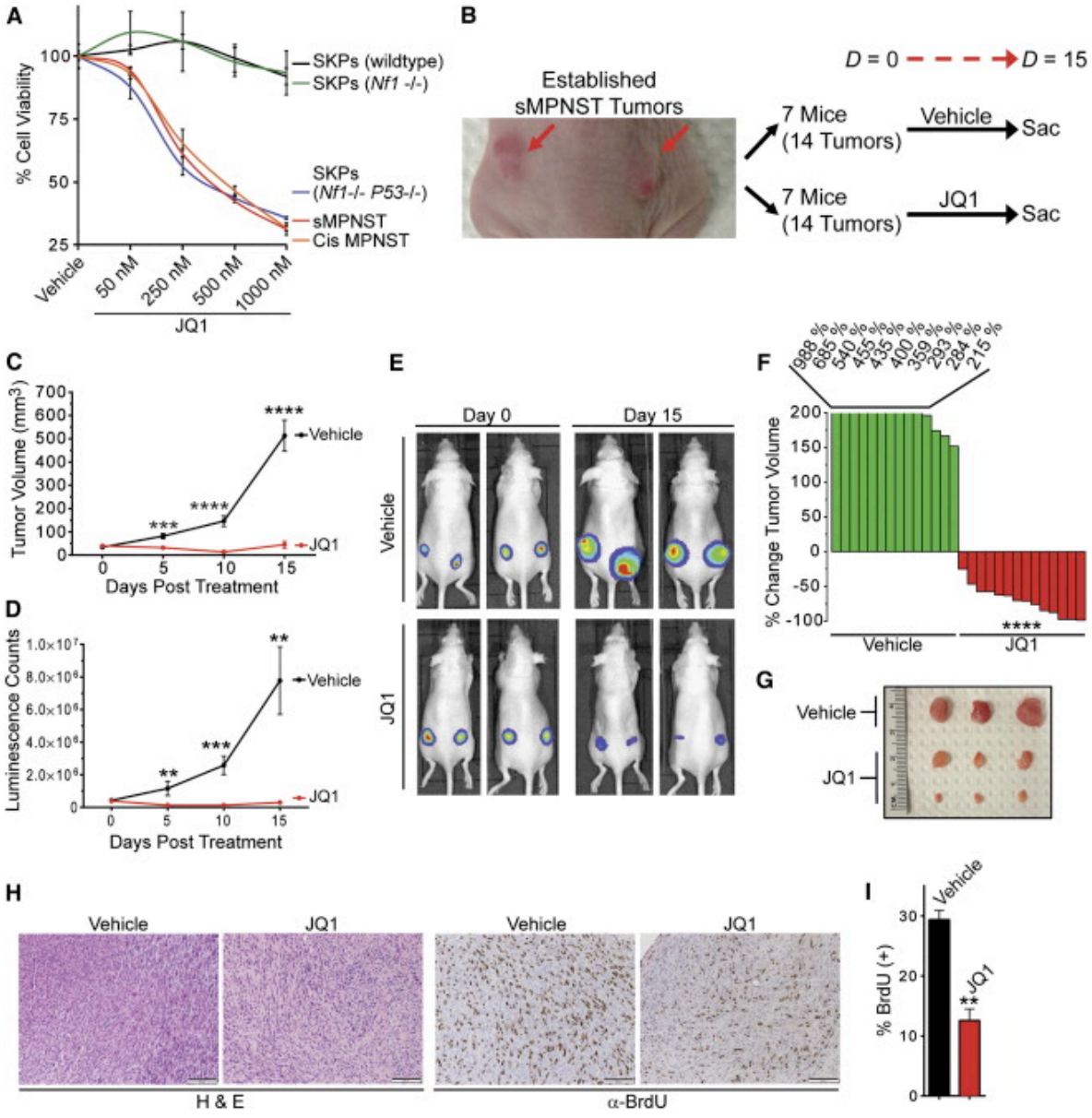

Figure 17. JQ1 Induces MPNST Regression *In Vivo*.
(A) Dose response curves for 2 day JQ1 treatment on primary murine SKPs (wildtype, *Nf1*$^{-/-}$, *Nf1*$^{-/-}$ *P53*$^{-/-}$) and MPNST cells (SKP model and *cisNP* model). ATP CellTiter-glo assay was used to measure cell viability, and normalized to DMSO (Vehicle) for each cell type.
(B) Overview of JQ1 drug trial with nude mice bearing sMPNST allografts.
(C) Average sMPNST tumor volume measured during JQ1 drug trial (n = 14 tumors per treatment group).
(D) Average sMPNST tumor bioluminescence counts measured during JQ1 drug trial (n = 14 tumors per treatment group).

(E) Bioluminescence imaging of sMPNST allografts in mice before and after the JQ1 drug trial.
(F) Waterfall plot showing the percentage change in sMPNST tumor volume from before starting (Day 0) and after 10 days of JQ1 treatment.
(G) Representative pictures of sMPNST allografts excised from mice treated with vehicle or JQ1 for 15 days.
(H) Staining of sections from sMPNST allografts (vehicle or JQ1 treated) with hematoxylin and eosin (H&E) or immunostaining with BrdU antibody.
(I) Quantification of BrdU(+) cells from vehicle and JQ1 treated sMPNST tumor sections (scale bars represent 100 mm).
All statistics are represented as the mean +/- SEM (*$p \leq 0.05$, **$p \leq 0.01$, ***$p \leq 0.001$, ***$p \leq 0.0001$). [Adapted from (Patel et al., 2014)]

Interestingly, during the course of the experiment, we observed sMPNST tumor regression in JQ1 treated mice both visually and through bioluminescence imaging (Figure 17E). Remarkably, we observed 50% to near complete regression of tumor volume in as little as 10 days of JQ1 treatment, which resulted in much smaller tumors compared to Vehicle tumors (Figures 17F and 17G). Moreover, analysis of tumor proliferation revealed significantly fewer BrdU-positive cells in JQ1 treated sMPNST-allografts compared to Vehicle (Figures 17H and 17I). Importantly, we observed no significant changes in body weight nor behavior of mice during JQ1 treatment (data not shown), which is consistent with JQ1 tolerance observed in published mouse studies (Cheng et al., 2013; Delmore et al., 2011; Filippakopoulos et al., 2010; Zuber et al., 2011). These data strongly suggest great therapeutic potential for JQ1 in the treatment of established NF1-associated MPNSTs *in vivo*. Given that BRD4 levels increased upon loss of both *Nf1*/*P53* in SKPs, and further increased upon progression to MPNST, we hypothesized that BRD4 plays a role in NP-SKP progression or initiation to MPNST development.

Acquisition of Brd4 dependency as pre-tumorigenic NP-SKPs progress to MPNST in vivo

Thus, to examine whether BRD4 inhibition could subvert or delay MPNST initiation, primary SKPs were derived from post-natal day 1 mice (*Nf1*$^{F/F}$ *P53*$^{F/F}$ Rosa26-Luciferase), followed by Cre mediated recombination to generate *Nf1*$^{-/-}$ *P53*$^{-/-}$ SKPs (NP-SKPs). NP-SKPs were stably transduced with doxycycline inducible shRNA lentiviruses encoding control or 2 distinct *Brd4* shRNAs as described earlier in this chapter. *Brd4* knockdown was validated, followed by analysis of growth, which revealed that genetic inhibition of *Brd4* in NP-SKPs did not subvert their growth *in vitro* after 4 days (Figure 18A, 18B, 18C). Paradoxically, the very same NP-SKPs remained sensitive to BET bromodomain inhibitor JQ1 (Figure 18D). Given that we originally identified BRD4 upregulation as NP-SKPs progressed to sMPNST tumors *in vivo*, we reasoned that perhaps BRD4 dependency is acquired as NP-SKPs undergo malignant progression to MPNSTs in vivo.

To address this, we subcutaneously implanted NP-SKPs (with doxycycline inducible *Brd4* shRNA) into nude mice (Figure 19A), followed by continuous shRNA induction by dox (doxycycline) or no dox (vehicle) 3days later, and evaluated tumor volume and bioluminescence. During this experiment, we observed no difference in tumor volume or luminescence during the first 10 days of shRNA induction, but by 15 days, we observed that *Brd4* shRNA induced tumors had significant reduction in tumor bioluminescence, followed by sustained inhibition of tumorigenesis when compared to the "No Dox" group (Figures 19B and 19C). Towards the end of this study, we found that tumors with *Brd4* shRNA induction were markedly smaller in weight in size when compared to "No Dox" tumors

(Figure 19D and 19E). Collectively, these *in vitro* and *in vivo* studies suggest that BRD4 dependency might be acquired during malignant progression to MPNST, but does not rule out other possibilities as will be addressed in the discussion section of this chapter.

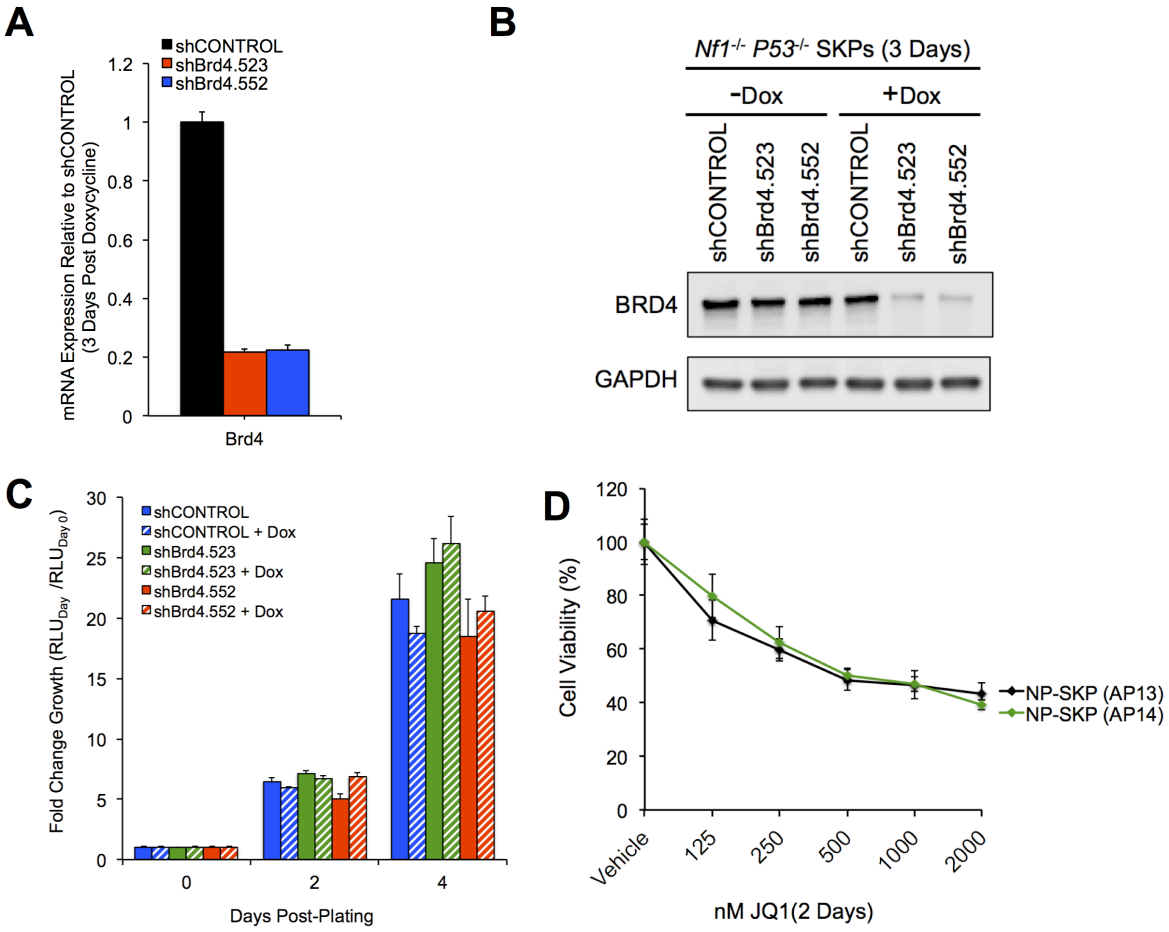

Figure 18. Pre-tumorigenic *Nf1*$^{-/-}$ *P53*$^{-/-}$ SKPs are sensitive to JQ1 but not *Brd4* knockdown *in vitro*.

(A) qRT-PCR analysis of *Brd4* mRNA expression after 3 days induction of indicated doxycycline inducible control or *Brd4* shRNAs in NP-SKPs.

(B) Western blot analysis of BRD4 protein expression after 3 days induction of indicated doxycycline inducible control or *Brd4* shRNAs in NP-SKPs.

(C) Growth of NP-SKPs was not affected by shRNA-mediated knockdown of *Brd4* in NP-SKPs as measured by ATP-cell titer Glo assay at the indicated time points.

(D) NP-SKPs are sensitive to BET bromodomain inhibitor JQ1 as measured by ATP-cell titer glo assay 2 days after indicated drug treatments. AP13 and AP14 represent two different batches/preparations of NP-SKPs (biological replicates).

All statistics are represented as the mean +/- SEM (*p ≤ 0.05, **p ≤ 0.01, ***p ≤ 0.001, ***p ≤ 0.0001).

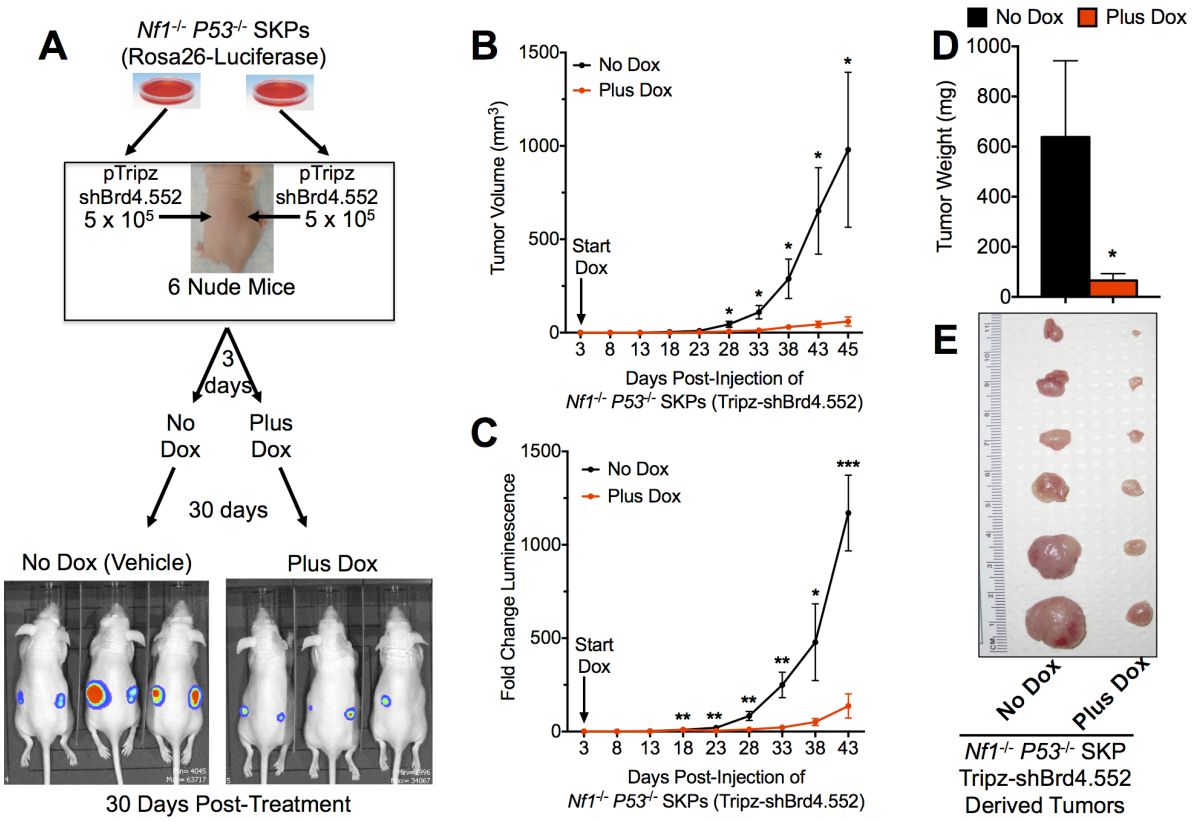

Figure 19. *In vivo* knockdown of *Brd4* blunts tumor initiating potential of *Nf1*$^{-/-}$ *P53*$^{-/-}$ SKPs.

(A) Diagram of experiment, and below is bioluminescence imaging of NP-SKPs(dox-inducible shBrd4.552) derived tumors in mice with indicated treatments.

(B) Tumor volume analysis.

(C) Tumor bioluminescence analysis

(D) Final tumor weight.

(E) Final tumors harvested from mice.

All statistics are represented as the mean +/- SEM (*p ≤ 0.05, **p ≤ 0.01, ***p ≤ 0.001, ***p ≤ 0.0001).

JQ1 exerts therapeutic efficacy against NF1-human MPNST xenograft tumors in vivo

The data thus far suggest an important role for BET bromodomains in MPNST pre-clinical mouse models, but human NF1-associated MPNSTs are likely to have additional

genetic alterations in addition to loss of *Nf1* and *P53*, and thus it is not clear whether BET bromodomain inhibitors will maintain therapeutic efficacy in late-stage or advanced MPNSTs. To address this, we utilized human NF1-associated MPNST cell line (S462), which was derived from a primary human MPNST tumor (WHO grade IV), and previously characterized to have loss of heterozygosity for 3 tumor suppressors (*Nf1*, *P53*, *p16*) (Frahm et al., 2004). These cells were engineered to express Luciferase via low titer transduction with Luciferase carrying retrovirus (by Chung-Ping Liao in Le lab). These cells were highly sensitive to JQ1 *in vitro*. These cells were subcutaneously implanted to nude mice (Figure 20A) followed by an initial scan of palpable tumors after 11 days post-implantation for bioluminescence in order to assign tumors to vehicle or JQ1 treatment groups (Figure 20B). Next day, mice were administered with either vehicle or 50mg/kg daily dose of JQ1 per day for 15 days, and harvested tumors. It was observed that JQ1 treated tumors had decreased tumor volume over time during this experiment, and accordingly, the final tumors weighed much less in the JQ1 arm compared to vehicle (Figures 20C, 20D, 20E, 20F). Although, some tumors in the JQ1 arm were larger, which either represents variation or resistance to JQ1 *in vivo* (Figure 20F). Nevertheless, thus study suggests that BET bromodomain inhibition with JQ1 can exhibit therapeutic efficacy against advanced human MPNST tumors *in vivo*, and perhaps development of combination therapies may be appropriate for improving overall therapeutic efficacy and ultimately patient survival.

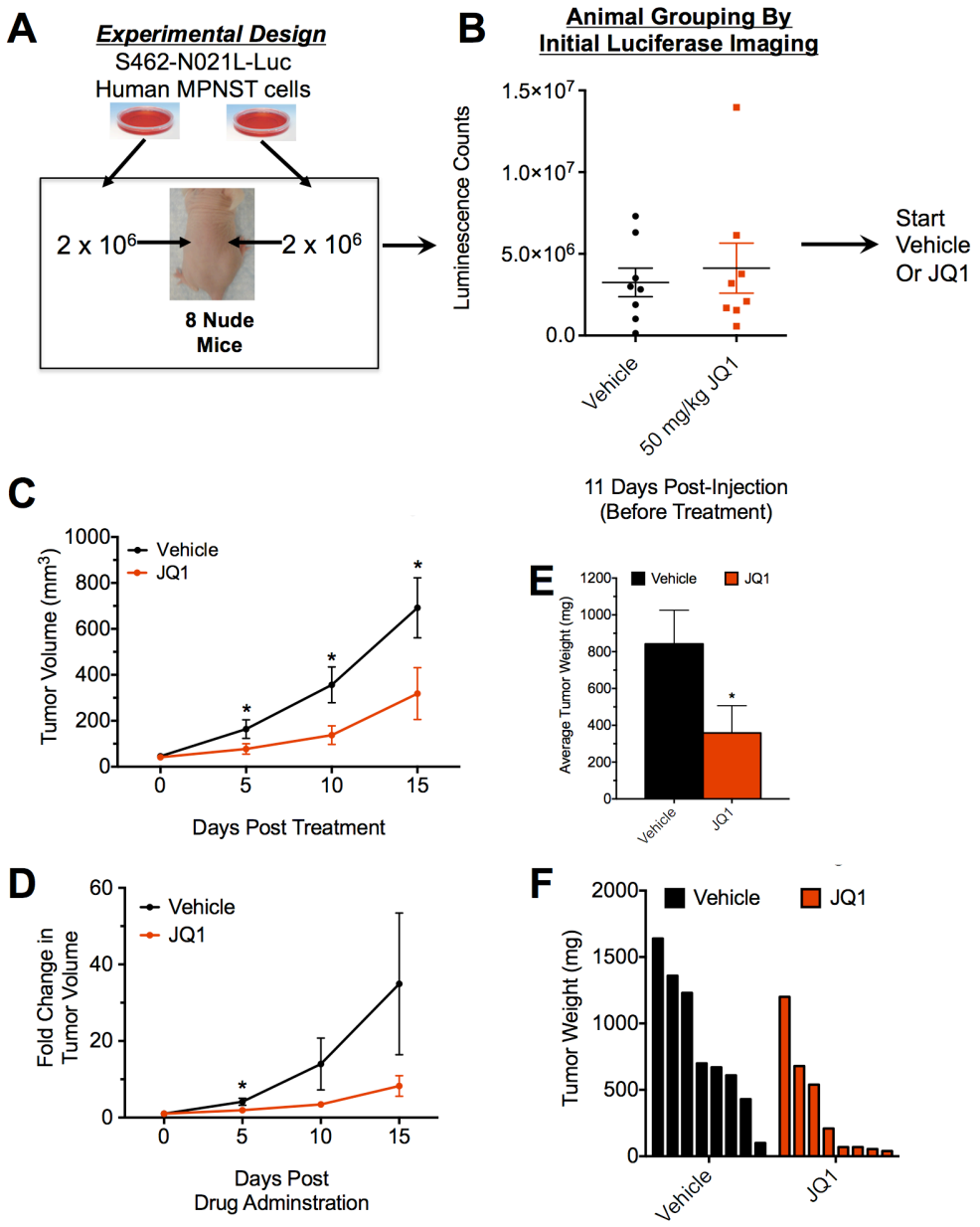

Figure 20. *In vivo* therapeutic efficacy of JQ1 against human MPNST xenografts.
(A) Experimental design for generating xenografts using S462-Luciferase tagged human MPNST cells in vivo in nude mice. (B) After 11 days injection, visible/palpable tumors were evident, and mice were scanned for tumor bioluminescence, followed by separation of mice into 2 groups with relatively similar tumor bioluminescence signals. Mice were started on JQ1 or vehicle the very next day.(C) Tumor volume analysis of S462 xenografts treated with vehicle (n=8 tumors) or JQ1 (n=8 tumors).(D) Fold change tumor volume analysis of S462 xenografts treated with vehicle or JQ1. Relative to day 0 of prior to drug treatment.(E) Average final tumor weight at the end of the drug trial. (F) Waterfall plot of individual tumor weights at the end of the drug trial. All statistics are represented as the mean +/- SEM (*p $\leq$ 0.05, **p $\leq$ 0.01, ***p $\leq$ 0.001, ***p $\leq$ 0.0001).

3.4 – Discussion

The elevated expression of *Brd4* in our sMPNST transcriptome data drew our attention in the previous chapter. In this chapter, through use of genetic and pharmacological approaches coupled with MPNST models and imaging technology, we have established an important role for BRD4 or BET bromodomains in MPNST pathogenesis. These results highlight the strength and speed in which novel, non-germline GEMMs can accelerate discovery of tractable therapeutic targets for rare malignancies that represent an unmet medical need (Heyer et al., 2010).

Naturally, the next step is to decipher the mechanism of action by which BRD4 inhibition or BET bromodomain inhibitors exert their potent effects on MPNSTs. Based on *in vitro* and *in vivo* studies presented in this chapter, it could be inferred that proliferation and survival are reduced. From the literature, studies indicate that shRNA mediated knockdown of either *Brd2*, *Brd3*, or *Brd4* individually in human glioblastoma cells leads phenotypically similar rates of growth and survival inhibition (Cheng et al., 2013). However, based on our studies in Figure 18, it is unclear whether the effects of BRD4 shRNA or JQ1 on MPNST cells are caused by the same set or distinct molecular signaling events. In other words, is *Brd4* shRNA redundant with BET bromodomain inhibitor JQ1? If they are redundant, then one would anticipate that *Brd4* shRNA would not have additive effects on JQ1 treated cells nor vice-versa should JQ1 have additive effects on *Brd4* shRNA cells (which we will address experimentally in Chapter 7). However, given the highly similar selectivity of BET bromodomain inhibitors (including JQ1) towards BRD4, BRD2 and BRD3 (Asangani et al., 2014; Dawson et al., 2011; Filippakopoulos and Knapp, 2014; Filippakopoulos et al., 2010;

Nicodeme et al., 2010), it is certain that effects of BRD2 or BRD3 inhibition with JQ1 cannot be teased apart from BRD4 inhibition without assaying the effects through RNAi-mediated knockdown of the individual BET protein members in MPNST cells.

From a functional perspective in regards to chromatin/genomic occupancy, ChIP-seq studies from various groups indicate that *Brd2*, *Brd3*, and *Brd4* have overlapping sites of genomic occupancy in addition to distinct sites (Anders et al., 2014; Asangani et al., 2014; Nicodeme et al., 2010). More recently, a biotinylated derivative of JQ1 (bio-JQ1) was used to perform Chem-seq (similar to ChIP-seq) to identify genome wide targets of JQ1 compared to BRD2, BRD3, and BRD4 in a multiple myeloma cell line (Anders et al., 2014). This study revealed that genomic occupancy sites of JQ1 were highly correlated to BRD4 sites, while BRD2 and BRD3 sites were less significant (Anders et al., 2014). However, it was also evident that BRD2, BRD3, and BRD4 had overlapping genomic occupancy sites at gene promoters including *Ccnd2* (encodes cell cycle regulator Cyclin D2) (Anders et al., 2014). In this type of scenario where multiple BET proteins occupy the same site of a gene promoter, it is unclear whether eviction of all BET proteins is required for complete disruption of transcription elongation from such promoters. Furthermore, it is unclear whether one or more BET proteins can compensate for the lack of another BET protein at a genomic occupancy site. Therefore, the observations made in Figure 18 could suggest either overlapping or distinct roles for BET proteins in MPNST tumorigenesis. Thus, plans for an investigation of the phenotypic and molecular effects of additional BET proteins and their pharmacological inhibitors (e.g. JQ1) will be detailed in Chapter 8 of this dissertation. Nevertheless, it clear from the data presented here that BRD4 plays role in MPNST tumor

development, but the underlying mechanism is unclear. In subsequent chapters, we further characterize the phenotypic consequences of BRD4 inhibition in MPNSTs, and delineate the mechanisms of action.

CHAPTER FOUR

BRD4 Maintains Cell Cycle Progression and Expression of Cyclin D1 in MPNST

4.1 – Introduction

BRD4 was first described by the Ozato and Zhou research groups to regulate G_1 to S phase progression in the cell cycle of normal non-transformed cells (NIH 3T3 and MEFs) and tumor cells (HeLa) (Mochizuki et al., 2008; Yang et al., 2008). Molecularly, by expression microarray analysis, they uncovered that BRD4 promoted the expression of numerous genes that regulate G_1 to S phase progression (*Ccnd1*, *Ccnd2*, *E2f2*, *E2f7*, *c-Myc*, *Jun*, *Orc2*, *Mcm2*, *Dhfr*, *Top2a*, *Pcna*) (Mochizuki et al., 2008). Mechanistically, they found that BRD4 achieved this at least in part by recruitment to the promoter of these genes (e.g. *Ccnd1*, *Ccnd2*, *Orc2*, *Mcm2*) upon cellular re-entry to G_1 phase of the cell cycle (Mochizuki et al., 2008; Yang et al., 2008).

More recently in the transformed or malignant state, BRD4 has been described to regulate or maintain transcription elongation of oncogenes in a cancer specific manner. For instance, in a variety of mouse and human leukemia samples, genetic inhibition of *Brd4* with shRNAs led to a substantial reduction of *c-Myc* transcription, and almost complete loss of expression with pharmacological inhibitors (e.g. JQ1 or I-BET 151) (Dawson et al., 2011; Delmore et al., 2011; King et al., 2013; Zuber et al., 2011). Re-expression of *c-Myc* rescued proliferation but not apoptosis of leukemia cells with either *Brd4* knockdown or JQ1 treatment (Delmore et al., 2011; King et al., 2013; Zuber et al., 2011). Interestingly, these

groups did not observe reduced of *c-Myc* transcription in a panel of more normal cells (including immortalized MEFs) nor in various cancer cell lines derived from non-hematopoietic lineages/tissues (Delmore et al., 2011; Zuber et al., 2011). All together, these studies reinforce the role of *Brd4* in promoting cell cycle progression (in some cases via regulation of *c-Myc*).

However, despite lack of *Myc* regulation in various non-hematopoietic malignancies, they undergo growth inhibition via genetic or pharmacological inhibition of BRD4 (Zuber et al., 2011). In fact, sensitivity to BRD4 inhibition in some tumors cells (e.g. prostate cancer, glioblastoma multiforme) has been reported to associate with reduced levels of *c-Myc*, but re-expression of *c-Myc* fails to restore proliferation in those tumor cells (Asangani et al., 2014; Cheng et al., 2013). This suggests cell type specific regulation of growth genes via BRD4. In support of this idea, studies from the lab of Richard Young indicate that certain tumor types establish wide-spanning enhancers called "super enhancers," which accumulate an exceptionally high amount of BRD4 molecules (Lovén et al., 2013). These super-enhancers are typically in the vicinity of genes important for regulating cellular identity, and cancer cell growth and survival (Lovén et al., 2013). These super enhancer regulated genes tend to be highly expressed, and perturbation via BRD4 inhibition has been found to be associated with a sharp decline in their expression while genes with typical enhancers are less affected (Lovén et al., 2013). These groundbreaking observations indicate a mechanism for cell type specificity for BRD4 action in normal biology and disease. Thus, in light of this emerging role for BRD4 in regulating aberrant transcription of particular genes in specific tumor types, it would important to identify the genes that are under the control of BRD4 in MPNSTs, and

how their misregulation through genetic or pharmacological inhibition of BRD4 may contribute suppression of tumorigenesis and survival that we have observed thus far. To this end, in the following section of this chapter, we employed a systematic approach to characterize the phenotypic consequences of BRD4 inhibition on MPNST cell growth and associated affects on transcription of cell cycle components to ultimately delineate the underlying mechanism.

4.2 – Experimental Procedures

Reagents

(+)JQ1 (Cayman Chemical). Doxycycline (Sigma-aldrich). Methanol free formaldehyde (Thermo Scientific).

qRT(quantitative, reverse transcription)-PCR

RNEasy mini kit (Qiagen) was used to isolate total RNA from cells, followed by cDNA synthesis with iScript Select cDNA synthesis kit (Bio-Rad), and then qRT-PCR using iTaq Universal SYBR Green Supermix (Bio-Rad) on the CFX Connect Real-Time PCR platform (Bio-Rad). Data was quantified by ΔCt method, and normalized relative to Gapdh. See Appendix E for list of oligonucleotide primers used.

Chromatin-Immunoprecipitation (ChIP) qPCR

ChIP experiments were conducted as described in detailed protocol from Abcam, Inc. Briefly, chromatin equivalent to 25 μg DNA was 10-fold diluted in IP dilution buffer, pre-cleared by 1 hour incubation with ChIP-Grade Protein A/G Plus Agarose beads (Thermo

Scientific), then incubated overnight with BRD4 or control IgG antibody, 2 hours with protein A/G agarose beads, followed by wash, elution, and DNA purification (phenol/chloroform extraction followed by ethanol precipitation). For qPCR analysis, each IP signal was normalized to input signal to plot data as percentage of input. *Antibodies Used*: BRD4 (Bethyl Labs), and control IgG (Cell Signaling Technology). See Appendix J for detailed protocol.

Western Blot

Protein isolation, and subsequent Western blot analysis was performed as described previously (Mo et al., 2013). Antibodies Used: Cyclin D1 (Millipore), Gapdh (Santa Cruz Biotechnology). See Appendix F for detailed protocol.

BrdU Cell Cycle Analysis and Annexin V Flow Cytometry

Cell cycle studies were conducted using BrdU Flow kit (BD Biosciences) as per manufacturer's instructions. All flow cytometry was performed using FACSCalibur Flow Cytometer (BD Biosciences) at the UTSW Flow Cytometry core facility. Data was analyzed using FlowJo software (Tree Star). See Appendix H for detailed protocol.

4.3 – Results

Brd4 Regulates MPNST Cell Cycle Progression and Cyclin D1 Expression

To gain insight into the mechanism of action for BRD4 in MPNST tumorigenesis, we first evaluated the effect of genetic and pharmacological inhibition of BRD4 on sMPNST cell number. On average, we found that induction of *Brd4* shRNAs led to 60-65% reduction in

cell number after 5 days in culture compared to cells without induction or shCONTROL cells (Figure 21A). We observed a similar effect on sMPNST cells treated 4 days with JQ1 (Figure 21B). These data suggested inhibition of MPNST proliferation through BRD4 inhibition. Indeed, we found that BRD4 inhibition restrains MPNST cell cycle progression. Analysis of proliferation via BrdU incorporation and DNA content by flow cytometry led us to find that BRD4 depletion leads to significant reduction of BrdU incorporation, a predominant increase in percentage of cells in G_1 phase and modest effect on the percentage of cells in G_2/M phase (Figure 21C). We observed similar results in both sMPNST cells and S462 human MPNST cells treated with JQ1 (Figures 21C and 21D). Collectively, these data suggest that genetic and pharmacological inhibition of BRD4 impedes MPNST cell cycle progression.

Previously we and others described a role for the CXCR4/β-catenin signaling pathway in stimulating MPNST cell cycle progression via control of *Cyclin D1* mRNA expression, which highlights the importance of *Cyclin D1* maintenance in MPNST cell cycle control (Mo et al., 2013). How *Cyclin D1* transcription is regulated in MPNSTs remains unknown, but previous reports indicate *Cyclin D1* as a potential target of BRD4 (Mochizuki et al., 2008; Yang et al., 2008). Therefore, we sought to determine if BRD4 directly regulates *CyclinD1* transcription in MPNSTs. Through ChIP-qPCR analysis we found that BRD4

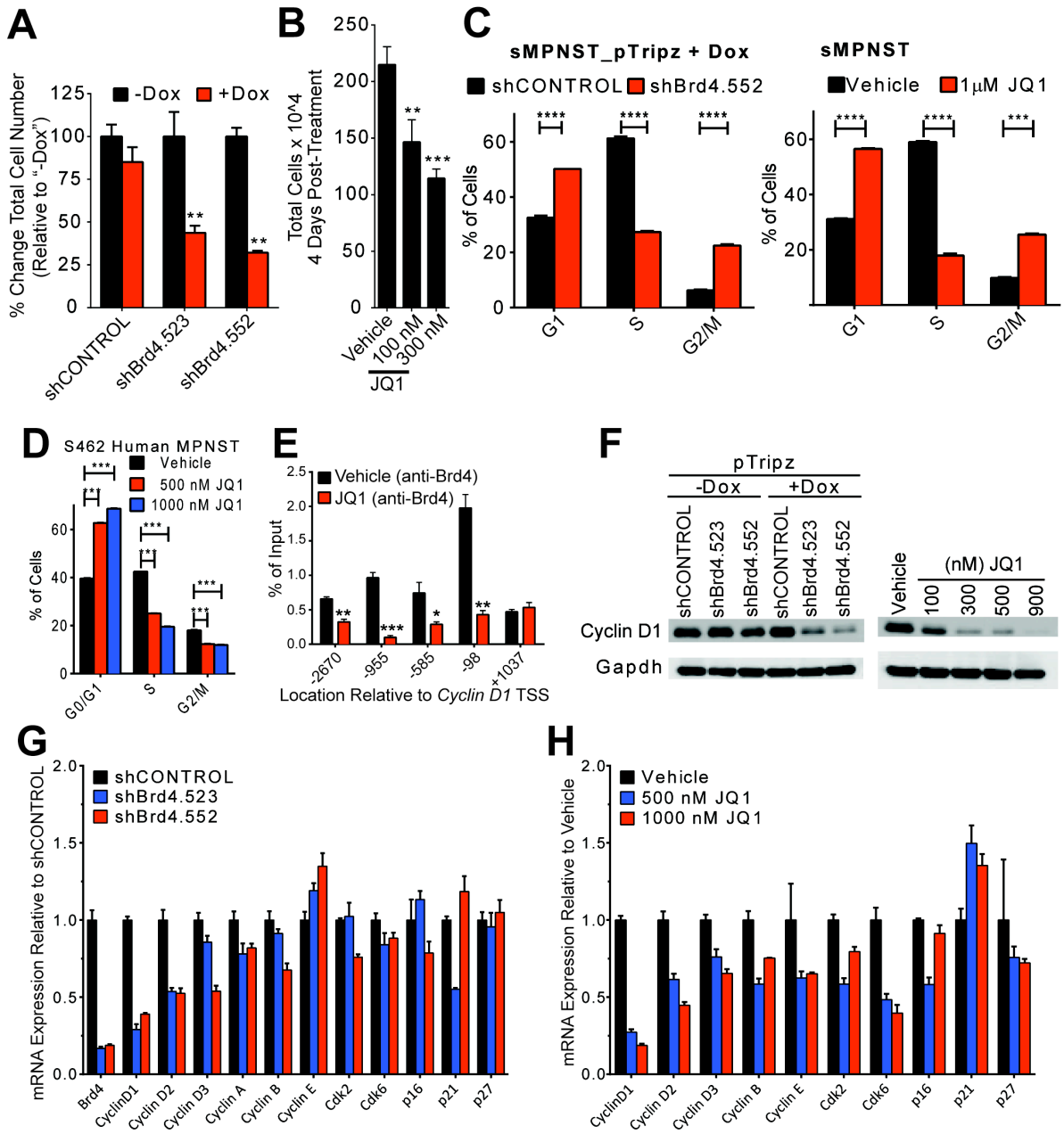

Figure 21. BRD4 Maintains CyclinD1 Expression and Cell Cycle Progression in MPNSTs.

(A) sMPNST cells harboring doxycycline (Dox) inducible shRNAs were counted after 5 days culture (+ or – Dox) and normalized to cell count of "-Dox" cells.

(B) sMPNST cells were counted 4 days after culturing in the presence of vehicle (DMSO) or JQ1.

(C) sMPNST cells were harvested 4 days after *Brd4* shRNA induction or 3 days after JQ1 treatment for processing, and subsequent analysis of BrdU uptake and DNA content by flow cytometry to determine the percentage of cells in the indicated cell cycle phases.
(D) Cell cycle analysis of 48 hour treated S462 cells through flow cytometry for BrdU(+) cells and DNA content (PI).
(E) sMPNST cells treated 24 hours with vehicle or 1000 nM JQ1 were harvested for chromatin immunoprecipitation (ChIP)-PCR analysis at different regions relative to *Cyclin D1* transcription start site (TSS).
(F) Western blot analysis of Cyclin D1 protein levels in sMPNST cells with *Brd4* knockdown (3 days) or JQ1 treatment (2 days).
(G and H) qPCR analysis of cell cycle regulatory genes in sMPNST cells with *Brd4* knockdown (3 days) or JQ1 treatment (2 days) respectively.
All statistics are represented as the mean +/- SEM (*$p \leq 0.05$, **$p \leq 0.01$, ***$p \leq 0.001$, ***$p \leq 0.0001$). [Adapted from (Patel et al., 2014)}

occupies the promoter of *Cyclin D1*, and that displacement of BRD4 from chromatin by JQ1 treatment led to reduced promoter occupancy in sMPNST cells (Figure 21E). Consequently, we found that shRNA mediated knockdown or pharmacological inhibition of BRD4 leads to substantial decrease in *Cyclin D1* mRNA and protein abundance in MPNST cells while other cell cycle regulators are less affected by *Brd4* shRNA or JQ1 in sMPNST cells (Figures 21F, 21G, and 21H). Together, these data point to a mechanism of BRD4 mediated epigenetic control of *Cyclin D1* transcription, and suggests BRD4 as a therapeutic target for inhibiting oncogenic Cyclin D1 in MPNSTs, further supporting the established roles of cellular growth pathways known to control MPNST cell cycle.

4.4 – Discussion

Control of MPNST cell cycle progression and tumorigenesis has been linked to a variety of pathways. The first pathway is the RAS/MEK/MAPK pathway given that *Nf1* loss can sustain RAS in the active GTP-bound state (Jessen et al., 2013; Malone et al., 2014).

The second being the mTOR growth control pathway that was demonstrated to be activated in *Nf1* deficient cells (Dasgupta et al., 2005; Johannessen et al., 2008). While previous groups have found that inhibition of these 2 growth pathways with pharmacological inhibitors for MEK or mTORC1 exhibit potent cytostatic effects on MPNSTs (Jessen et al., 2013; Johannessen et al., 2008), more recent studies indicate mild cytostatic effects on MPNSTs (Chau et al., 2013b). We and others recently identified a new pathway in MPNST growth signaling. In this pathway, MPNST cells secrete chemokine CXCL12, which then acts in an autocrine manner to activate CXCR4 receptor on MPNST cell surface, and thus downstream intracellular activation of β-catenin, and subsequent transcription of *Ccnd1* (Cyclin D1), which promotes cell cycle progression (Mo et al., 2013). However, the precise mechanism(s) by which CyclinD1 transcription is regulated in this underlying pathway was unknown.

Here in this chapter, through systematic characterization of cell cycle genes upon genetic and pharmacological inhibition of transcriptional regulator BRD4, we find that BRD4 inhibition leads to a substantial reduction in the expression of D-type Cyclins (most notably Cyclin D1), which correlates with reduced proliferation observed. Conversely, other cell cycle genes evaluated were less affected. Further, we find that BRD4 occupies regions upstream of the Cyclin D1 transcription start site (TSS), which is consistent with previous studies (Mochizuki et al., 2008; Yang et al., 2008), but importantly, pharmacological inhibition leads to reduction in occupancy. Contrary to the role of BRD4 in maintaining high levels of *c-Myc* transcription in leukemia, we did not observe this feature in NF1-associated MPNST cells (Figure 22). All together, our findings point to BRD4 as a CyclinD1 regulator

underlying the CXCR4/CXL12/β-catenin signal transduction network in MPNSTs. Thus pharmacological inhibition of BRD4 with JQ1 presents an opportunity for more direct inhibition of Cyclin D1 in scenarios whereby resistance to CXCR4 inhibitors may be subverted by alternative pathways that may re-engage CyclinD1 (like that observed for re-activation of MAPK signaling in BRAF-mutant tumors) (Wilson et al., 2012). More broadly, the ability of BET bromodomain inhibitors to selectively inhibit different tumor oncogenes may point to additional mechanisms by which BRD4 inhibition is potently therapeutic to MPNSTs; specifically, in the next chapter, we describe additional mechanisms of BET bromodomain inhibitors on MPNST cell survival.

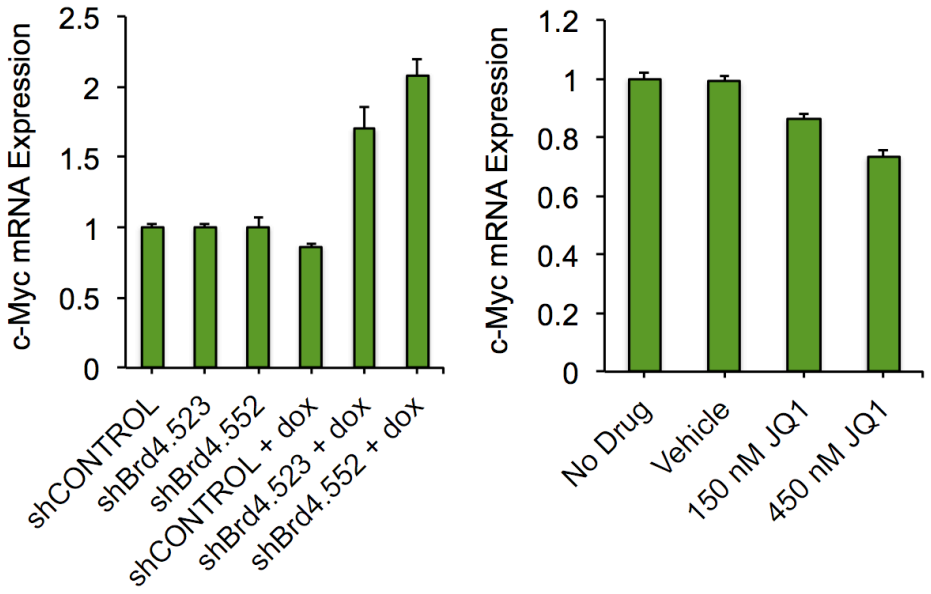

Figure 22. qRT-PCR analysis of c-Myc mRNA levels in *Brd4* knockdown and JQ1 treated MPNST cells

(Left panel) sMPNST cells harboring doxycycline (Dox) inducible shRNAs were cultured 3 days with or without Dox followed isolation of RNA for analysis of *c-Myc* mRNA levels relative to *Gapdh* by qRT-PCR.

(Right Panel) sMPNST cells were treated with the indicated treatments (x-axis) for 2 days followed by RNA isolation for analysis of *c-Myc* mRNA levels relative to *Gapdh* by qRT-PCR.

CHAPTER FIVE

Regulation of MPNST survival through BET bromodomain inhibition

5.1 – Introduction

While BET bromodomain inhibitors are well known for anti-proliferative or cytostatic effects on a wide range of genetically diverse tumor cells, they are known to have potent cytotoxic (death inducing) effects. Two research groups revealed that MLL-fusion driven leukemias' undergo substantial cellular apoptosis upon BET bromodomain inhibition with either JQ1 or I-BET151 (Dawson et al., 2011; Mo et al., 2013; Zuber et al., 2011). Zuber and colleagues have demonstrated that re-expression of *c-Myc* restores proliferation of JQ1 treated leukemia cells, but fails to block apoptosis (Zuber et al., 2011). Thus indicating that JQ1 triggers apoptosis independent of *c-Myc* perturbation. On the other hand, Dawson and colleagues identified substantially reduced expression of *Bcl2*, a pro-survival oncogene (Dawson et al., 2011). Interestingly, re-expression of *Bcl2* rescued leukemia cells from apoptosis via I-BET51 (Dawson et al., 2011). Alternatively, Cheng and colleagues observed apoptosis associated with suppression of pro-survival gene *Bcl-xL* in JQ1 treated glioblastoma cells, and the re-expression of *Bcl-xL* was sufficient to rescue from apoptosis induction by JQ1 (Cheng et al., 2013). These findings highlight a role for BET bromodomains in regulating cancer cell survival, but perhaps through distinct mechanisms depending on the cancer cell type.

However, less is known about the mechanisms of when or how tumor cells become sensitive to cell death via BET bromodomain inhibitors. Furthermore, the mechanism(s)

of resistance to cell death remains a relatively unexplored frontier of BET bromodomain inhibitor action. In the following section of this chapter we explore the role of BET bromodomains in maintaining MPNST survival.

5.2 – Experimental Procedures

Reagents

(+)JQ1 (Cayman Chemical). ABT-263 (Selleck Chemicals). Doxycycline (Sigma-aldrich).

qRT(quantitative, reverse transcription)-PCR

RNEasy mini kit (Qiagen) was used to isolate total RNA from cells, followed by cDNA synthesis with iScript Select cDNA synthesis kit (Bio-Rad), and then qRT-PCR using iTaq Universal SYBR Green Supermix (Bio-Rad) on the CFX Connect Real-Time PCR platform (Bio-Rad). Data was quantified by ΔCt method, and normalized relative to Gapdh. See Appendix E for list of oligonucleotide primers used.

Quality control analysis of total RNA samples for expression microarray analysis

For microarray analysis of shBrd4 and JQ1 effect on sMPNST cells, technical replicates (n = 3) were used for the experiment. RNA quality was assessed using Bioanalyzer chips (Agilent) by the UT Southwestern Microarray core facility.

Expression microarray and data analysis

Microarray experiments were conducted using Mouse Genome 430 2.0 microarrays (Affymetrix) by the UT Southwestern Microarray core facility. Data was analyzed with GeneSpring GX software (Agilent Technologies).

Western Blot

Protein isolation, and subsequent Western blot analysis was performed as described previously (Mo et al., 2013). Antibodies Used: BIM, Cleaved Caspase-3 (Cell Signaling Technology); Cleaved PARP (Millipore); BCL-2, GAPDH (Santa Cruz Biotechnology). See Appendix F for detailed protocol.

Annexin V Flow Cytometry for apoptotic cells

For analysis of cellular apoptosis/death, Annexin V-FITC Kit (Miltenyi Biotec) was used as per manufacturer's instructions. All flow cytometry was performed using FACSCalibur Flow Cytometer (BD Biosciences) at the UTSW Flow Cytometry core facility. Data was analyzed using FlowJo software (Tree Star). See Appendix I for detailed protocol.

Lentiviral and Retroviral Constructs

To knockdown *Bim*, pLKO.1-puro shRNA lentivectors containing either scrambled shRNA (shCONTROL) or mouse *Bim* shRNAs were purchased from Open Biosystems, and packaged into lentivirus. shBim.92 (TRCN0000009692), shBim.94 (TRCN0000009694). For lentivirus production, psPAX2 and pMD2.g (Addgene plasmids 12260 and 12259) packaging vectors were used. To re-express BCL-2, PCR primers (F: TCGAGGAATTCatggcgcaagccgggagaa, R: GCACGGTCGACtcacttgtggcccaggtatgc) were

designed for introducing cloning sites for (5'EcoRI and 3'SalI), and used to amplify *Bcl2* from total mouse sMPNST cell cDNA pool followed by restriction digestion with EcoRI and SalI (New England Biolabs) of gel purified *Bcl2* cDNA PCR product and pBabe-Neomycin retroviral vector, and subsequent DNA ligation and transformation into subcloning efficiency DH5α chemically competent bacterial cells (Life Technologies). Mini-prep plasmid DNA was isolated from bacterial clones followed by DNA sequencing to identify clones that contain a sequence verified *Bcl2* cDNA in pBabe-Neomycin plasmid. pBabe-*Bcl2*_cDNA-Neomycin plasmid was packaged into ecotropic (mouse specific) retrovirus using pCL-Eco (Addgene Plasmid 12371) packaging plasmid. See Appendix B for plasmids used. See Appendix C for virus packaging protocol, and Appendix D for virus infection protocol.

5.3 - Results

BET bromodomain inhibition triggers apoptosis of MPNSTs through induction of pro-apoptotic Bim

Cell cycle arrest can lead to subsequent cellular apoptosis (Pietenpol and Stewart, 2002). Further analysis of acute knockdown of *Brd4* in MPNST led us to observe increased floating cells in culture (Figure 23A), which was suggestive of apoptosis induction. Indeed, we found an increase in apoptotic cells and activation of apoptotic markers in both mouse and human MPNST cells with BRD4 inhibition (Figures 23B, 23C, and 23D). To elucidate how BRD4 inhibition triggers apoptosis of MPNSTs, we performed gene expression microarray analysis to first identify differentially expressed genes in MPNST cells with or without BRD4 inhibition (both shRNA and JQ1), which led us to identify upregulation of

pro-apoptotic BIM (*Bcl2l11*), which represents a novel finding (Figure 23E). We also found that BRD4 inhibition decreased expression of anti-apoptotic *Bcl2* in our microarray data (data not shown). Quantitative RT-PCR and Western blot analyses confirm that BRD4 inhibition (shRNA or JQ1) leads to induction of BIM and down-regulation of BCL-2, and relatively minor effect on the expression of additional apoptosis regulators evaluated (Figures 23F and 23G). BIM is a pro-apoptotic, BH3 domain containing protein that is thought to play a central role in apoptosis through activation of pro-apoptotic BAX and BAK, which leads to mitochondrial permeabilization that is followed by activation of caspases and apoptosis (Bean et al., 2013; Tait and Green, 2010; Wei et al., 2001). BCL-2 is an anti-apoptotic protein that is thought to prevent BAX/BAK activation (Cheng et al., 2001). One of the mechanisms is through inhibition/sequestration of pro-apoptotic BH3-only proteins, such as BIM and PUMA (Cheng et al., 2001; Letai et al., 2002; Youle and Strasser, 2008).

To determine if BRD4 inhibition mediated downregulation of *Bcl2* expression promotes MPNST apoptosis, we first re-expressed BCL-2 in MPNSTs by stable retroviral mediated transfer of mouse *Bcl2* cDNA, and observed that these cells were rescued from JQ1 induced apoptosis (Figure 24A and 24B). However, given that *Bcl2* suppression is likely to be one many events as a consequence of JQ1 treatment, we tested whether direct inhibition of BCL-2 is sufficient to phenocopy JQ1 induced apoptosis. Thus, we treated MPNST cells with ABT-263, a selective small molecule that inhibits BCL-2/BCL-X_L, which prevents sequestration of pro-apoptotic BIM or PUMA. We observed that BCL-2/BCL-X_L inhibition with ABT-263 is not sufficient to trigger robust apoptosis of MPNST cells (Figure 25B),

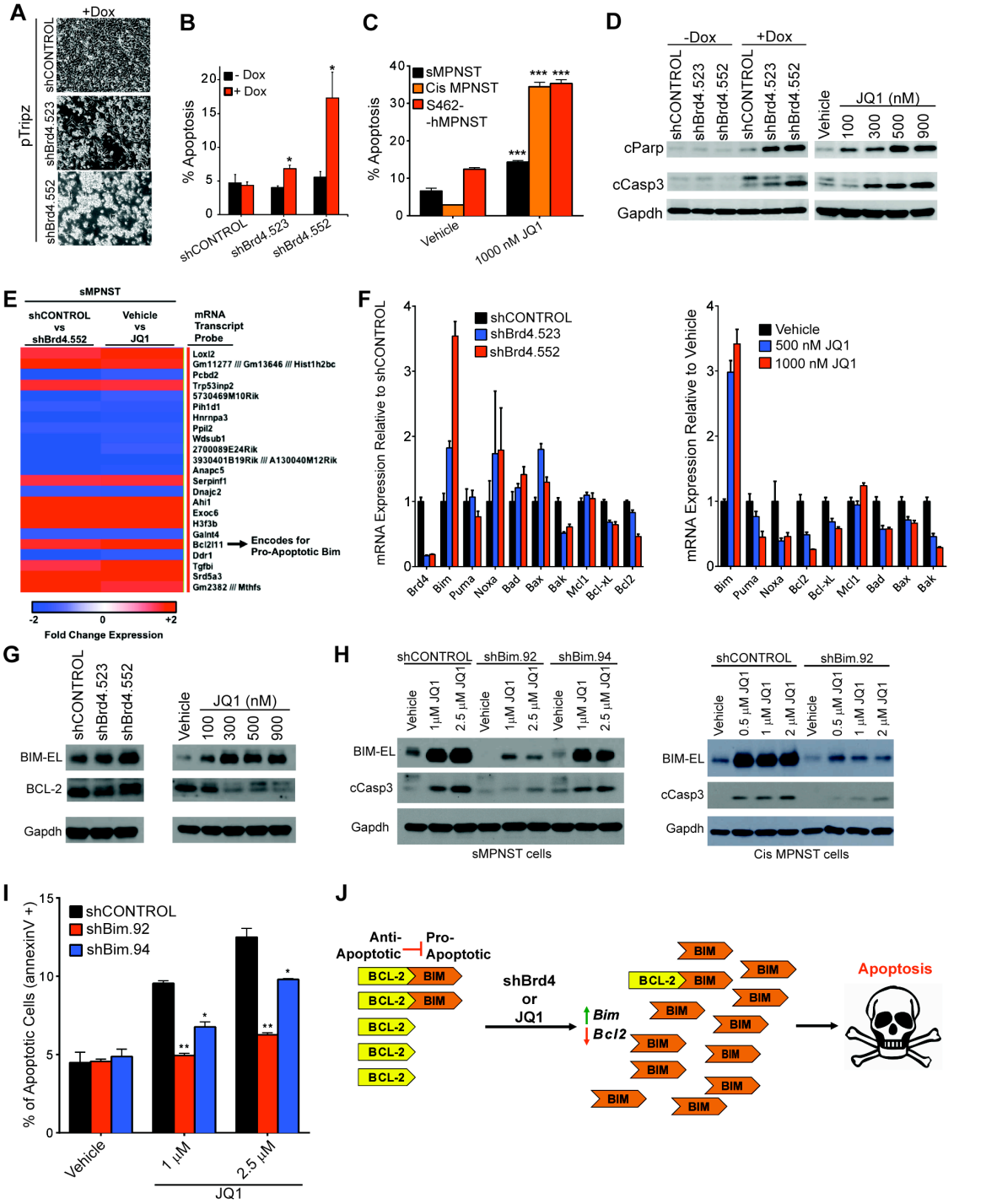

Figure 23. BET Bromodomain Inhibition Triggers MPNST Apoptosis Through *Bim* Induction.

(A) Microscopy images of sMPNST cells after 5 days of shRNA induction in vitro. (B) Percentage apoptosis in sMPNST cells with and without *Brd4* shRNA induction (5 Days) by flow cytometry analysis of Annexin V (+) cells.

(C) Apoptosis induction by 3 days of JQ1 treatment in mouse and human MPNSTs cells through flow cytometry analysis for Annexin V (+) cells.
(D) Western blot analyses of lysates from sMPNST cells with (3 days) *Brd4* knockdown or (2 days) JQ1 treatment for activation of apoptosis (cCasp3 = cleaved caspase 3, cParp = cleaved Parp).
(E) Expression microarray analysis comparing the effect of *Brd4* shRNA or JQ1 on sMPNST cells reveals induction of pro-apoptotic effector *Bim*.
(F) qPCR analysis of the effect of (3 days) *Brd4* shRNA or (2 days) JQ1 treatment on the expression of apoptosis regulators in sMPNST cells.
(G) Western blot validation of BIM induction and BCL-2 down-regulation through *Brd4* shRNA (3 days) or JQ1 (2 days) treatment in sMPNST cells.
(H) Western blot analysis of BIM knockdown leading to attenuation of cleaved caspase 3 in sMPNST and Cis MPNST cells treated with JQ1 (2 days).
(I) Flow cytometry analysis of Annexin V (+) cells reveals attenuated apoptosis through *Bim* shRNAs in sMPNST cells treated with JQ1 for 4 days.
(J) Model for how BET bromodomain inhibition modulates the ratio of pro-apoptotic and anti-apoptotic molecules in favor of apoptosis.
All statistics are represented as the mean +/- SEM (*p ≤ 0.05, **p ≤ 0.01, ***p ≤ 0.001, ***p ≤ 0.0001). [Adapted from (Patel et al., 2014)]

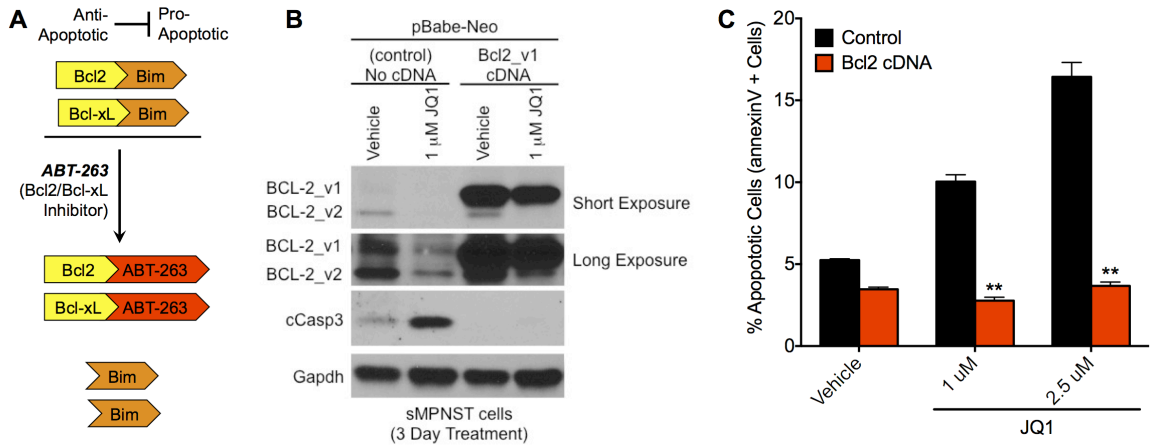

Figure 24. Re-expression of BCL-2 rescues MPNST cells from JQ1 induced apoptosis.
(A) Diagram illustrating mechanism by which ABT-263 inhibits BCL-2/BCL-XL bindings with BH3 death proteins such as BIM or PUMA.
(B) Western blot analysis of lysates from sMPNST cells (with or without stable transduction of retrovirus carrying mouse BCL-2 variant 1 encoding cDNA) treated with vehicle or JQ1. cCASP3 = cleaved caspase 3(Asp175).
(C) Flow cytometry analysis for annexinV positive cells after sMPNST cells with or without ectopic BCL-2 expression were treatmed with vehicle or JQ1 for 4 days.
All statistics are represented as the mean +/- SEM (*p ≤ 0.05, **p ≤ 0.01, ***p ≤ 0.001, ***p ≤ 0.0001)

which suggests that perhaps inhibition of BRD4 leading to induction of *Bim* initiates MPNST apoptosis. Indeed, we found that constitutive knockdown of *Bim* attenuates/rescues JQ1 induced apoptosis in multiple MPNST cell types as indicated by reduced caspase-3 cleavage and fewer apoptotic cells (Figures 23H and 23I). Collectively, these findings lead us to propose a model in which BRD4 inhibition or JQ1 treatment initiates apoptosis through induction of pro-apoptotic *Bim*, and suppression of anti-apoptotic *Bcl2* to trigger apoptosis of

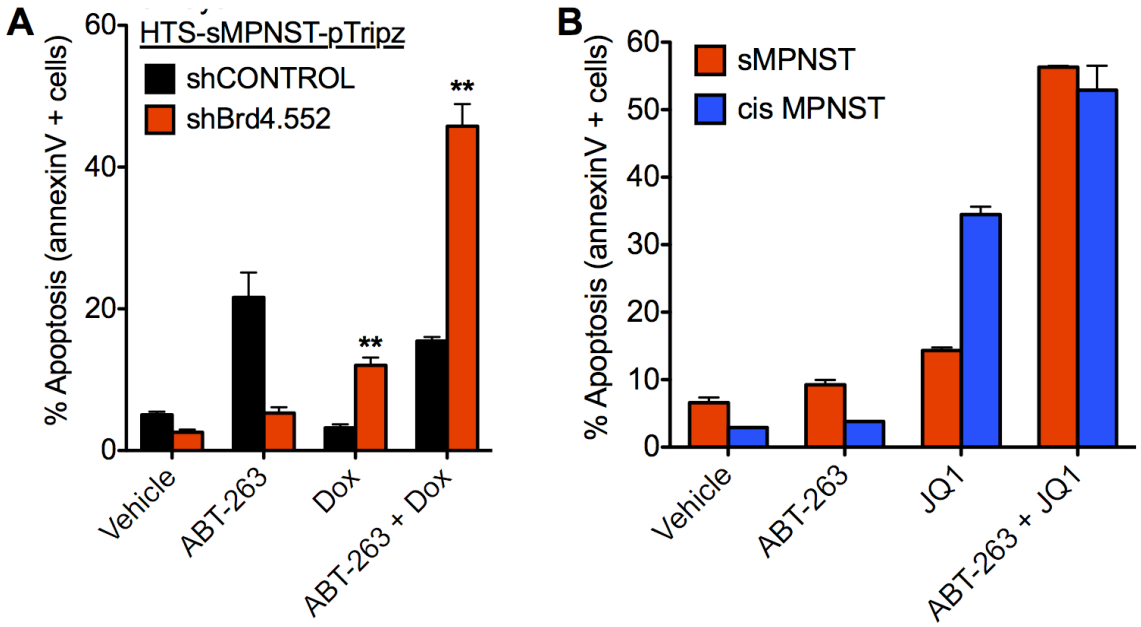

Figure 25. BRD4 inhibition combined with ABT-263 potently induces MPNST cell death.

(A) Dox (doxycycline) inducible *Brd4* shRNA more potently induces sMPNST apoptosis when combined with 1μM ABT-263 (BCL-2/BCL-XL inhibitor). Apoptosis assayed 5 days after indicated treatments by flow cytometry for annexinV positive (apoptotic) cells.

(B) 1μM JQ1 more potently induces MPNST apoptosis when combined with 1μM ABT-263. Apoptosis assayed 3 days after indicated treatments by flow cytometry for annexinV positive (apoptotic) cells.

All statistics are represented as the mean +/- SEM (*$p \leq 0.05$, **$p \leq 0.01$, ***$p \leq 0.001$, ***$p \leq 0.0001$). [Only Figure 25B Adapted from (Patel et al., 2014)]

NF1-associated MPNSTs (Figure 23J). Our observations suggest that BET bromodomain inhibition with JQ1 induces *Bim* and downregulates *Bcl2* expression, leading to an imbalance of pro- and anti-apoptotic effectors which favors induction of apoptosis (Figure 23J), and supports the model for an anti-apoptotic/pro-apoptotic BCL-2 rheostat (Bean et al., 2013; Corcoran et al., 2013). In support of this model, we found that further inhibition of BCL-2 alongside BCL-XL with ABT-263 leads to potent induction of MPNST apoptosis when combined with shBrd4 or JQ1 (Figure 25A and 25B).

5.4 – Discussion

Both BCL-2 and BCL-XL are found at high levels in diverse tumor types where in which they maintain or support tumor cell survival. In some instances, BCL-2 is over-expressed in human follicular B-cell lymphoma through t(14;18) chromosomal translocation that juxtaposes the *Bcl2* coding sequence with IgH enhancer, which drives high level of transcription (Cleary et al., 1986; Tsujimoto et al., 1984; Xiang et al., 2011). Mice engineered with this translocation have long lived B cells that eventually progress to lymphomas (McDonnell et al., 1989; McDonnell and Korsmeyer, 1991; Xiang et al., 2011). In support of the role of BCL-2 in maintaining lymphoma and lung cancer survival, genetic and pharmacological approaches to directly inhibit BCL-2 lead to a marked induction of apoptosis *in vitro* and regression *in vivo* (Oltersdorf et al., 2005). However, resistance prior to or after direct inhibition of BCL-2 or BCL-XL has been a limitation in the therapeutic efficacy of such agents (Bean et al., 2013; Corcoran et al., 2013; Oltersdorf et al., 2005). Studies suggest that induction of BH3 only proteins including BIM, PUMA, and NOXA as a requisite for triggering effective apoptosis in the context whereby their antagonists (BCL-2

and BCL-XL) are functionally inhibited (Bean et al., 2013; Corcoran et al., 2013). Thus, pharmacological interventions to induce BH3 only proteins (e.g. BIM) will be necessary to improve upon the therapeutic efficacy of BCL-2/BCL-XL inhibitors against cancer cells.

In this chapter, we identify BET bromodomain inhibition as novel strategy to potently induce pro-apoptotic BIM, and improve efficacy of BCL-2/BCL-XL inhibitors against MPNSTs. Prior to our studies, BET bromodomain inhibition had been described to trigger apoptosis, and associated or demonstrated to occur through suppression of either BCL-2 or BCL-XL in leukemia and glioblastoma. Our studies in this chapter re-affirm that BCL-2 is suppressed upon BET bromodomain inhibition, but now for the first time in the context of NF1-associated MPNSTs. We demonstrate that re-expression of BCL-2 blocks JQ1 induced apoptosis. However, direct inhibition of BCL2/BCL-XL with ABT-263 was insufficient to trigger apoptosis of MPNSTs, while JQ1 was sufficient. Through systematic analysis of a wide range of apoptosis regulators in cells treated with JQ1, we discovered that BET bromodomain inhibition led to a potent induction of pro-apoptotic BIM alongside suppression of BCL-2. Through genetic suppression of BIM induction in JQ1 treated MPNST cells, we observed a recue from apoptosis induction. All together, in light of these new findings, we propose a new model or mechanism of action by which BET bromodomain inhibition triggers cancer cell apoptosis via induction of pro-apoptotic BIM alongside suppression of its inhibitor (BCL-2), thus leading apoptosis of MPNSTs. In light of this new finding, in the next chapter, we endeavor to delineate the mechanism by which BET bromodomain inhibition triggers BIM in MPNSTs.

CHAPTER SIX

BET bromodomain inhibition regulates ER stress/UPR pathway in MPNSTs

6.1 – Introduction

Our findings reveal BIM as key death effector engaged by induction upon BET bromodomain inhibition for the first time. Specifically, we found this mechanism operant in NF1-associated MPNSTs with as few as 2 known genetic alterations (*Nf1* and *P53* loss). Since the time of our publication, it is now evident from more recent publications that BET bromodomain inhibitors such as JQ1 and now I-BET151 can induce BIM in additional human malignancies such as acute myeloid leukemia (AML) and melanoma (Fiskus et al., 2014; Gallagher et al., 2014). Furthermore, suppression of BIM in melanoma can rescue from BET bromodomain inhibitor induced apoptosis, which is consistent with our findings in MPNSTs (Gallagher et al., 2014). These new data support a broad role for BET inhibitors in regulating BIM in cancer cells, and thus warrants further investigation into mechanisms by which BET bromodomain proteins regulate BIM.

BIM is tightly regulated at the transcriptional and post-translation level through distinct, context dependent mechanisms as described in published literature. Withdrawal or deprivation of growth factors, cytokines, or glucose is reported to lead to induction or pro-apoptotic proteins including BIM and PUMA (Bean et al., 2013; Mason and Rathmell, 2011; Puthalakath et al., 2007). Conversely, oncogenes such as RAS can suppress BIM via downstream activation of MAPK family of kinases (ERK1/2 or JNK), which in turn

phosphorylates BIM protein for degradation PUMA (Bean et al., 2013; Mason and Rathmell, 2011; Puthalakath et al., 2007).

Similarly, AKT can suppress transcription of *Bim* via phosphorylation-mediated retention stress-responsive transcription factor FOXO3 in the cytoplasm (Figure 26B) (Bean et al., 2013; Luo et al., 2013; Sunters et al., 2003; You et al., 2006). On the other hand, ER (endoplasmic reticulum) stress via downstream activation of UPR (Unfolded Protein

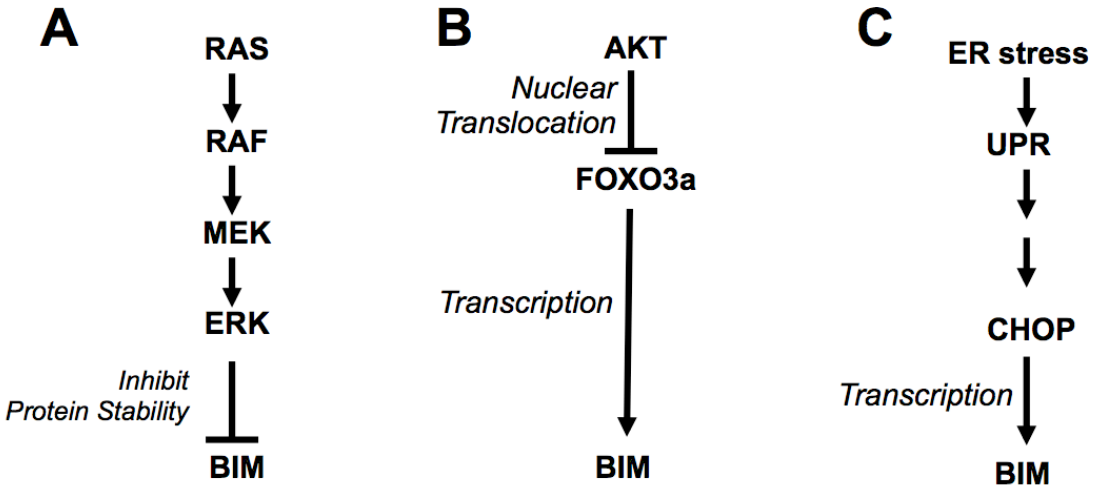

Figure 26. Context-dependent mechanisms underlying BIM regulation in mammalian cells.
(A) Phosphorylated-ERK, a downstream effector of RAS/MAPK signaling can phosphorylate BIM protein leading to its degradation.
(B) Transcription factor FOXO3a, when phosphorylated by effectors such as AKT, is translocated from nucleus to cytoplasm, thus prevent transcriptional induction of BIM.
(C) Various forms of ER stress stimuli lead to downstream activation of UPR, and subsequent induction of pro-apoptotic transcription factor CHOP, who then can induce BIM transcriptionally

transcription; furthermore, ER stress at same time is also reported to stabilize BIM protein levels by phosphatase mediated dephosphorylation (Altman et al., 2009; Puthalakath et al., 2007; Youle and Strasser, 2008). How BIM along with BCL-2 are perturbed by BET bromodomain inhibition remains unknown. Given the importance of this regulation in cell

death induction by BET bromodomain inhibitors, in the next section of this chapter, we explored the above mechanisms to define how BET bromodomain inhibition may trigger BIM in MPNSTs.

6.2 Experimental Procedures

Cells and reagents

Low passage/primary mouse sMPNST cells and cisMPNST cells. S462 human MPNST cells (a kind gift from the Dr. Karen Cichowski (Brigham and Women's Hospital, MA). All MPNST cells (mouse and human) are cultured in standard DMEM (10% fetal bovine serum, 1% penicillin-streptomycin, 1% L-glutamine, 1% sodium pyruvate). For time course experiments, cells were plated at least overnight, followed by a fresh media change (plus or minus treatment), and fresh media (plus or minus treatment) was replenished every12 hours to maintain ER homeostasis afterwards. Thapsigargin (Santa Cruz Biotechnology), (+)JQ1 (Cayman Chemical). See Appendix A for growth media formulations and reagents.

Expression microarray analysis

Same as microarray experiment from previous chapter. See methods section of Chapter 5.

qRT-PCR

RNEasy mini kit (Qiagen) was used to isolate total RNA from cells, followed by cDNA synthesis with iScript Select cDNA synthesis kit (Bio-Rad), and then qRT-PCR using iTaq Universal SYBR Green Supermix (Bio-Rad) on the CFX Connect Real-Time PCR platform

(Bio-Rad). Data was quantified by ΔCt method, and normalized relative to *Gapdh*. See Appendix E for list of oligonucleotide primers used.

Western blot

Protein isolation, and subsequent Western blot analysis was performed as described previously (Mo et al., 2013). Antibodies Used: Phospho-AKT (Ser473), ATF4, BIM, BiP, CHOP, Cleaved Caspase-3 (Asp175), Phospho-eIF2α (Ser51), Phospho-ERK1/2 (Thr202/Tyr204), Phospho-PERK (Thr980) (Cell Signaling Technology); GAPDH (Santa Cruz Biotechnology). See Appendix F for detailed protocol.

Electron microscopy

S462 human MPNST cells were seeded into MatTek plates (catalog: P35G-1.5-14-C), and allowed to sufficiently attach before treatment. For treatment, fresh (37^{o}C pre-warmed) media with added treatments were fed to cells while old media was aspirated completely. Cells were cultured for 12 hours in 37^{o}C incubator followed by a aspiration of media, and addition of a glutaraldehyde fixative solution, and stored in 4^{o}C overnight. Fixed samples were submitted to UT Southwestern Electron Microscopy Core Facility for processing and sectioning. Trained electron microscopy core facility staff under our supervision analyzed and recorded images from multiple sections. Representative images per treatment group are displayed.

6.3 – Results

To determine how BIM is regulated by BET bromodomain inhibition in MPNSTs, we first sought to determine if existing mechanisms as mentioned in the Chapter 6.1 are engaged. MAPK family of kinases including phosphorylated(P)-ERK1/2 are reported to phosphorylate BIM protein leading to its degradation by the proteasome. Conversely, deactivation of AKT, leads to translocation of transcription factor FOXO3 to the nucleus where it promotes *Bim* transcription. (Figure 27A). We found that *Brd4* shRNA induction or

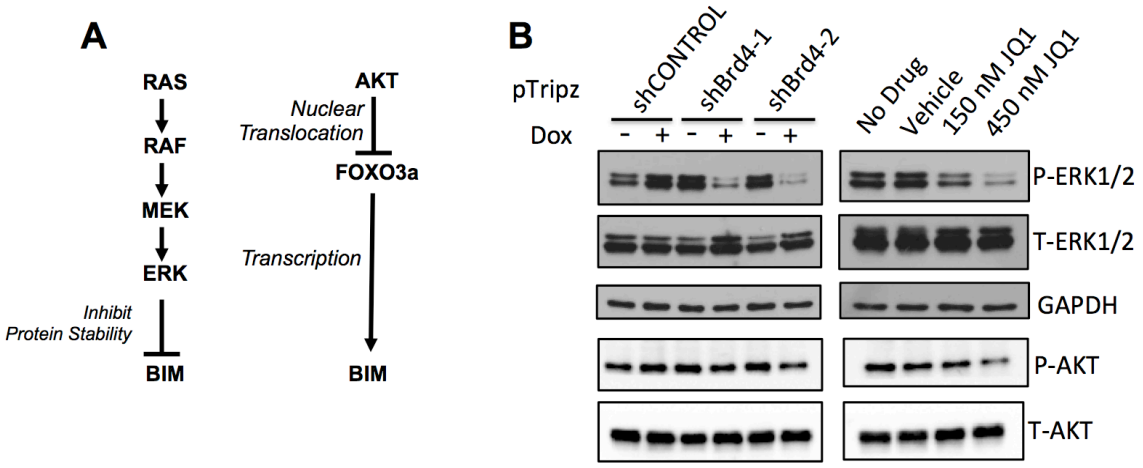

Figure 27. BRD4 inhibition attenuates ERK but not AKT signaling in MPNST.
(A) Diagram illustrating oncogenic pathways reported in literature to regulate BIM expression.
(B) Western blot analysis of phosphorylation status of key signaling pathways in sMPNST cells with doxycycline-inducible Brd4 shRNA induction (3 days) or JQ1 treatment (2 days)

JQ1 lead to reduced but not absent phosphorylation of ERK1/2, while AKT phosphorylation was unaffected in MPNST cells (Figure 27B). This observation suggests a hypothesis whereby BET bromodomain inhibition stabilizes BIM protein stability via suppression of ERK1/2 phosphorylation. To address this hypothesis, a post-doctoral researcher in the Lu Le laboratory (Chung-Ping Liao) stably introduced a dominant active cDNA for MEK (upstream activator of ERK1/2) MPNSTs, and found that restoration of ERK1/2 phosphorylation did

not rescue MPNST cells from BET bromodomain inhibition. This observation suggests perhaps additional or alternative modes of BIM regulation may be downstream of BET proteins.

Thus, we explored other mechanisms of BIM regulation underlying BET bromodomain inhibition. Seminal research from the lab of Andreas Strasser indicates that multiple types of ER stress stimuli induce BIM, which participates in triggering apoptosis of multiple cell types during this stress process (Puthalakath et al., 2007). To assess whether BET bromodomain inhibition triggers ER stress pathway in MPNSTs, we first reviewed the literature to determine what events occur downstream of ER stress, and which of those could be utilized as surrogate markers of this pathway being engaged. We summarized the events and markers of ER stress pathway from the literature as a representative diagram (Figure 28A). The endoplasmic reticulum (ER) is an essential cellular organelle that consists of 2 types; there is the smooth ER and the rough ER (Xu et al., 2005). The smooth ER participates in lipid synthesis and storage of metabolic enzymes (Xu et al., 2005). On the other hand, the rough ER is studded with ribosomes, participates in protein folding and synthesis of secretory proteins (Xu et al., 2005). A variety of stress events including accumulation of misfolded proteins, glucose or amino acid starvation, misregulation of intracellular calcium, defects in N-linked protein glycosylation, or viral infection can compromise the function/performance of the rough ER (Xu et al., 2005). As a result, unfolded proteins can accumulate leading to activation of the UPR (Unfolded Protein Response), which serves to restore ER homeostasis or function by activating its 3 main

pathway effectors (IRE1α, PERK, and ATF6α) to promote attenuation of protein synthesis and selective induction of protein folding chaperones (e.g. BiP, ERDJ4) to handle misfolded proteins, and ultimately lead to restored ER homeostasis and deactivation of the UPR (Clarke et al., 2014; van Galen et al., 2014; Xu et al., 2005). However, prolonged or overwhelming ER stress can lead to induction of pathways and genes (e.g. *Txnip*, *Bim*, *Chop*, *Dr5*, *Chac1*) that promoting cellular suicide or apoptosis (Lerner et al., 2012; Lu et al., 2014; Mungrue et al., 2009; Puthalakath et al., 2007).

To evaluate the activity of the ER stress/UPR pathway in MPNST cells with BET bromodomain inhibition, we assayed for several different pathway events. Downstream of the UPR pathway underlies transcriptional induction of stress-regulated genes that have pro-survival benefits (e.g. BiP, Erdj4) while others have pro-death effects (e.g. *Chop*, *Bim*, *Chac1*, *Txnip*) (Figure 28A). Through comparative transcriptome analysis of sMPNST cells with *Brd4* shRNA or JQ1 treatment, we found that several of the downstream UPR targets were transcriptionally induced by BET bromodomain inhibition (Figure 28B), and further validated by quantitative RT-PCR of mRNA levels (Figure 28C). Given that BET bromodomain proteins can serve as coactivators or repressors of gene transcription, it is plausible that these UPR markers are induced by de-repression of transcription if BET proteins physically occupy and regulate these genes at the epigenomic level. However, we also found that BET bromodomain inhibition with JQ1 could also induce upstream UPR markers (ATF4 and CHOP) at the protein level in MPNST cells (Figure 28D). Furthermore,

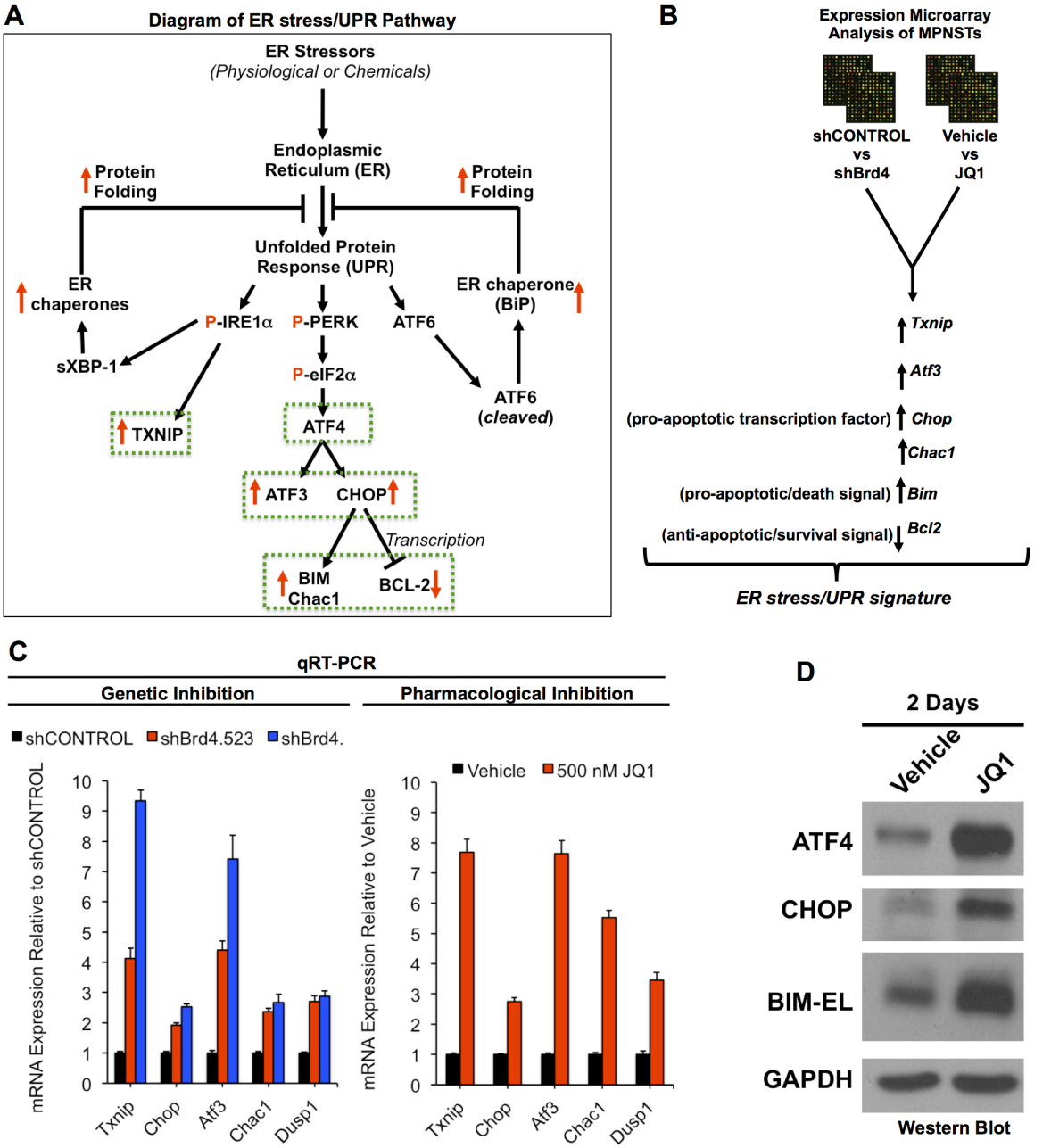

Figure 28. Genetic and pharmacological inhibition of BRD4 associated with activation of UPR targets in MPNST cells.

(A) Representative diagram of UPR (Unfolded Protein Response) pathway based on survey of the literature (Clarke et al., 2014; Lerner et al., 2012; Lu et al., 2014; Mungrue et al., 2009; Puthalakath et al., 2007; van Galen et al., 2014; Xu et al., 2005).

(B) Transcriptome analysis of BRD4 inhibition identifies activation of ER stress/UPR gene set signature in sMPNST cells.

(C) Validation of UPR target induction at the transcriptional level via qRT-PCR of sMPNST cells with shBrd4 (3 days) or 500 nM JQ1 treatment (2 days). Normalized relative to *Gapdh* mRNA levels.
(D) Validation of UPR pathway component induction in 1μM JQ1 treated sMPNST cells by Western blot. Normalized relative to *Gapdh* mRNA levels.

time course analysis of JQ1 treated MPNST cells revealed activation of upstream UPR pathway members in as little as 3-6 hours upon treatment (Figures 29A and 29B). Specifically, we consistently observed phosphorylation of PERK and eIF2α prior to induction of ATF4, CHOP, and BIM (Figure 29B). Furthermore, protein chaperones like BiP, which are induced upon ER stress, were also induced by JQ1 treatment in MPNSTs (Figure 29B). ER stress inducer thapsigargin (TG) also induced BIM expression in our MPNST cells, which is consistent with observations in other cell types (Puthalakath et al., 2007). All together, these cardinal features of ER stress/UPR pathway were found to be activated by BET bromodomain inhibition, which is consistent with what we observed with classical chemical inducers of ER stress such as thapsigargin (TG) in MPNST cells (Figure 29B).

On the other hand, other mechanisms in addition to ER stress have been reported to co-opt or trigger the UPR in mammalian cells. A more recent example is the discovery that VEGF maintains endothelial cell survival by activating the PERK and ATF6 arms of the UPR in an ER stress-independent manner (Karali et al., 2014). Thus far, the data presented here indicates that JQ1 may trigger the UPR pathway in MPNST cells, but evidence of ER stress in JQ1 treated MPNST cells or other cell types is unknown. Classically, ER stress is physically evaluated by electron microscopy for dilation of the ER lumen, and other features including lipid droplets (Basseri and Austin, 2012; Beck et al., 2013; Fei et al., 2009;

Oslowski and Urano, 2011). By electron microscopy analysis of MPNST cells treated with JQ1 and compared to either vehicle or thapsigargin (positive control ER stress inducer), we observed that vehicle treated cells typically featured more intact, a well-structured rough ER and less dilated ER lumen (Figure 30). Conversely, JQ1 treated cells featured areas where the ER was dilated, presence of lipid droplets, and lack of well-structured rough ER, which were all observed similarly in thapsigargin treated MPNST cells (Figure 30). All together, these data suggest that BET bromodomain inhibition is associated ER stress in MPNST cells.

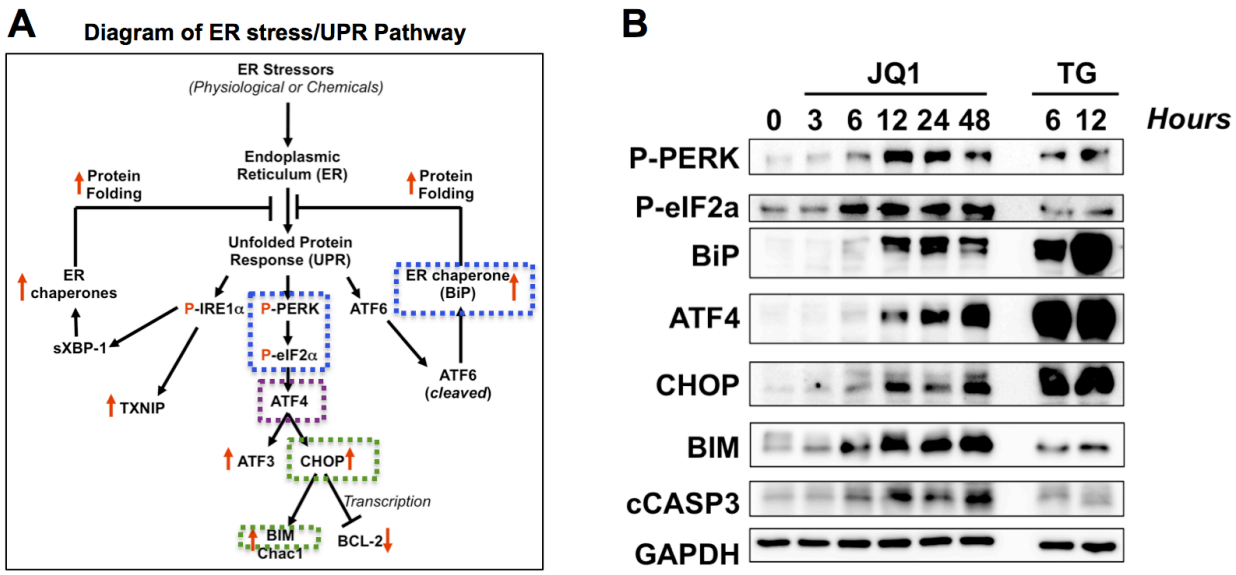

Figure 29. BET bromodomain inhibition triggers UPR pathway components in a time dependent manner in MPNST cells.

(A) Representative diagram of UPR (Unfolded Protein Response) pathway based on survey of the literature (Clarke et al., 2014; Lerner et al., 2012; Lu et al., 2014; Mungrue et al., 2009; Puthalakath et al., 2007; van Galen et al., 2014; Xu et al., 2005).

(B) Time course analysis of UPR pathway member induction via JQ1 compared to positive control ER stress inducer (TG) in cis MPNST cells in vitro. Cellular lysates from time course analyzed by Western blot. JQ1 = 1000 nM JQ1, TG = 1000 nM Thapsigargin (ER stress inducer)

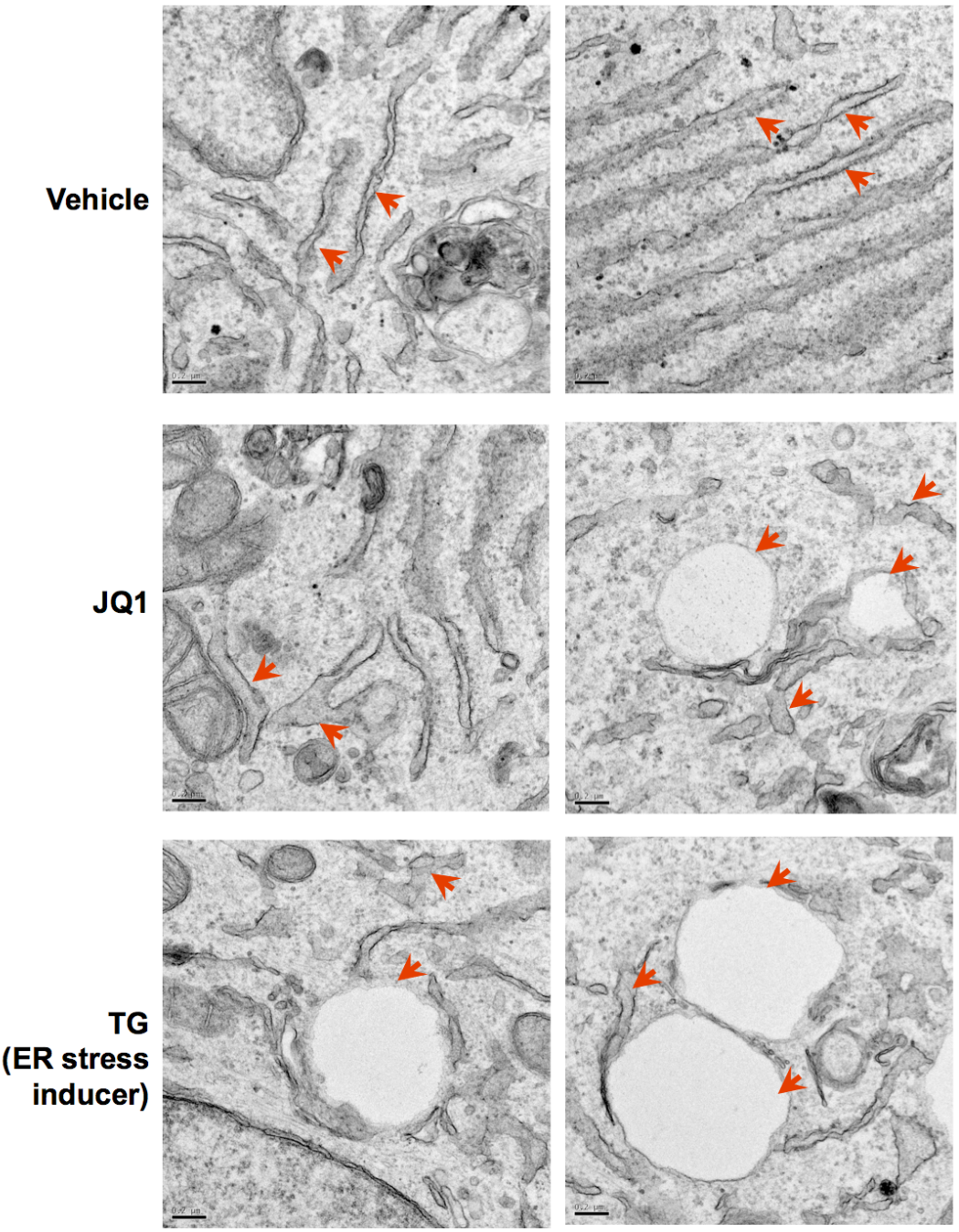

Figure 30. Electron microscopy reveals features of ER stress in JQ1 treated NF1-associated human MPNST cells *in vitro*.
Electron microscopy analysis of sections from S462 human MPNST cells in vitro with indicated treatments for 12 hours.

6.4 – Discussion

BET bromodomain inhibitors display broad efficacy against a variety of human cancer types, but their mechanism of action remains incompletely understood. Here, we show for the first time that BET bromodomain inhibition is associated with ER stress and induction of UPR pathway signaling components, and downstream stress-regulated genes (e.g. *Bim*, *Txnip*, *Chac1*). While these findings were observed in mouse and human MPNST cells with at least *Nf1* and *P53* tumor suppressor loss, they may also extend to other cancer types. Recently, after our publication, additional research groups published that BET bromodomain inhibitors such as JQ1 and I-BET151 can induce BIM in human malignancies such as acute myeloid leukemia (AML) and melanoma (Fiskus et al., 2014; Gallagher et al., 2014). Furthermore, additional UPR regulated genes such as *Txnip* were consistently found upregulated in microarray data from published studies in the context of neuroblastoma, lymphoma, and multiple myeloma (Bhadury et al., 2014; Chaidos et al., 2014; Mertz et al., 2011; Puissant et al., 2013). However, in many of these published studies, a central focus is on the regulation of *Myc* or *Mycn* by BET bromodomain proteins while genes such as *Txnip* are not addressed in text, but rather on a long list of genes or exists in public data sets but not explored. Collectively, our data coupled with these more recent public data sets highlights an unappreciated yet novel mechanism underlying BET bromodomain inhibition.

While our studies suggest that BET bromodomain inhibition leads to ER stress and UPR, the mechanism by which BET proteins regulate these pathways is not understood. However, we know that BET proteins can largely coactivate but also repress transcription elongation. Thus, the ER stress/UPR events observed in MPNST cells may be a consequence

of one or more genes being de-activated or de-repressed upon BET bromodomain inhibition. In support of this hypothesis, a recent study analyzed existing ChIP-seq data sets for occupancy of BRD4, CDK9, MED1, and RNAPII in multiple myeloma cells treated with vehicle or JQ1; they reported that BRD4 occupies a distal upstream enhancer of stress-regulated gene *Txnip*, while MED1 and CDK9 (activators for RNAPII dependent transcription elongation) were less abundant under vehicle conditions; however, upon JQ1 treatment, BRD4 occupancy was reduced while MED1 and CDK9 occupancy were increased at the enhancers and gene body of *Txnip*, which was associated with increased mRNA transcripts for *Txnip* in JQ1 treated cells (Bhadury et al., 2014). Thus, this finding suggests that transcription of *Txnip* is repressed by BET proteins (e.g. BRD4), and leads to a hypothesis whereby BET proteins may repress transcription of stress-regulated genes (e.g. *Txnip*, *Bim*, *Chop*, *Chac1*). This hypothesis can be addressed in future ChIP-seq analysis of BET protein occupancy in MPNST cells or analysis of pre-existing data sets from other cancer cell types. Taken together, out results indicate a novel mechanism or consequence of BET bromodomain inhibition in MPNST cells. However, less is known about how MPNST or other tumor cells become sensitive or may resist BET bromodomain inhibition; thus, in the next chapter, we explored those two important issues of sensitivity and resistance.

CHAPTER SEVEN

Mechanisms underlying sensitivity and resistance to BET bromodomain inhibition

7.1 – Introduction

BET bromodomain inhibitors show great potential as selective, anti-cancer therapeutics, but the mechanisms underlying sensitivity and resistance to apoptosis in the presence of these inhibitors is less clear. For example, do specific cancer alterations including activation of oncogenes or deletion of tumor suppressors dictate response? Recently, inactivation of tumor suppressor *Lkb1* was shown to be associated with resistance to JQ1 in *Kras*-mutant non-small cell lung cancer (Shimamura et al., 2013). While MPNSTs are not known to harbor mutations in *Lbk1*, other tumor suppressors are inactivated in these tumors (e.g. *Nf1*, *P53*, *RB1*, *Suz12*). The impact of these frequent mutations on resistance and sensitivity to JQ1 in MPNSTs remains unknown to date.

Moreover, the recent concept of super-enhancers in development and diseases such as cancer illustrates a novel mechanism by which nature establishes a dependency or sensitivity to BRD4 inhibition either genetically or pharmacologically (Lovén et al., 2013; Whyte et al., 2013). The first example arose from the groundbreaking research in Richard Young's lab. They demonstrated that diverse human cancer cells contain super-enhancers that are abundantly loaded with BRD4 compared to typical enhancers (Lovén et al., 2013). These super-enhancer regulated genes typically encoded oncogenes that are important for maintaining the identity and tumorigenic potential of these cancer cells (Lovén et al., 2013).

Therefore, this suggests super-enhancer formation at oncogenes as a mechanism for sensitivity to BET protein inhibitors. However, less is known about how these super-enhancers are established in cancer cells except for situations where oncogenes are chromosomally re-arranged to super-enhancers (e.g.*Myc* translocation to IgH super enhancer in multiple myeloma, re-arrangement of *Gata2* enhancer to *Evi1* oncogene in acute myeloid leukemia) (Gröschel et al., 2014; Lovén et al., 2013; Yamazaki et al., 2014). Additional mechanisms governing the establishment of super-enhancers remains on open area for investigation. Given that BET proteins target acetyl-lysine residues of histones, the histone acetylation patterns of cancer versus normal cells may represent one such plausible mechanism.

On the other hand, mutations in drug targets are a classical mechanism of resistance to their cognate pharmacological inhibitors. A prime example of this scenario is mutations found in kinase domain of BCR-ABL fusion oncogene that mediate resistance to Imatinib in chronic myelogenous leukemia (Burgess et al., 2005; Shah et al., 2002). A more recent example is mutations of the G protein-coupled receptor Smoothened, which confer resistance to Vismodegib in medulloblastoma (Yauch et al., 2009). However, mutations in BET proteins have not been investigated thus far. A clear future direction may be to identify mutations that confer resistance to BET bromodomain inhibitors either through pharmacological selection of drug resistant clones or a systematic analysis of engineered point mutations on inhibitor efficacy.

Lastly, the lack of an effective readout of BET bromodomain inhibitor efficacy against its molecular targets may suggest an area for investigation. For example, the efficacy

of MEK inhibitors in living cells and tissues can be faithfully quantified by analysis of its downstream targets (e.g. ERK1/2 phosphorylation). Whereas for BET bromodomain inhibitor, its targets are several genomic positions genome-wide. The only feasible means to assess BET inhibitor efficacy would be either analysis of global genomic occupancy of BET proteins or target gene expression in presence and absence of the inhibitor. Target gene expression is informative if all targets are identified and analyzed. ChIP-seq for global genomic occupancy of BET proteins would likely serve as the best assay for evaluating inhibitor efficacy. Indeed, ChIP-seq analyses to evaluate the ability of JQ1 to chase off BRD4 from its chromatin targets in human multiple myeloma cell line (MM1.S) revealed that JQ1 efficiently displaced BRD4 from super-enhancers, and quite less effectively from typical enhancers even at concentrations as high as 5000 nM JQ1 (Lovén et al., 2013). This observation was concluded to be a reason for why BET inhibitors selectively inhibit cancer cells while sparing normal cells (Lovén et al., 2013). However, from a perspective of inhibitor resistance, one might view the fact that high a concentration of JQ1 was unable to displace BRD4 completely from typical enhancers, as a potential mechanism of inhibitor resistance. This striking observation raises an important question: Are BET bromodomain inhibitors effective against the total cellular pool of BET proteins or a subset, and does that dictate the apoptotic response to these drugs? In the following section of this chapter, we present evidence suggesting sensitivity and resistance to BET bromodomain inhibitors, which collectively support the idea that perhaps BET inhibitors may not be completely effective against it biological target *in vivo*.

7.2 – Experimental Procedures

Cells and Reagents

Primary sMPNST and Cis MPNST cells were established from SKP-MPNST and *cis*NP model mice as described (Mo et al., 2013; Vogel et al., 1999). S462 human MPNST cell line is a gift from Dr. Karen Cichowski (Brigham and Women's Hospital, MA). HEK 293T cells (a gift from Dr. Wei Mo). Human dermal fibroblasts (Life Technologies). All cells (mouse and human) are cultured in DMEM (10% FBS, 1% penicillin-streptomycin, 1% L-glutamine, 1% sodium pyruvate). SKPs were prepared and cultured as described (Biernaskie et al., 2007). (+)JQ1 (Cayman Chemical. Doxycycline (Sigma-Aldrich). See Appendix A for media formulations and reagents.

BrdU Cell Cycle Analysis and Annexin V Flow Cytometry

Cell cycle studies were conducted using BrdU Flow kit (BD Biosciences) as per manufacturer's instructions. For analysis of cellular apoptosis/death, Annexin V-FITC Kit (Miltenyi Biotec) was used as per manufacturer's instructions. All flow cytometry was performed using FACSCalibur Flow Cytometer (BD Biosciences) at the UTSW Flow Cytometry core facility. Data was analyzed using FlowJo software (Tree Star). See Appendices H and I for detailed protocols.

In Vitro Growth Assays

ATP CellTiter Glo assay (Promega – Catalog#G7572) was performed as per manufacturer's instructions. The FLUOstar OPTIMA 96-well plate reader (BMG Labtech) was used for luminescence measurements.

Retroviral and Lentiviral Constructs

Mouse *Brd4* shRNAs were generated by synthesizing 22mer sequences corresponding to *Brd4* shRNAs described previously (Zuber et al., 2011) for PCR cloning into pTripz lentiviral vector. LV(lentivirus)-Cre-puro and LV-control-puro plasmids (gift from Dr. Wei Mo). For lentivirus production, psPAX2 and pMD2.g (Addgene plasmids 12260 and 12259) packaging vectors were used. See Appendix B for plasmids used. See Appendix C for virus packaging protocol, and Appendix D for virus infection protocol.

Western blot

Protein isolation, and subsequent Western blot analysis was performed as described previously (Mo et al., 2013). Antibodies Used: BRD4 (Bethyl labs); FLAG (Cell Signaling Technology); GAPDH (Santa Cruz Biotechnology). See Appendix F for detailed protocol.

7.3 - Results

To delineate how BET bromodomain inhibition with JQ1 leads to selective induction of apoptosis and marked growth inhibition in MPNSTs, we screened a panel of SKPs with defined genetic changes for sensitivity to JQ1 induced apoptosis. We found that JQ1 induced apoptosis of sMPNST, cisMPNST, $Nf1^{-/-}P53^{-/-}$ SKPs, and HEK293T cells while wildtype

SKPs, *Nf1*$^{-/-}$ SKPs, and human dermal fibroblasts survived (Figure 31A). Because *Nf1* loss

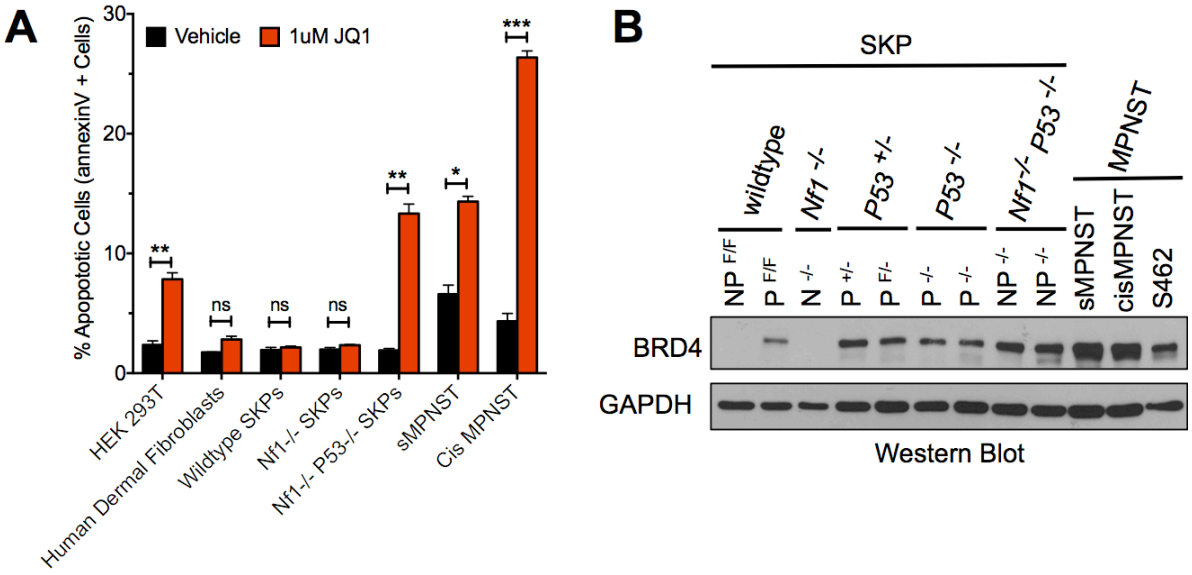

Figure 31. Loss of tumor suppressor *P53* is associated with increased BRD4 expression and sensitivity to BET bromodomain inhibition with JQ1.
(A) Flow cytometry analysis of indicated cells for annexinV+ (apoptotic) cells after 3 days of exposure to either 1μM JQ1 or vehicle (DMSO). All statistics are represented as the mean +/- SEM (*p ≤ 0.05, **p ≤ 0.01, ***p ≤ 0.001, ***p ≤ 0.0001). [Only Figure 31A adapted from (Patel et al., 2014)]
(B) Western blot analysis of indicated cells reveals increased BRD4 expression after loss of P53. (NP = *Nf1* & *P53*; P = *P53*; sMPNST = MPNST cells derived from NP-SKPs; cisMPNST = cells derived from spontaneous MPNST generated in *Nf1*$^{+/-}$ *P53*$^{+/-}$ mice; S462 = human MPNST cells with loss of heterozygosity for *Nf1*, *P53*, and *P16* alleles)

did not sensitize SKPs to JQ1 induced, we hypothesized that perhaps loss of *P53* alone or in combination with *Nf1* loss may sensitize cells to JQ1 induced apoptosis. In support of this idea, we observed upon Western blot analyses of various SKPs of different genetic configurations to MPNSTs, that BRD4 protein levels increased substantially upon loss of one allele for *P53*, further increased upon loss of both *Nf1* and *P53* in SKP, and more after malignant transformation to sMPNST (Figure 31B). Interestingly, HEK 293T cells carry the SV40 large T-antigen, which is known to inactivate the *P53*/*RB* tumor suppressor pathways,

and these cells were observed to undergo apoptosis in response to JQ1 (Figure 31A). All together, these observations suggest that perhaps loss of *P53* sensitizes SKPs to JQ1 induced apoptosis.

To address the role of *P53* in dictating response of SKPs to JQ1, we analyzed the effect of *P53* loss on primary SKPs to JQ1 treatment. Primary SKPs were isolated and cultured from newborn mice ($P53^{+/F}$ or $P53^{F/F}$) prior to post-natal day 2. These SKPs were infected with lentiviruses that transduce no cDNA (control) or Cre recombinase cDNA, and stably selected with puromycin to generate cells with or without recombination mediated loss of *P53* (Figure 32A). Through subsequent analysis, we found that one copy loss of *P53* was

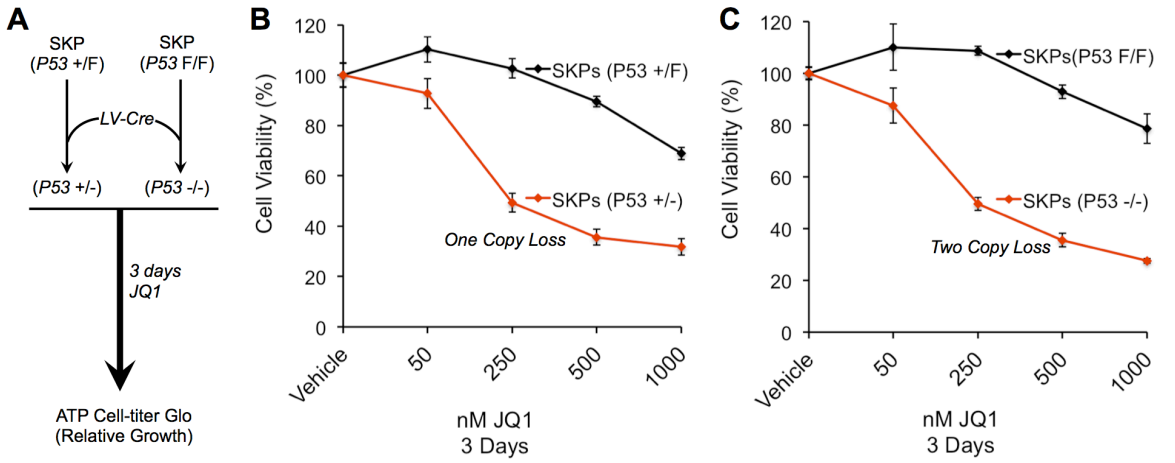

Figure 32. Loss of tumor suppressor *P53* sensitizes SKPs to growth inhibition by JQ1.
(A) Flow chart diagram illustrating the generation of SKPs with single- or two-copy loss of *P53*, and subsequent assay for growth inhibition via JQ1.
(B) ATP cell Titer glo assay of SKPs with indicated alleles for growth inhibition by JQ1. All statistics are represented as the mean +/- SEM (*$p \leq 0.05$, **$p \leq 0.01$, ***$p \leq 0.001$, ***$p \leq 0.0001$).

sufficient to exacerbate SKPs to JQ1 induced growth inhibition, and loss of the second copy did not significantly have further effects on growth inhibition (Figure 33B). In contrast, one copy loss of *P53* sensitized SKPs only to a marginal, but statistically significant amount of

cell death (Figures 33A and 33B). Remarkably, complete loss of *P53* led to a striking sensitization of SKPs to JQ1 induced apoptosis (Figure 33B). Thus, *P53* plays an important role in dictating the proliferative and survival response of SKPs to BET bromodomain inhibition with JQ1.

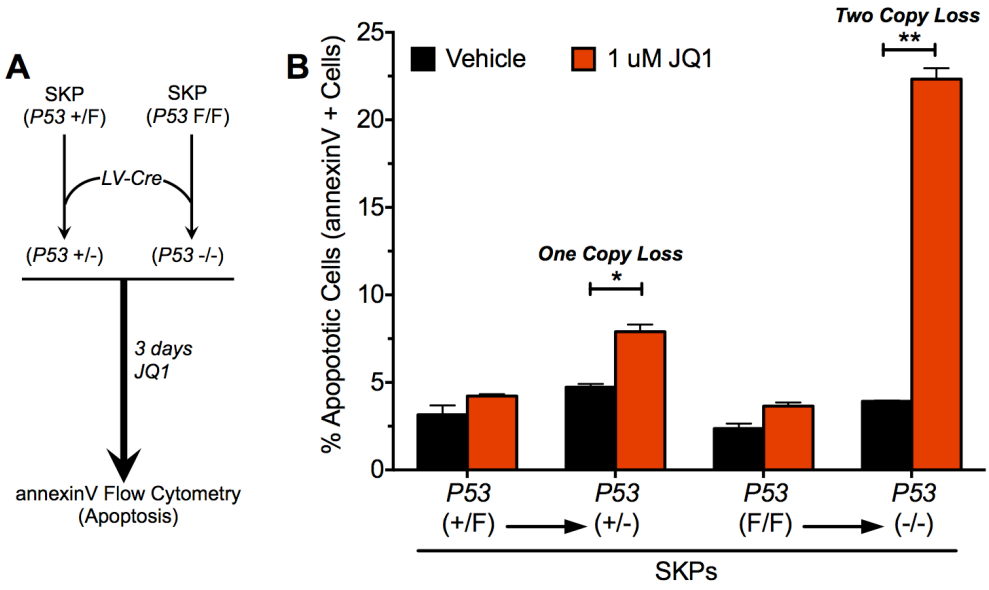

Figure 33. Loss of tumor suppressor *P53* sensitizes SKPs to apoptosis via JQ1.
(A) Flow chart diagram illustrating the generation of SKPs with single- or two-copy loss of *P53*, and subsequent assay for growth inhibition via JQ1
(B) Flow cytometry analysis of indicated cells for annexinV+ (apoptotic) cells after 3 days of exposure to either 1μM JQ1 or vehicle (DMSO). All statistics are represented as the mean +/- SEM (*$p \leq 0.05$, **$p \leq 0.01$, ***$p \leq 0.001$, ***$p \leq 0.0001$).

However, a majority (or at least 50%) of SKPs ($P53^{-/-}$ and $Nf1^{-/-}P53^{-/-}$) or MPNSTs with *P53* loss maintain survival, which suggests cells with either pre-existing or acquired resistance to JQ1 induced apoptosis. If there is pre-existing resistance or otherwise cells in the population already resistant to JQ1 induced apoptosis, then prior to treatment, the isolation of single cell clones from the population should yield clones that die or survive (resistant) in the presence of JQ1. On the other hand, if resistance is acquired after JQ1

treatment, then JQ1 resistant clones (after treatment) should be taken off JQ1, and then compared with the original population before and after re-dosing with JQ1. In both scenarios, *in vitro* cell autonomous modes of resistance can be feasibly identified, but other approaches could be also applied. For example, whole genome cDNA or shRNA screens could be performed to identify genes that modulate sensitivity of JQ1 resistant MPNST or other cancer cells. However, we stumbled upon a potential mechanism of resistance from a serendipitous observation while trying address a different question.

Specifically, to address the role of BRD4 isoforms in MPNSTs, we cloned the cDNA for FLAG-tagged human BRD4 isoform C into a retroviral transfer vector and a lentiviral transfer vector. After packaging these vectors to retrovirus or lentivirus, we stably infected sMPNST cells, and validated expression of FLAG-tagged BRD4 isoform C (Figure 34). We observed that under the retroviral LTR promoter, isoform C protein

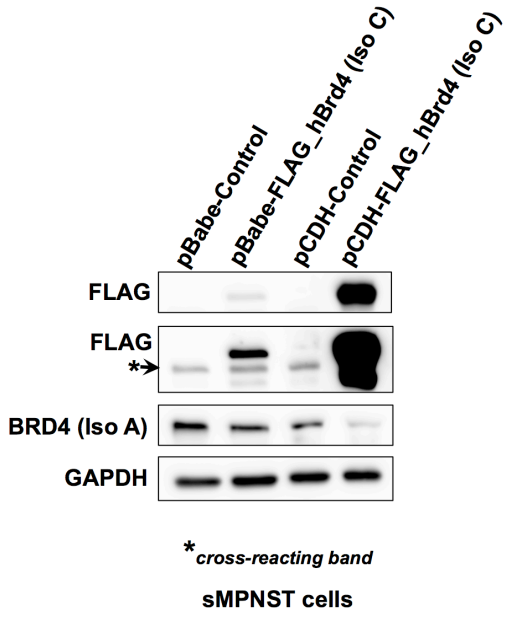

Figure 34. High levels of exogenous BRD4 Isoform C is associated with reduced levels of endogenous BRD4 Isoform A.
sMPNST cells were stably infected with indicted retroviral constructs (pBabe) or lentiviral constructs (pCDH). Cells were plated in standard growth medium followed by isolation of protein 2 days later, and subsequent Western blot analysis as shown here.

expression was adequate, but supra-physiological when expressed under the lentiviral EF1α promoter (Figure 34). Interestingly, supra-physiological levels of exogenous BRD4 isoform

C was consistently associated with a marked reduction in protein levels of endogenous BRD4 isoform A (Figure 34), but no change in mRNA levels (data not shown). Upon further characterization of these cells by ATP cell titer glo and cell cycle analysis, we observed that MPNST cells with high levels of isoform C have a slower growth rate compared to control cells, and further inhibition of growth when treated with JQ1 (Figures 35A and 35B). In fact, time course analysis of cells by ATP cell titer glo analysis revealed that cells with high levels of isoform C did not grow further when treated with JQ1, which is consistent with cell cycle data, but instead these cells underwent substantial loss of viability whereas control cells responded much less (Figure 35A). Consistent with observations from these assays, flow cytometry analysis for apoptotic cells revealed that cells with high levels of isoform C were extremely sensitive to JQ1 induced apoptosis (approximately 3-fold increase in apoptosis compared to control cells treated with JQ1) (Figure 36). Interestingly, cells with low level of exogenous isoform C did not have significant changes in growth nor survival under vehicle or JQ1 conditions, and this a was associated with no significant change in protein levels of endogenous isoform A (data not shown). All together, these observations suggest that Isoform C may not play a role in MPNST growth and response to JQ1, but rather the Isoform A plays a crucial role, which is consistent with the literature.

Given the serendipitous observation that exogenous isoform C leads to reduced levels of endogenous Isoform A with association to JQ1 hypersensitivity, we tested the effect of genetically inhibiting BRD4 prior to JQ1 treatment. Remarkably, and consistent with the most recent data, acute *Brd4* knockdown followed by JQ1 treatment was lethal to MPNST cells in vitro (Figure 37A). And vice-versa, pre-treatment of MPNST cells with JQ1

followed by doxycycline mediated induction of *Brd4* shRNA (that effectively reduces protein level by 24 hours), was again lethal to MPNST cells (Figure 37B). Interestingly, this complete loss of cellular viability or life occurred in a time dependent manner where total loss of survival could be achieved by 5 days at least. These striking observations may suggest that BET bromodomain proteins BRD4, BRD3, and BRD2 may play functionally redundant but vital roles in maintaining MPNST cell survival, and that resistance to BET bromodomain inhibitors such as JQ1 may be mediated by unknown mechanisms that prevent complete inactivation of BET proteins with their inhibitors. Importantly, our data suggests that pharmacological interventions aimed at fine-tuning or reducing the expression of BET proteins may improve the therapeutic efficacy of JQ1. And because pre-malignant wildtype cells such as SKPs maintain survival in the presence of JQ1 despite having low levels of BRD4, this new combination strategy has merits for further investigation in pre-clinical models of MPNST or tumors with *P53* inactivation for analysis of therapeutic efficacy and safety.

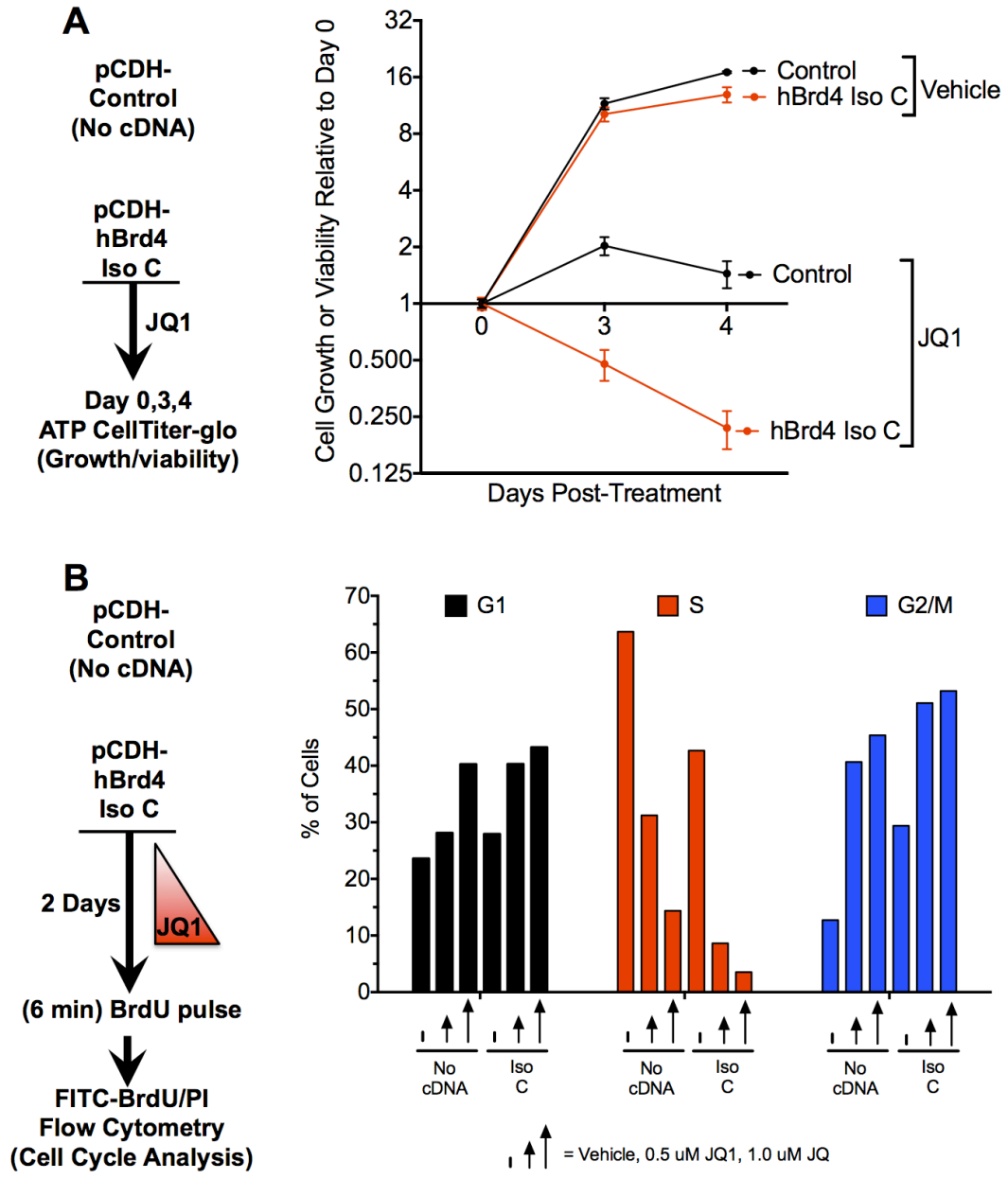

Figure 35. High levels of exogenous BRD4 isoform C is associated with reduced levels of endogenous isoform A along with reduced basal growth and extreme sensitivity to growth inhibition via JQ1.

(A) ATP cell titer glo analysis of indicated sMPNST cells in the presence of vehicle or 1000 nM JQ1. Triplicate per condition.

(B) Cell cycle analysis of indicated sMPNST cells in the presence of vehicle, 500 nM JQ1 or 1000 nM JQ1. Single replicate per condition

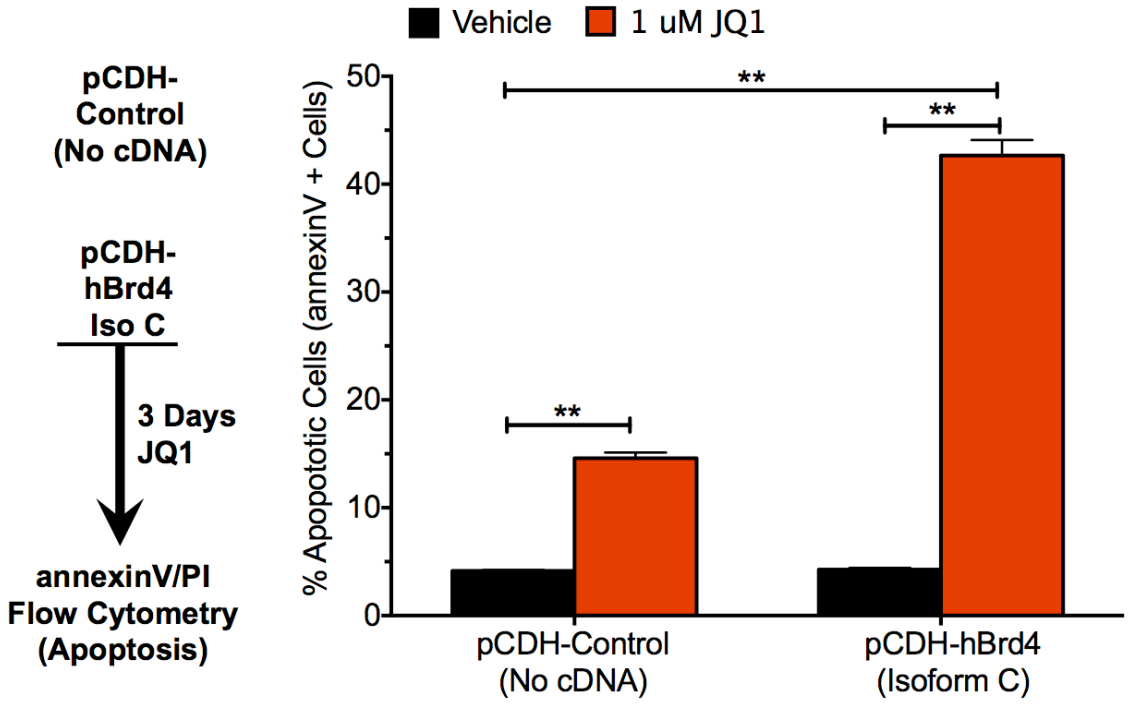

Figure 36. High levels of exogenous BRD4 isoform C is associated with reduced levels of endogenous isoform A along with extreme sensitivity to JQ1 induced apoptosis.
Flow cytometry analysis of indicated sMPNST cells for annexinV+ (apoptotic) cells after 3 days of exposure to either 1μM JQ1 or vehicle (DMSO). All statistics are represented as the mean +/- SEM (*$p \leq 0.05$, **$p \leq 0.01$, ***$p \leq 0.001$, ***$p \leq 0.0001$).

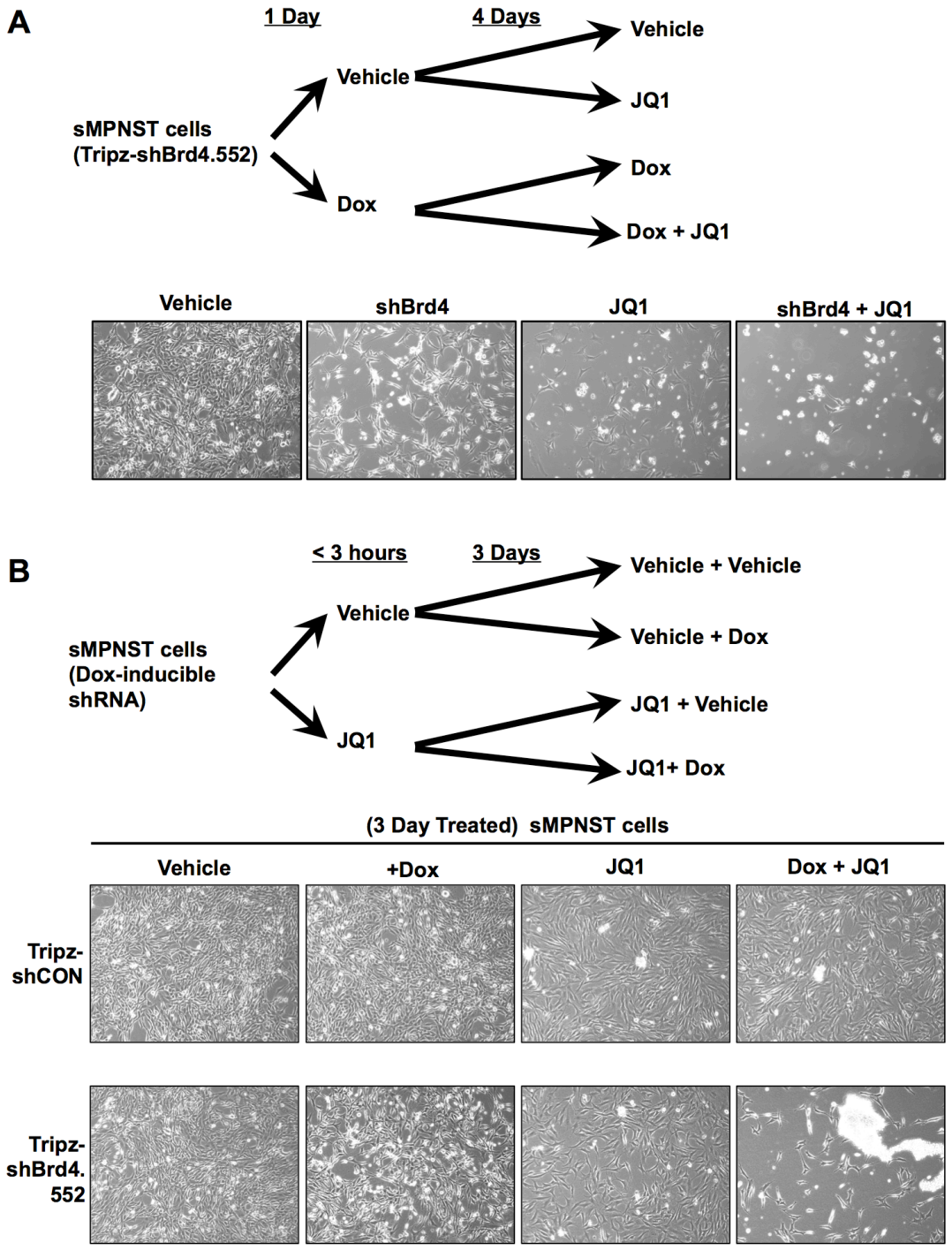

Figure 37. Genetic depletion of *Brd4* prior to or after JQ1 treatment is extremely lethal to sMPNST cells.

(A) sMPNST cells treated with 1μM JQ1 after genetic depletion of *Brd4* via shRNA

(B) sMPNST cells treated with 1μM JQ1 prior to genetic depletion of *Brd4* with shRNA.

7.4 – Discussion

In relatively short time, BET bromodomain inhibitors have emerged as important class of drugs with promising therapeutic efficacy in pre-clinical animal models of mouse and human tumors from various tissue and genetic origins, but the underlying mechanisms dictating sensitivity to such drugs are in dire need for guidance in patient selection for clinical trials and beyond. Here in this chapter, through genetic dissection of relevant tumor suppressors in NF1-associated MPNSTs, we have identified *P53* inactivation as an underlying mechanism for mediating sensitivity to JQ1 induced growth inhibition and apoptosis of SKPs. In support of this idea, HEK 293T cells with inactivation of *P53* and *RB1* tumor suppressor pathways through expression SV40 large T-antigen (Ahuja et al., 2005; Christensen and Imperiale, 1995; Linzer and Levine, 1979) are similarly sensitive to JQ1. The requisite for *P53* inactivation in other normal or malignant cells in modulating sensitivity to JQ1 remains to be explored in future studies. However, if this requisite holds true, it has far-reaching implications given that a majority of advanced human tumors frequently have *P53* inactivation (Muller and Vousden, 2013). Thus, *P53* inactivating mutations may serve as potential biomarker for selecting cancer patients for enrollment on BET bromodomain inhibitor therapy.

On the other hand, the mechanism by which *P53* loss may render cells sensitive to BET bromodomain inhibitor therapy remains unclear at the moment. However, our findings indicate an association between *P53* loss and increased protein expression of BET protein BRD4 in primary SKPs. During the course of my experiments, we observed that *P53* inactivation at least in primary SKPs allows for indefinite proliferation and escape from

senescence. This may allude to a potential mechanism whereby perhaps BET proteins such as BRD4 are either called upon or co-opted for maintaining proliferative and survival capabilities acquired after *P53* inactivation. On other hand, a recent report indicates that BRD4 binds with *P53* to regulate transcription of *P53* target genes (Wu et al., 2013b). At this time in our system, it is unclear whether *P53* interacts with or regulates BRD4, but this could be addressed in future studies by interaction analysis in primary wildtype SKPs or transient induction of *P53* cDNA in *P53* null MPNST cells.

In addition to identifying biomarkers, the identification of mechanisms underlying resistance to BET bromodomain inhibitor therapy is equally needed in anticipation of failed tumor responses to this therapy in the clinic. Indeed, the data presented here as well as in published studies indicate *in vitro* and *in vivo* mechanisms of resistance. In the case for *in vivo*, the short half-life of current BET bromodomain inhibitors (e.g. JQ1) in rodents is being addressed through second-generation derivatives (e.g. JQ2 by Tensha Therapeutics) in early stage clinical trials. *In vitro* mechanisms underlying resistance to this class of therapeutics has not been addressed to date. As with most therapeutics in early stages of development, mechanisms of resistance will surely be identified through a variety of approaches and insights. As testament to this, here in this chapter, we have identified through a serendipitous insight that BRD4 levels play an important role in protecting MPNST cells from complete lethality during exposure to BET bromodomain inhibitor JQ1. The mechanism underlying this insight remains unknown at the time being. Yet, we know that our *Brd4* shRNAs allow for ~80% reduction in total *Brd4* mRNA levels in our MPNSTs cells, and that JQ1 should inhibit BRD2, BRD3, and BRD4, which presents a paradox. All 3 of those BET proteins are

expressed in our cells as measured at the mRNA and protein level. Given that genomic occupancy analysis of these 3 proteins and JQ1 in other cancer cells indicate overlapping genomic targets, it is conceivable that all 3 BET proteins play some functionally redundant or distinct roles such that simultaneous targeting with JQ1 leads to profound therapeutic effects. Moreover, the precise levels of BET protein inhibition via JQ1 are not easily quantifiable in cells, thus posing a challenge to determining if the inhibitor is effective or encountering endogenous resistance. However, insights from ChIP-seq data evaluating genome wide occupancy of all 3 BET proteins indicates that JQ1 is highly efficient at displacing BET proteins from super-enhancers, but less effective at typical enhancers (Lovén et al., 2013). Super-enhancers are thought allow for high levels of transcription elongation compared to typical enhancers (Lovén et al., 2013; Whyte et al., 2013). Thus, BET proteins remaining at typical enhancers in the presence of JQ1 may signify the maintenance of BET protein target gene transcription at reduced levels, which may be compatible with cancer cell survival. This may allude to undetailed mechanism of resistance to JQ1. Thus, our findings may suggest that pharmacological interventions aimed at selective reduction of BET protein expression in cancer cells as a surrogate for displacement from typical enhancers may serve as a novel approach to further sensitize NF1-associated MPNST cells for complete eradication via BET bromodomain inhibitor therapy. Therefore, if applicable to other types of cancer, and tolerable with normal mammalian cell function and viability, our strategy may represent a significant step forward in advancement of BET bromodomain inhibitors for cancer therapy, and benefit for cancer patients in the clinic.

CHAPTER EIGHT

CONCLUSIONS AND FUTURE DIRECTIONS

8.1 Summary

Loss of tumor suppressors *Nf1* and *P53* are two major events underlying the development of NF1-associated MPNSTs, but little is known about the tumor promoting features or vulnerabilities as a consequence of those events in this disease. Through use of a novel/stem-progenitor model of MPNST, we were able for the first time to capture genetic and epigenetic events underlying malignant transformation of *Nf1*/*P53* deficient progenitors cells to MPNSTs. Through genetic and pharmacological dissection of these events, in this case, chromatin regulator BRD4, which we found abundantly expressed in the malignant state of MPNSTs, we show that BRD4 represents a dependency acquired during progression to MPNST. Given the global nature of chromatin regulators on transcription, the effect of BET bromodomain inhibition has been attributed to diverse transcriptional events observed. In our case, we find that BET bromodomain inhibition does not inhibit transcription elongation of *Myc* in NF1-associated MPNSTs. Instead we find that proliferation is correlated with reduced levels of D-type cyclins (predominantly Cyclin D1). This finding further supports our previous publication demonstrating a role of for Cyclin D1 in mediating cell cycle progression induced by a CXCL12/CXCR4 autocrine mechanism (Mo et al., 2013). Moreover, in agreement with a previous study (Dawson et al., 2011), we show that suppression of BCL-2 upon BET bromodomain inhibition plays a pivotal role in apoptosis

induction under this context. However, we find apoptosis in our context to be co-dependent on the induction of pro-apoptotic BIM upon BET bromodomain suppression, which represents a new mechanism of action for BET bromodomain inhibitor therapy. After publication our findings, two new studies reassuringly confirmed that BET bromodomain inhibition could trigger apoptosis through BIM induction in other malignancies (human leukemia and melanoma) (Fiskus et al., 2014; Gallagher et al., 2014). Given this novel mechanism of action for BET bromodomain inhibitors, we propose the following future directions to elucidate this mechanism, and delineate the pathways that mediate sensitivity and resistance to BET bromodomain inhibition under this mechanism.

8.2. Future Directions

Do BET proteins regulate ER stress/UPR/BIM pathways indirectly?

The precise mechanism by which BET bromodomain inhibition triggers expression of pro-apoptotic BIM remains unclear, but we entertain two distinct hypotheses that are testable. The first of which is a role for BET bromodomain inhibition in triggering a ER stress/UPR cascade to mediate downstream events such as BIM, and therefore promoting MPNST apoptosis. This hypothesis was inferred by ChIP-qPCR analysis of BRD4 occupancy at several promoter regions of BIM, which revealed no substantial evidence of occupancy when compared to background. If true, then perhaps BET proteins regulate BIM through an indirect mechanism (e.g. regulation of genes or proteins that control BIM expression). Consistent with a role for ER stress/UPR pathway in regulating apoptosis through mechanisms including BIM, we observed that BET bromodomain inhibition leads to

presentation of ER luminal features, and downstream UPR activation signals, and transcription. As part of our future experiments/research, a new member of the Le laboratory will employ genetic and pharmacological methods to modulate ER stress/UPR pathways to determine if BIM and subsequent apoptosis can be suppressed in the context of BET bromodomain inhibition (Figures 38A and 38B).

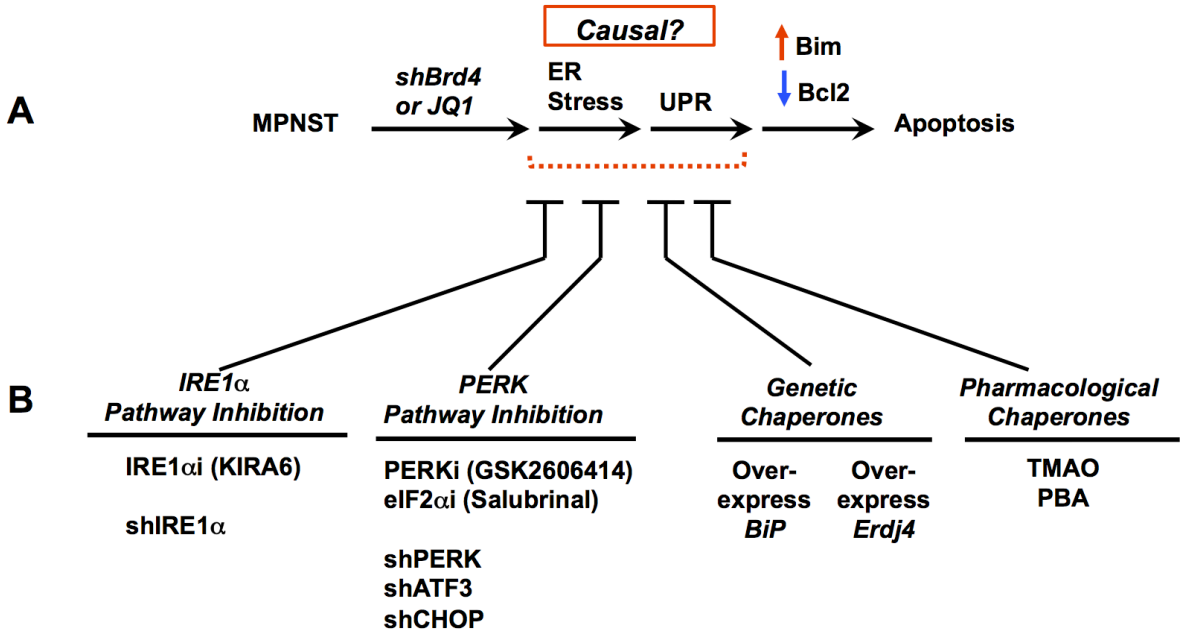

Figure 38. Genetic and pharmacological determination of ER stress/UPR signaling in BET bromodomain inhibition induced apoptosis of MPNSTs.
(A) Hypothesis: ER stress and UPR signaling events mediate either apoptotic or anti-growth effects of BET bromodomain inhibition in the context of NF1-associated MPNST cells.
(B) Genetic and pharmacological strategies to modulate distinct arms of the UPR pathway for evaluation of rescue from classical ER stress inducers or BET bromodomain inhibition.

Do BET proteins directly repress transcription of stress inducible genes (e.g. Bim)

As an alternative, our second hypothesis arises from differential interpretation of our ChIP-qPCR data, which had originally suggested to us an indirect mode of BIM regulation in MPNSTs upon BET bromodomain inhibition (Figure 39A). Given that ChIP-qPCR assay

probes for occupancy at selected sites, we cannot rule out other sites of occupancy at the BIM promoter (Figure 39B). To address this issue, a new member of our lab will continue

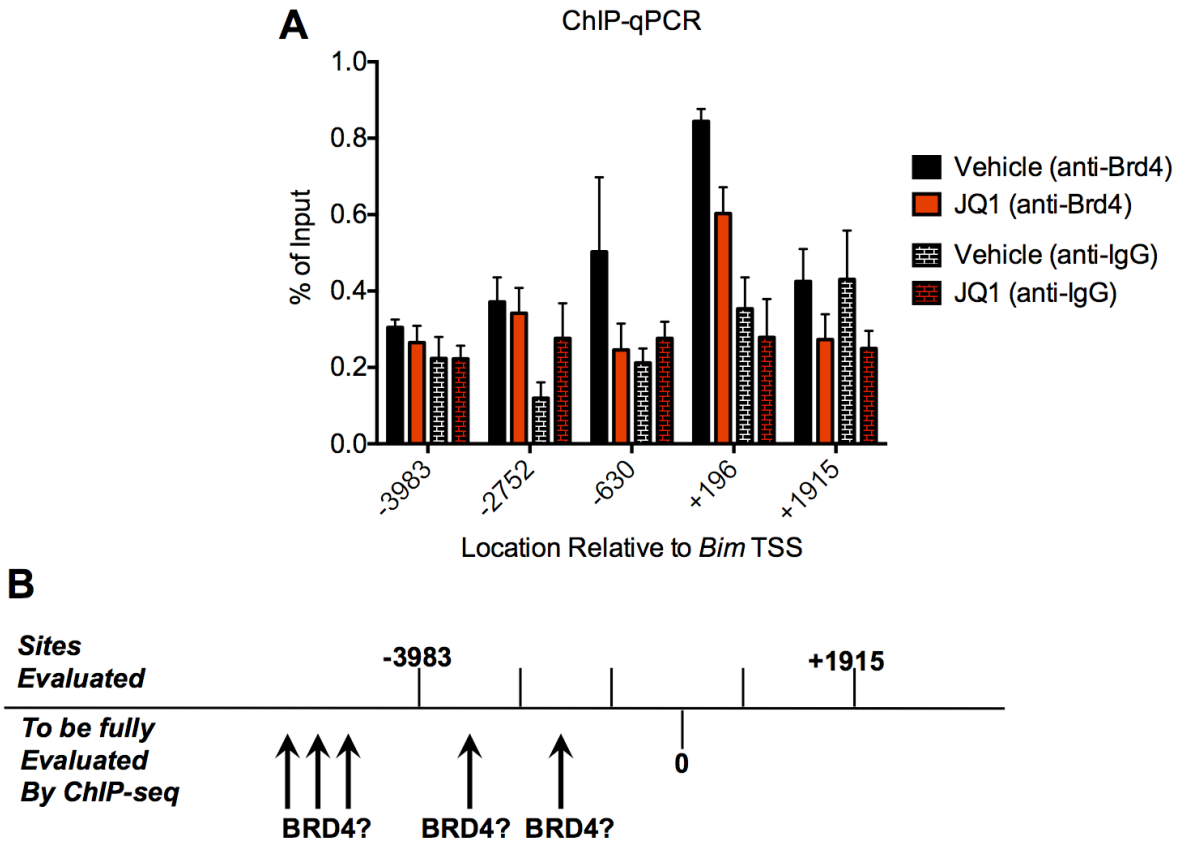

Figure 39. Targeted (ChIP-PCR) versus genome-wide (ChIP-seq) analysis of BET protein occupancy in MPNST cells.
(A) Lack of strong evidence for BRD4 occupancy at promoter of *Bim* in sMPNST cells. ChIP-PCR analysis of specified genomic regions relative to *Bim* TSS (transcription start site) in sMPNST cells with or without BRD4 displacement from chromatin via 1000 nM JQ1.
(B) Illustration of ChIP-PCR (targeted approach) compared to future plan to comprehensively characterize BRD4 genomic occupancy in proximity of *Bim* TSS and genome-wide in MPNST cells.

the work presented here by conducting a comprehensive genome-wide analysis to identify BET protein occupancy sites in MPNSTs (Figures 39B). In further support of this aim, a recent study that analyzes publically available BRD4 ChIP-seq data sets has identified a role

for BET protein BRD4 in repression of transcription for numerous genes, most notably, those that are stress inducible (Bhadury et al., 2014). One of these genes identified was *Txnip*,

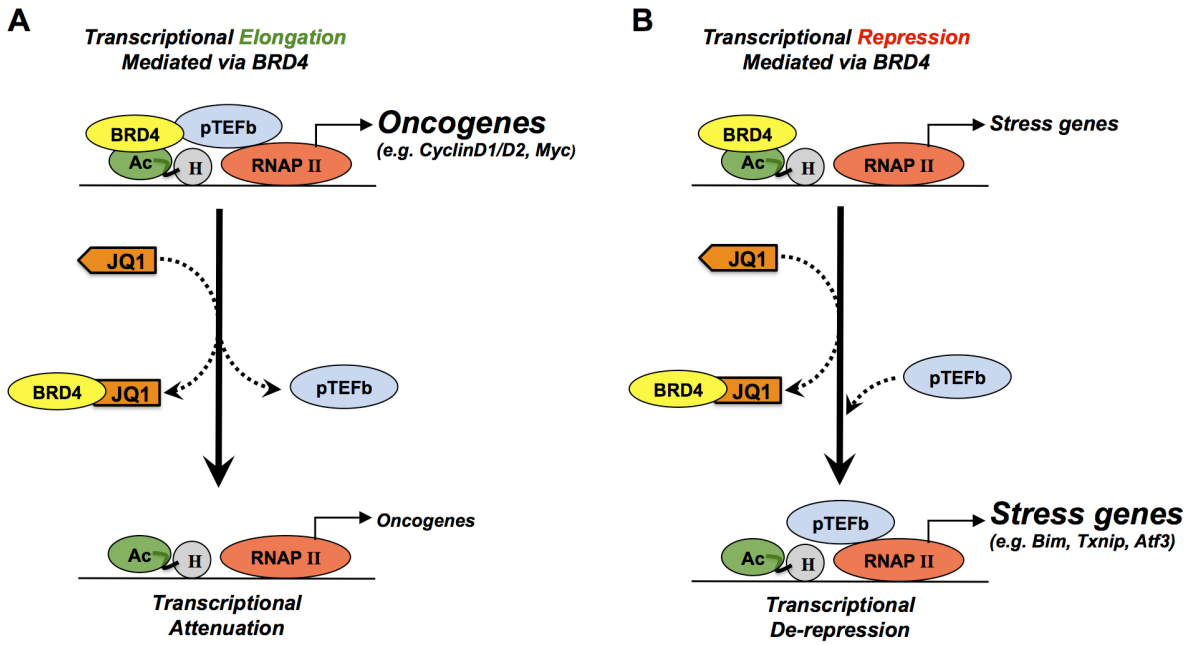

Figure 40. Models for BRD4 mediated transcriptional elongation and repression.
(A) Model in which BRD4 recruits pTEFb to stimulate RNAPII (RNA polymerase II) dependent transcript elongation (expression of genes such as oncogenes in cancer). JQ1 competitively displaces BRD4 from acetyl-histone (Ac-H) leading to attenuation but not elimination of transcript elongation (Lovén et al., 2013; Wu and Chiang, 2007; Yang et al., 2005).
(B) Model in which BRD4 antagonizes pTEFb recruitment, and therefore repression of transcriptional elongation of genes (e.g. stress inducible genes as observed in the literature). Upon JQ1 mediated displacement of BRD4, pTEFb is recruited to stimulate higher levels of transcript elongation (de-repression) (Bhadury et al., 2014).

which we found upregulated in via BET protein inhibition in our cells, and as a known target of downstream UPR events (Bhadury et al., 2014). Given this recent revelation, it may be plausible that induction of UPR downstream genes via BET bromodomain inhibition may be a consequence of de-repressed transcription. If true, this would suggest that BET proteins

play secondary role in maintaining repression of genes that would antagonize tumorigenesis and survival (Figures 40A and 40B). In that case, given that various death stimuli can activate stress inducible genes, it would interesting to explore the effects of death stimuli or stress events on genome-wide BET protein occupancy. Thus, to delineate roles for BET proteins in promoting or repressing transcription elongation in MPNSTs, we plan to conduct a comprehensive analysis of BET protein occupancy and function by ChIP-sequencing and RNA-sequencing to identify direct target genes (e.g. *Bim*, *Bcl2*, *Txnip*?) that are relevant to the mechanism of BET bromodomain inhibitor efficacy against MPNST cells (see Figure 41). To further complement our studies in MPNST, we will take a parallel approach to analyze public ChIP-seq and expression data sets to compare and contrast BET protein mechanisms across different cancer types.

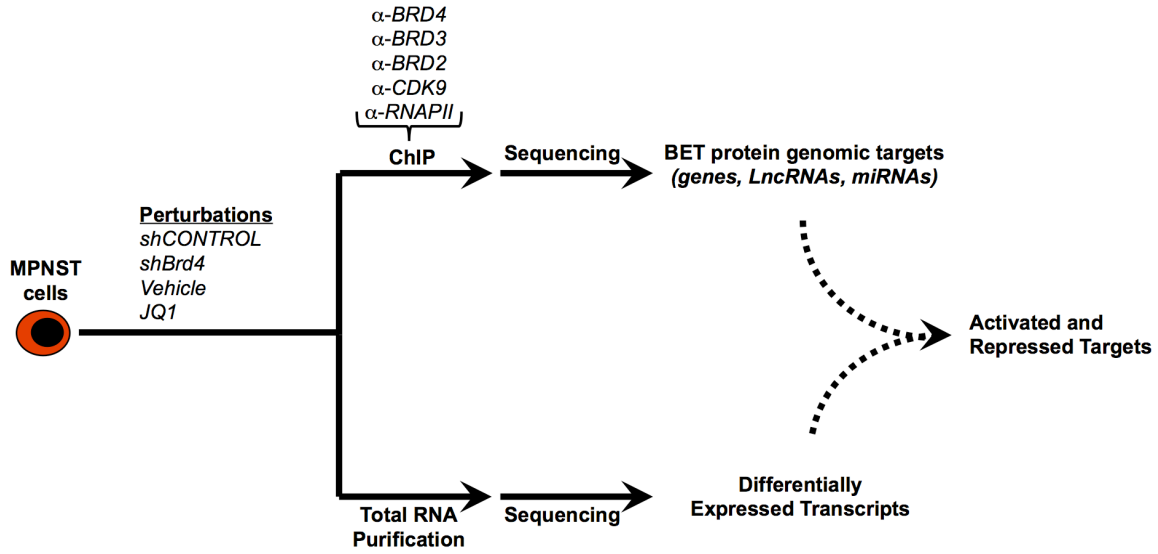

Figure 41. Multi-dimensional analysis for therapeutic targets underlying BET bromodomain inhibition.
A two-pronged, comprehensive strategy to dissect the chromatin binding events (ChIP-seq) underlying individual or combined BET bromodomain inhibition, and the downstream transcriptional consequences (RNA-sequencing) ultimately leading to the identification of direct targets and mechanistic insights.

Regulation of BET protein expression and JQ1 sensitivity

Our recent discovery that *P53* loss leads to higher levels of BRD4 and sensitivity to JQ1 represents a new finding in the BET bromodomain field. However, caution must be taken in interpreting these results. First, this finding is limited to primary SKPs, and we know from the literature that many findings can be cell type- or context-dependent (e.g. *Myc* regulation via *Brd4* in leukemia but not in most solid tumors) (Delmore et al., 2011; Zuber et

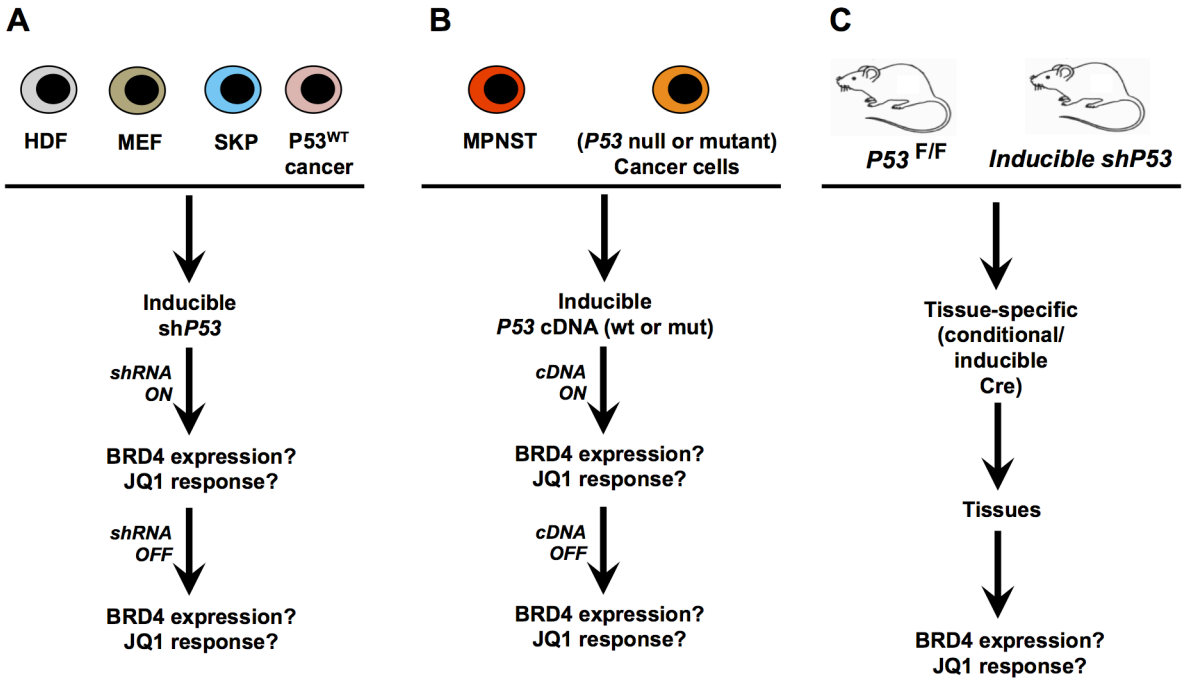

Figure 42. Strategies to validate and dissect the role of *P53* in regulating BRD4 expression and JQ1 sensitivity.
(A) Inducible *P53* shRNA as an alternative approach to determine if *P53* can broadly regulate BRD4 expression or JQ1 response in a wide range of cell types in vitro. (HDF: human dermal fibroblast, MEF: mouse embryonic fibroblast, SKP: mouse skin-derived precursor cell, $P53^{WT}$ cancer: cells that have wildtype *P53*.
(B) Inducible *P53* cDNA to assess reversibility of BRD4 expression and JQ1 sensitivity in genetically complex cancer cell lines.
(C) Strategies to explore the effect of constitutive or temporal *P53* inactivation on BRD4 expression or JQ1 response in mouse tissues *in vivo*.

al., 2011). To address this, we plan to evaluate the role of *P53* on BRD4 expression and JQ1 response in other cell types through *in vitro* and *in vivo* experiments as outlined (Figure 43A, 43B, 43C). Second, there could be another interpretation to our observation. We observed and showed that some wildtype SKPs had higher BRD4 expression than others. Interestingly, those wildtype SKPs with higher BRD4 levels were high passage and had reduced growth and senescent morphology, which we typically observe during prolonged culture of these stem-like cells. It may be feasible that other mechanisms can regulate BRD4 expression, which would be reasonable given the diverse contexts in which BRD4 is implicated (e.g. cancer, heart failure, DNA damage). Because *P53* loss is likely to have a wide-range of effects on SKPs, it is unclear whether induction of BRD4 expression is an indirect downstream consequence of *P53* loss in the context of SKPs. Thus to determine if *P53* has a role in regulating BRD4 expression, we plan to utilize inducible systems to upregulate or downregulate *P53* levels to further validate our findings, and determine if this regulation if reversible or bi-directional in multiple cell types *in vitro* and *in vivo* (Figure 43A, 43B, 43C).

Role of additional BET bromodomain proteins in MPNST

The finding that BRD4 depletion sensitizes to JQ1 induced apoptosis of MPNST cells suggests that inhibition of other BET proteins may have partial overlapping molecular and phenotypic effects on MPNSTs. Although we did not observe differential expression of neither *Brd2* nor *Brd3* in our first expression microarray array comparing pre-tumorigenic NP-SKPs to MPNSTs, it should be noted that these cells expressed these genes, and that

there could other mechanisms (e.g. protein levels, acetyl-lysine target availability) dictating the activity of *Brd2* or *Brd3* in different stages of tumorigenesis. Moreover, compared to *Brd4*, less is known about *Brd2*, and even less about *Brd3*. Thus, given the importance of BET bromodomain inhibitor therapy in pre-clinical models of MPNST, and scarcity of biological knowledge regarding *Brd2* and *Brd3*, a fruitful opportunity exists to characterize or shed new light on these BET genes in tumorigenesis. Thus, our future studies entail the use of genetic approaches (e.g. shRNA, sgRNA) to define the precise role of *Brd2* and *Brd3* in MPNST development, and whether their inhibition (like *Brd4*) can overcome resistance to JQ1.

Are there JQ1 or BET bromodomain inhibitor off-targets?

On the other hand, the finding that BRD4 depletion overcomes resistance to JQ1 could be alternatively interpreted as an off-target phenomenon. First, it may be possible that our *Brd4* shRNA have unforeseen off-target effects that may cooperate with JQ1 to produce the phenotype. To address, we could test additional *Brd4* shRNAs with similar knockdown efficiency to rule out this possibility. As an alternative approach, CRISPR/Cas9 mediated gene editing to create *Brd4* loss of protein expression or knockout alleles may be used in place of shRNAs. However, this approach may also have it's own off-target effects or cell clone dependent phenotypes that would need to be addressed. Lastly, JQ1 may have off-target effects that are unknown. Although high JQ1 concentrations (>10 μM) may have off-target effects, perhaps depletion of specific JQ1 targets such as BRD4 in our situation may favor non-specific JQ1 interactions at lower concentrations. To address this issue, we could

evaluate whether alternative BET bromodomain inhibitors (with different chemical scaffolds) can phenocopy the effect that JQ1 has upon BRD4 depleted cells. In the case that JQ1 does have off-target effects causing lethality to BRD4 depleted cells, it would be useful to delineate those effects. Specifically, off target information would be useful if BET bromodomain inhibitors are used in human patients or in pre-clinical studies. Moreover, off-target identification may potentially offer a novel therapeutic target or biomarker for use of JQ1 in the clinic. Thus, to address this issue, we could employ a recently validated, biotinylated version of JQ1 (bio-JQ1) as a probe to locate and immunoprecipitate off-targets of this small molecule in cancer cells (Anders et al., 2014). Nonetheless, the observation that P53 wildtype cells with low BRD4 expression (e.g. SKPs) being resistant to JQ1 suggests a therapeutic opportunity for eradicating *P53* deficient cells (e.g. MPNSTs).

8.3 Conclusion

In conclusion, we believe that our studies point to BET bromodomain proteins as an Achilles heel in MPNST development. Therefore, BET bromodomain inhibition with JQ1 represents a viable therapeutic strategy for disrupting MPNST tumor maintenance. Given that NF1-associated MPNSTs are life threatening malignant sarcomas that are associated with poor patient prognosis and survival despite available therapeutic options (chemotherapy and surgery), our findings present a viable therapeutic alternative for further investigation of efficacy and improvement of patient survival. More broadly, because *P53* inactivation is a frequent event in cancer progression, our findings suggest that *P53* inactivation may serve as potential biomarker for JQ1 sensitivity in various human tumor types. And although

resistance to JQ1 is likely to be unavoidable in the clinic, our studies for the first time suggest that strategies aimed at modulation of BET protein expression may override resistance to JQ1. All together, our studies illustrate the importance and relevance of familial tumor pre-disposition genetic disorders and novel GEMMs in advancing our knowledge regarding tumor development, and understanding mechanisms of sensitivity and resistance to inhibition of key therapeutic targets in cancer, and translation to therapy for cancer patients.

APPENDIX A
Mammalian Tissue/Cell Culture Reagents

D10 Media
435 mL DMEM (Sigma-Aldrich, catalog# D5796)
*5 mL Penicillin-streptomycin (Sigma-Aldrich, catalog# P0781-100mL)
*5 mL L-glutamine (Sigma-Aldrich, catalog# G7513)
*5 mL Sodium Pyruvate (Sigma-Aldrich, catalog# S8636)
*50 mL Heat-inactivated fetal bovine serum (Sigma-Aldrich, catalog# F4135-500mL)
Add components to 435mL DMEM media.
*Before adding to DMEM, filter sterilize with 0.2 μm syringe filter (Millipore, catalog#).

D10 media used for culturing all mouse and human tumor cell lines, HEK 293T, human dermal fibroblasts.

SKP base media
Advanced DMEM/F12,1X (Life Technologies, catalog# 12634-010)
*5 mL Penicillin-streptomycin (Sigma-Aldrich, catalog# P0781-100mL)
*5 mL L-glutamine (Sigma-Aldrich, catalog# G7513)
*5 mL Sodium Pyruvate (Sigma-Aldrich, catalog# S8636)
*5 mL 100x N-2 Supplement (Life Technologies, catalog# 17502-048)
*1 mL Heparin (0.2%)
*1 mL D-glucose (30%)
*0.750 mL $NaHCO_3$ (7.5%)
*0.250 mL HEPES (1M)
*Before adding to DMEM, filter sterilize with 0.2 μm syringe filter (Millipore, catalog#).

SKP complete media (Prepare fresh, storage at 4^{o}C, use within 1 week)
40mL SKP base media
800 μL 50x B-27 Supplement, serum free (Life Technologies, catalog# 17504, 044)
40 μL 1000x Fibroblast growth factor (Sigma-Aldrich, catalog# F0291-25UG)
40 μL 1000x Epidermal growth factor (Life Technologies, catalog# PHG0311-100μg)
160 μL Amphotericin B

SKP complete media used for culturing all SKPs (wildtype, *Nf1*$^{-/-}$, *P53*$^{-/-}$, *Nf1*$^{-/-}$ *P53*$^{-/-}$)

- All cells maintained in water humidified tissue culture incubator at 37^{o}C with 5% CO_2.

APPENDIX B
Plasmids Used

Mammalian expression vector
p6345 MSCV-CMV-Flag-HA-Brd4 1-722 (Isoform C) (Addgene, Plasmid 31352)

Lentiviral transfer vector
pCDH-EF1α-control-IRES-Puro (System Biosciences, catalog# CD532A-1)
pCDH-EF1α-Cre-IRES-Puro
pCDH-EF1α-Flag_HA_human_Brd4_Isoform C_cDNA-IRES-Puro (Lu Le lab-AJP)
pLKO-shCONTROL (Addgene, Plasmid 1864)
pLKO-shBim.92 (TRCN0000009692)
pLKO-shBim.94 (TRCN0000009694)

Retroviral transfer vector
pBabe-Neo-Control (Addgene, Plasmid 1767)
pBabe-Neo-mouse_Bcl2(transcript variant 1) cDNA (Lu Le lab-AJP)
pBabe-Neo-mouse_ human_Brd4_Isoform C_cDNA (Lu Le Lab-AJP)
MSCV-Luciferase-PGK-Hygro (Addgene, Plasmid 18782)

Virus packaging and envelope vectors
psPAX2 (Addgene, Plasmid 12260)
pMD2.g (Addgene, Plasmid 12259)
pCL-Eco (Addgene, Plasmid 12371)

APPENDIX C
Protocol: Lentivirus or Retrovirus Production in HEK293T cells

1. Maintain 293T cells by regularly in 10cm tissue culture plates. When cells reach 80-90% confluency, passage 1/4th of cells to a new 10cm plate. Passage 1/4th of cells consistently every 2 days.

2. Plate cells for transfection.
- When cells reach ~90% confluency, passage 1/3rd of cells to a new 10cm plate (1 plate per transfection)
- Prepare at least 3 plates for transection (1 x untransfected, 1 x Chloroquine only, 1x transfection)

3. Approximately 24 hours after plating cells, pre-warm D10 media in 37^{o}C water-bath. For each transfection plate, add 10 mL of 100 mM Chloroquine (light-sensitive) to 10 mL D10 media (pre-warmed). Aspirate all media from plate of 293T cells, and immediately replace with Chloroquine-D10 media. Return to tissue culture incubator.
- *Note: Chloroquine can be used as an inhibitor of lysosomal degradation of DNA, which is thought to improve efficiency of DNA transfection such as in this case. Thus chloroquine is optional.*

4. Prepare precipitated DNA for transfection. For each transfection, do the following:
- Keep all reagents on ice or 4^{o}C during this preparative step.
- Add 0.5 mL of 2X HBS to a sterile 15 mL conical tube.
    - 2X HBS buffer is at pH 7.05-7.15, and consists of the following: 42 mM HEPES, 274 mM NaCl, 10mM KCl, 1.8 mM Na_2HPO_4. Sterile filtered, and stored at 4^{o}C. Test different pH batches in the indicated range for the pH that yields the finest particles during subsequent precipitation or transfection efficiency.
- Mix the following in a sterile 1.5 mL tube.
    - For lentivirus: 12.5 μg transfer vector, 8.5 μg psPAX2 (packaging vector), 5 μg pMD2.g (envelope vector), 62 μL 2M $CaCl_2$, water to a final volume of 0.5 mL
    - For retrovirus: 15 μg transfer vector, 15 μg pCL-Eco (packaging/envelope vector), 62 μL 2M $CaCl_2$, water to a final volume of 0.5 mL
- Collect all DNA/$CaCl_2$ mixture with a 1 mL pipetman, and add to the 0.5 mL 2X HBS aliquot (kept under a medium vortex) in a drop-wise manner.
- Incubate on ice for at least 30 minutes prior to use for transfection.

Note: Do not leave this mixture at room temperature. In some instances, depending of the pH of your 2X HBS buffer, the calcium phosphate mixture will precipitate very quickly, and tend to be very coarse and clumpy after adding to your cells later. This will reduce your transfection efficiency. Thus, please keep reagents for this preparative procedure at 4^{o}C as a preventative measure.

5. Transfect chloroquine-D10 pre-treated 293T cells with the above DNA/Calcium phosphate mixture. Note: mix DNA mixture by pipetting up and down several times followed by gentle drop-wise addition evenly across the cell monolayer, and then gentle distribution by swirling or side-to-side motions. Return cells to incubator.

- After 1 hour, a fine/sand-like precipitate of DNA/Calcium phosphate particles should be settled throughout the plate. In general, more finer/smaller the particles should lead to better transfection results than coarse/larger particles.

6. Upon 8-12 hours after transfection, aspirate media, and immediately replace with 10 mL of pre-warmed D10 media per plate. Return to incubator.

7. Next day, compare chloroquine treated cells to untransfected cells. If chloroquine treated cells appear healthy, continue with experiment. If unhealthy, consider decreasing cell exposure or concentration of chloroquine to reduce toxicity to 293T cells. Otherwise, chloroquine can be eliminated from protocol, but lower virus titers may result.

8. Approximately 2 days after transfection collect virus-containing media into a sterile 15 mL conical tube. Centrifuge at 1000 rpm for 5 min. Pass viral supernatant through a 0.45 μm syringe filter, and prepare 1 mL aliquots in sterile 1.5 mL tubes for long-term storage in -80^{o}C. Virus can be stored at 4^{o}C for at least 2 days if multiple viral media batches are to be serially collected and pooled together until eventual -80^{o}C storage.

APPENDIX D
Protocol: Lentiviral or Retroviral Infection

Day 1

1. In the evening, plate target cells into three 6-well plates (w/ 50,000 cells per well for primary murine MPNST cells). Also plate on a 6cm dish as well to serve as positive control for antibiotic effectiveness.

Day 2

2. In the morning, check status of plated cells. If cells look like they are well dispersed (not too much crowding), then proceed wtih infecting them with your lenti-/retro-virus.
3. Pre-warm media to 37^{o}C in water bath.
4. Quickly thaw vials of lenti-/retro-virus in 37^{o}C water bath (2 minutes).
5. Prepare dilutions of lenti-/retro-virus for infection. Add polybrene (to a final concentration of 8 μg/mL from 1mg/mL stock) to each dilution (and for un-diluted). See below for details.

Dilution Factor	***uL of Lenti-/Retro-virus***	***Media***
Un-diluted	1000 μL of Undiluted	
1:100	10 μL of Un-diluted	990 μL
1:1,000	100 μL of 1:100	900 μL

Prepare 3 sets of these for triplicate Assay. If virus titer low, then adjust dilution factors accordingly.

6. Remove all media in wells from each plate below, and replace with lentivirus or retrovirus dilutions prepared above. Then place plates back into 37^{o}C/CO_2 incubator.

Day 3

1. 24 hours later, change media to fresh media (pre-warmed to 37^{o}C)
2. In the evening, quickly assess lentiviral infection by assaying for reporter activity. In this case, check for GFP by fluorescence microscopy.

Day 4

3. 48 hours post-infection (or by day 4), select for infected cells with antibiotic
4. Once non-infected cells die, and float up, aspirate media from wells, and replace with 2mL media with selection antibiotic. Visually compare infection efficiency by referencing to uninfected cells with or without antibiotic treatment.

APPENDIX E
Mouse qRT-PCR Primers Used

Oligo Name	Oligo Seqeunce (5'-->3')
mGapdh_F	AGG TCG GTG TGA ACG GAT TTG
mGapdh_R	TGT AGA CCA TGT AGT TGA GGT CA
mCyclinD1_F	GCC CTC CGT ATC TTA CTT CAA G
mCyclinD1_R	GCG GTC CAG GTA GTT CAT G
mCyclinD2_F	GCG TGC AGA AGG ACA TCC A
mCyclinD2_R	CAC TTT TGT TCC TCA CAG ACC TCT AG
mCyclinD3_F	CGA GCC TCC TAC TTC CAG TG
mCyclinD3_R	GGA CAG GTA GCG ATC CAG GT
mCyclinA_F	GTC CTT GCT TTT GAC TTG GC
mCyclinA_R	ACG GGT CAG CAT CTA TCA AAC
mCyclinB_F	CTG ACC CAA ACC TCT GTA GTG
mCyclinB_R	CCT GTA TTA GCC AGT CAA TGA GG
mCyclinE_F	GCG AGG ATG AGA GCA GTT C
mCyclinE_R	AAG TCC TGT GCC AAG TAG AAC
mCDK2_F	CCT GCT TAT CAA TGC AGA GGG
mCDK2_R	TGC GGG TCA CCA TTT CAG C
mCDK4_F	ATG GCT GCC ACT CGA TAT GAA
mCDK4_R	TCC TCC ATT AGG AAC TCT CAC AC
mCDK6_F	GGC GTA CCC ACA GAA ACC ATA
mCDK6_R	AGG TAA GGG CCA TCT GAA AAC T
mp21_F	CCT GGT GAT GTC CGA CCT G
mp21_R	CCA TGA GCG CAT CGC AAT C
mp16_F	CGC AGG TTC TTG GTC ACT GT
mp16_R	TGT TCA CGA AAG CCA GAG CG
mp27_F	TCA AAC GTG AGA GTG TCT AAC G
mp27_R	CCG GGC CGA AGA GAT TTC TG
mMyc_F2	AGT GCT GCA TGA GGA GAC AC
mMyc_R2	GGT TTG CCT CTT CTC CAC AG
mCdk8_F	CGG GTC GAG GAC CTG TTT G
mCdk8_R	TGC CGA CAT AGA AAT TCC AGT TC

Oligo Name	Oligo Seqeunce (5'-->3')
mBclxl_F	GAC AAG GAG ATG CAG GTA TTG G
mBclxl_R	TCC CGT AGA GAT CCA CAA AAG T
mBcl2_F	ATG CCT TTG TGG AAC TAT ATG GC
mBcl2_R	GGT ATG CAC CCA GAG TGA TGC
mSurvivin_F	TGG CAG CTG TAC CTC AAG AA
mSurvivin_R	CCA AAT CAG GCT CGT TCT CG
mMcl1_F	CTT GTA AGG ACG AAA CGG GAC
mMcl1_R	TCT AGG TCC TGT ACG TGG AAG
mBax_F	TGA AGA CAG GGG CCT TTT TG
mBax_R	AAT TCG CCG GAG ACA CTC G
mBak_F	ACT GCA TCA TTA CAT CGC CAG
mBak_R	CCC AAC AGA ACC ACA CCA AAA
mPuma_F	GAC CTC AAC GCG CAG TAC
mPuma_R	CCT AGT TGG GCT CCA TTT CTG
mNoxa_F	ACT GTG GTT CTG GCG CAG AT
mNoxa_R	TTG AGC ACA CTC GTC CTT CAA
mBim_F	AGT CAA CAC AAA CCC CAA GTC
mBim_R	TCC TGA GAC TGT CGT ATG GAA G
mBad_F	AAG TCC GAT CCC GGA ATC C
mBad_R	GCT CAC TCG GCT CAA ACT CT
mTxnip_F	GCAGGTGAGAACGAGATGGT
mTxnip_R	GAGAAAAGCCTTCACCCAGTAG
mAtf3_F	CGCCATCCAGAATAAACACCTC
mAtf3_R	CGCCTCCTTTTCCTCTCATCT
mChac1_F	CAGCGACAAGATGCCTGG
mChac1_R	CTCACATTCAGGTACTTCAGGG
mDusp1_F	CGTCTCAGCCAATTGTCCTAAC
mDusp1_R	TCCCTCCAGCATCCTTGAT
mChop_F	GCACCTATATCTCATCCCCAGG
mChop_R	ACTGGAATCTGGAGAGCGAG

APPENDIX F
Protocol: Protein Isolation and Western blot

1. **Lyse cells**
    a. Prepare ice-cold lysis buffer (keep on ice). Add fresh protease and phosphatase inhibitors if necessary for your intended application.

Tris/Triton Lysis buffer
20mM Tris-HCl (pH 7.6), 150mM NaCl, 1mM EDTA, 1mM EGTA, 1% Triton X-100, Protease inhibitor, Ser/Thr Phosphatase inhibitor, Tyrosine phosphatase inhibitor, ddH_20)

PIERCE RIPA lysis buffer
25mM Tris-HCl (pH 7.6), 150mM NaCl, 1% NP-40, 1% Sodium Deoxycholate, 0.1% SDS, Protease inhibitor, Ser/Thr Phosphatase inhibitor, Tyrosine phosphatase inhibitor, ddH_20)

Whole Cell Lysate Buffer 1 (SR Floyd et al. Nature 2013)
120mM Tris-HCl pH6.8, 4% SDS, Protease inhibitor, Ser/Thr Phosphatase inhibitor, Tyrosine phosphatase inhibitor, ddH_20)

    b. Harvest cells for lysis (optional: include floating cells if necessary)
        i. Option 1: Trypsinize cells, recue with serum media, then pellet cells (5min at 2100 rpm), remove supernatant (sup). Wash pellet with ice-cold 1x PBS. Pellet cells again, remove as much sup without taking up cells. Store cell pellet in -80^oC for lysis in future or continue with cell lysis step.
        ii. Option 2: Place your plate of cells on ice. Remove/discard media or collect for pooling later. Wash cell monolayer 2x with ice-cold PBS. Add small amount of PBS to cells (1-5ml), use cell scraper to detach, and collect cells to one side of plate in PBS (keep on ice). Pipet up and down to break up cell monolayer, and collect cells into a pre-chilled tube on ice. Pellet cells (5min at 2100 rpm at 4^oC). Remove as much PBS. Store pellet in -80^oC or continue with cell lysis step.
        iii. Option 3: Similar to option 2. Instead of scraping cells in PBS, add lysis buffer directly to cell monolayer (important to keep sample cold during this step).
    c. Cell lysis: For cell pellet, lyse cells in ice-cold lysis buffer of desired volume. Pipet up and down 50x (avoid generating bubbles). Incubate on ice for 5-10min. Pipet up and down 10-20x.
    d. (Optional) Sonicate lysate (to improve protein yield and fragment genomic DNA to reduce viscosity). Do NOT sonicate if you are doing a co-immunoprecipitation experiment. Sonicate samples in cold room or cold-

water bath. 5 sec sonication pulses should be followed by 10-20sec cool down to avoid excessive heat (up to 12 pulses).

e. Clear debris/insoluble material by 15-25 min centrifuge at 4°C at 13,000 rpm. Transfer supernatant (solubilized protein) to pre-chilled 1.5mL tube. If insoluble material desired for analysis, do not spin down or discard.
f. Store protein sample in -20°C (short-term) or -80°C (long-term). Or go directly to assess protein concentration with BCA assay.

2. Assess protein concentration using BCA protein assay kit (PIERCE, catalog #23225) in 96-well clear bottom plate

a. Thaw prepared BSA standards (A through I). Mix well by quick vortex, and add 25μL per well (duplicate or triplicate wells per standard).
b. Mix your thawed protein sample well by gentle pipetting or tube tapping. Add 5μL of your sample per well (single or triple replicates as desired).
c. Prepare BCA working reagent by mixing 20 parts reagent A with 1 part reagent B (1mL of reagent A per 20μL of reagent B). Prepare enough working reagent to add 200μL per well of standard and sample added to 96-well plate.
d. Add 200μL working reagent per well (use multi-channel pipetman if too many sample wells)
e. Rotate at room-temp (RT) on orbital shaker for 30sec (do not let solution from one well spill over to other wells).
f. Place plate lead or seal wells to prevent evaporation. Incubate 30min at 37°C. Repeat step 2e. Remove lid, and analyze plate with absorbance plate reader (preferably at 562nm wavelength).
g. Use absorbance data for BSA standards of defined protein concentration to generate a standard curve to calculate protein concentration from absorbance data for your samples.

3. Prepare protein samples to run on gel.

a. Mix desired amount of protein with 4x Laemmli sample buffer (200mM Tris-HCl pH6.8, 8% SDS, 40% glycerol, 50mM EDTA, 0.08% bromophenolblue), and add water to bring to final of 1x Laemmli sample buffer. Note: Make sure final volume does not exceed maximum capacity of wells in your SDS-PAGE gel.
b. Incubate at 95-100°C for 10min. Spin down.(Prepare SDS-PAGE apparatus during incubation.)

4. SDS-PAGE

a. Prepare 1L of 1x Tris/Glycine/SDS running buffer = running buffer
    i. Dilute 10x Tris/Glycine/SDS buffer pH8.3 (250mM Tris, 1920mM glycine, 1% SDS) to 1x in ultrapure water.
b. Choose pre-cast gel. For most proteins, use 4-20% gel (Bio-Rad catalog# 1123).

c. Remove green plastic seal under bottom of gel (If not removed, sample migration will not occur during electrophoresis). Assemble inner chamber for SDS-PAGE. (use plastic dam if only one gel is used). Fill inner chamber completely with running buffer (or at least above your wells). Remove combs evenly. Flush wells using pipetman if necessary.
d. Load protein samples and protein ladder. Place inner chamber into outer chamber tank (fill with running buffer).
e. Start with 75V for 20min, and then ramp up to 120-150V all the way down.

5. Gel Transfer

a. Prepare ice-cold transfer buffer:
    i. Add 100mL of 10x Tris/Glycine buffer pH8.3 (250mM Tris, 1920mM glycine) and 200 mL of 100% methanol to 700 mL ultrapure water.
b. Separate SDS-PAGE gel plates using tool provided in gel box. Cut off wells and bottom flap.
c. Cut rectangular Whatman 0.2μm nitrocellulose membrane (Protran Ref No. 10 402 495) for low molecular weight proteins. Use 0.4μm for larger proteins.
d. Wet membranes and sponge pads with transfer buffer.
e. Prepare sandwich

Red electrode (+)
Clear panel
1x Sponge pad
2x filter paper sheet
Nitrocellulose membrane sheet
2x filter paper sheet
1x sponge pad
black panel
black electrode (-)

f. Add ice pack, and close tank with lid. Run at 45V for 2 hours @ 4^{o}C in cold room. May need longer time for high-molecular weight proteins.

6. Block membrane in PBS-T (0.1% Tween-20) with 5% BSA for 30-60min at RT.
7. Incubate overnight at 4^{o}C while rotating in **Primary antibody** solution (antibody + PBS-T with 5% BSA).
8. Recycle or discard primary antibody solution.
9. Wash membrane 3x 5min with PBS-T.
10. Incubate membrane in **secondary antibody** solution (antibody + PBS-T) for 2 hours at RT.
    a. Dilute secondary antibody (anti-mouse-IgG-HRP or anti-rabbit-IgG-HRP) at 1:10,000 dilution in PBS-T. Dilution in PBS-T (5%BSA) is optional depending on what kind of background you obtain.
11. Wash membrane 3x 5min with PBS-T

12. **Prepare** 1:1 mixture of Bio-Rad **ECL reagent** (follow manufacturer protocol, catalog# 170-5061). Use just enough ECL to cover membrane.
13. **Cover/soak membrane in ECL** for 3-5min (make sure ECL does not dry out during this step). Briefly drain excess ECL from membrane (leave some). Cover membrane in saran or plastic wrap. Do not let membrane dry up.
14. Expose membranes in **chemiluminescence imager**.

Antibodies used for Western blot

Manufacturer	Catalog #	Antibody	Dilution
Abcam	ab128874	BRD4 (human isoform A,B,C)	1:1,000
Bethyl Labs	A301-985A100	BRD4 (mouse/human isoform A)	1:5,000
Cell Signaling Technology	4060	Phospho-AKT (Ser473)	1:1,000
Cell Signaling Technology	9272	Total AKT	1:1,000
Cell Signaling Technology	11815	ATF4	1:1,000
Cell Signaling Technology	2933	BIM	1:1,000
Cell Signaling Technology	3177	BiP	1:1,000
Cell Signaling Technology	2895	CHOP	1:1,000
Cell Signaling Technology	9661	Cleaved caspase-3 (Asp175)	1:500
Cell Signaling Technology	3398	Phospho-eIF2a (Ser51)	1:1,000
Cell Signaling Technology	4370	Phospho-ERK1/2 (Thr202/Tyr204)	1:1,000
Cell Signaling Technology	4695	Total ERK1/2	1:1,000
Cell Signaling Technology	2368	DYKDDDDK (FLAG) Tag	1:1,000
Cell Signaling Technology	2813	SETD7	1:1000
Cell Signaling Technology	3179	Phospho-PERK(Thr980)	1:500
Millipore	04-1151	CyclinD1	1:2,000
Millipore	04-576	PARP-1 (cleaved p25)	1:1,000
Santa Cruz Biotechnology	sc-492	BCL-2	1:200
Santa Cruz Biotechnology	sc-32233	GAPDH	1:10,000
Santa Cruz Biotechnology	sc-2030	Anti-Rabbit-IgG-HRP	1:10,000
Santa Cruz Biotechnology	sc-2031	Anti-Mouse-IgG-HRP	1:10,000

APPENDIX G
Protocol: Immunohistochemistry

Day 1

For Paraffin Embedded Sections:

1) **De-Paraffinize:** in Xylene, 3x, 3 min each

2) **Rehydrate:**
   a. 100% Ethanol, 2x, 1 min each
   b. 95% Ethanol, 2x, 1 min each
   c. ddH_2O, 1x 1min

3) **Antigen Retrieval:**
   Antigen retrieval solution: 0.01 M Citric acid pH 6,0.05% Tween-20, in PBS
   a. Bring antigen retrieval solution to a boil by microwaving.
   b. Place re-hydrated tissue sample slides in that boiling solution. Place lid on.
   c. Leave covered with lid for 5min at room temperature. Then remove lid, and allow solution with slides to cool to room temperature before proceeding.
   d. Rinse in dH_2O, 2x, 5 min each

4) **Quench:**
   13.3 mL 30% H_2O_2
   186.7 mL PBS
   200 mL PBS (2% H_2O_2)
   a. Quench for at least 1 min
   b. Rinse in PBS, 5 min

5) **Block (at least 1 hour in humidity chamber):**
   9 mL PBS
   +1 mL 100% goat serum
   PBG = PBS (10% goat serum) = Blocking solution

6) **1^o Antibody:**
   a. Dilute antibody in PBG (2% goat serum)
   b. Remove blocking solution from tissue, and replace with diluted antibody. Do let tissues dry during this step.
   c. Leave in humidity Chamber at 4^{o}C for overnight

Day 2

1) **Rinse slides in PBS**, 2x, 5 min each

2) **2^{o}Antibody**
   Need VECTASTAIN Elite ABC kit (Vector Laboratories – Catalog #PK-6100)

a. 1:200 dilution of biotinylated secondary Rabbit IgG- in (from ABC kit) in PBG(2%)
b. Incubate in humidity chamber at room temperature for 1 hr

Meanwhile, make avidin-biotinylated peroxidase conjugate (reagents from ABC kit)
5 mL PBS
2 Drops Reagent A. Mix Well
+2 Drops Reagent B. Mix Well
VectaStain Elite ABC reagent
(Let sit at room temperature for 30 min before use)

d. Rinse Slides in PBS, 2x 5 min each

3) **VectaStain Conjuagation:**
   a. 30 min at room temperature
   b. Rinse in PBS, 2x for 5 min each

4) **Visualization:** DAB HRP substrate kit(Vector Laboratories – Catalog# SK-4100)
5 mL dH_2O
2 drops buffer → mix well
4 drops DAB substrate → mix well
2drops H_2O_2 → Mix well
This yields your DAB HRP substrate

a. Use DAB HRP substrate immediately upon making solution (stain until desired signal is achieved and before presence of non-specific signal) by adding directly to tissue section after removing PBS.
b. Stop reaction by rinsing with dH_2O, 5 min
c. Counterstain if desired with Hematoxylin for 2 min

5) **Dehydrate**
   a. 95% Ethanol, 2x, 1 min each
   b. 100% Ethanol, 2x, 1 min each
   c. Xylene, 3x, 1 min each

6) **Seal Slides:** Drain off excess xylene (no need to remove all completely). Apply Cytoseal 60 solution (Thermo Scientific – Catalog# 8310-4), and mount cover slip to seal tissues in slide (make sure Cytoseal solution covers your tissues, and avoid bubbles to be trapped in sealed slide. Dry slides overnight at room temperature.

Antibodies used for Immunohistochemistry on Tissue Sections

Manufacturer	Catalog #	Antibody	Dilution
Abcam	ab6326	BrdU	1:200-1:1000
Abcam	ab75810	GAP43	1:400-1:1000
Bethyl Labs	A301-985A100	BRD4 (mouse/human isoform A)	1:400-1:2000
Dako	00067790	S100β	1:800-1:2000

Notes for IHC

- Fixation
    - Under-fixation can lead to edge staining, with strong signal on the edges of the section and no signal in the middle.
    - Over-fixation can mask the epitope. Antigen retrieval step can help overcome this masking.
    - If tissue is fixed for a long period of time (i.e. over a weekend), there may be no signal even after antigen retrieval.

- Use at least 5 micron tissue sections.
- Sections are best mounted on positively charged or APES (amino-propyl-ethoxy-silane) coated slides.
- Incomplete paraffin removal can cause poor staining of the section.
- Drying out of the section will cause non-specific antibody binding, and therefore high background staining.
- Fixation procedure causes the formation of methylene bridges, which cross-link w/ proteins and therefore mask antigenic sites.
- Antigen retrieval step serves to break the methylene bridges and expose the antigenic sites in order to allow the antibodies to bind.
- H_2O_2 (peroxide) suppresses endogenous peroxidase activity and therefore reduces background staining/signal.
- Abcam recommends TBS to give a cleaner background than PBS.
- 0.025% Triton X-100 in the TBS or PBS helps reduce the surface tension, thus allowing the reagents to cover the whole tissue section with ease. Also believed to dissolve Fc receptors, therefore reducing non-specific binding.
- BSA is included to reduce non-specific binding caused by hydrophobic interactions.

APPENDIX H
Protocol: Cell Cycle Analysis via BrdU and Propidium Iodide Flow Cytometry

Reagents

- D10 media
- *BrdU (Sigma-Aldrich – catalog #B5002)
- 100% Ethanol (ice-cold)
- 2N HCL/Triton X-100 (83.33 mL 12N HCl, 2.5 mL 100% Triton X-100, 414.17 mL ddH_2O)
- 0.1M $Na_2B_4O_7$, pH 8.5 (19.07g $Na_2B_4O_7$, bring 500mL with ddH_2O, then adjust pH with HCl)
- 1x PBS
- RNaseA (10mg/mL in ddH_2O)
- BSA
- Tween-20
- *FITC-Anti-BrdU-IgG (BD Biosciences – catalog #556028)
- FITC-Anti-Isotype control-IgG1 (BD Biosciences – catalog #556028)
- *Propidium Iodide = PI (Life Technologies – catalog #P3566)

*Light-sensitive reagents.

Protocol

1. Plate ~200,000 MPNST cells in 10cm tissue culture plate.
    a. Triplicate plates per condition tested
    b. Include 3 plates for controls (Isotype Control only, PI only, or no staining)

2. Next day, aspirate media, and replace with media containing drug of interest or vehicle.

3. Two to 3 days later or before cells reach 75% confluency, pulse cells with BrdU.
    a. Using a 32.56 mM stock of BrdU, add BrdU directly to media to a final concentration of 10μM. Place cells back into 37°C incubator. (Note, do not give cells any new media with serum as this can stimulate proliferation of cells leading to increased BrdU uptake by cells. BrdU is light-sensitive)

4. Stop BrdU pulse by aspirating media, and washing with PBS followed by trypsinization, neutralization with D10 media, and collection into 15mL conical tubes.
    a. For most mouse MPNST cells, 5-10min BrdU pulse is sufficient to label cells that are synthesizing DNA. For human MPNST cells (S462), do a 30min BrdU pulse.

5. Centrifuge cells at 2100rpm for 5min. Remove supernatant. Wash cell pellet once with at least 5mL cold 1x PBS.

6. Centrifuge cells at 2100 rpm for 5min. Remove supernatant. Keep cells on ice. Protect from light when possible.

7. Resuspend cells in 100μL of ice-cold 1x PBS. While vortexing cells, fix cells by drop-wise addition of 5mL of ice-cold 100% ethanol to cells in 15mL conical tube. Do not vortex more than 10seconds.

8. Incubate overnight at 4^{o}C (protected from light) to allow fixation of cells.

9. Next day, centrifuge cells at 2100 rpm for 5 min at 4^{o}C. Remove as much supernatant without disturbing pellet. Leave small amount (less than 80 μL of fluid).

10. Resuspend cell pellet well with 200 μL pipetman to get a roughly single cells suspension, and then immediately add 1mL of 2N HCl/Triton X-100.
    a. The acid is used to denature the DNA such that the BrdU antibody will be able to access the incorporated BrdU in genomic DNA.
    b. If pellet is not resuspended before addition of acid, then immediate addition of acid can result in more clumpy solution. Single cells are desired flow cytometry rather than cells stuck together as clumps.

11. Incubate at room temperature for 30 minutes (protected from light).

12. Centrifuge cells at 2100 rpm for 5 min at 4^{o}C. Remove as much supernatant without disturbing pellet. Neutralize acid by resuspending pellet in 100 μL of 0.1M $Na_2B_4O_7$, followed by additional 900 μL of this solution.

13. Centrifuge cells at 2100 rpm for 5 min at 4^{o}C. Remove as much supernatant without disturbing pellet.

14. For each sample, prepare master mix (for FITC-BrdU antibody staining) that includes the following:

    + 60 μL of 0.5% Tween-20/1%BSA/PBS solution
    + 10 μL of FITC-anti-BrdU (or Isotype control for negative control)
    + 5 μL of RNase A (10 mg/mL)

    75 μL antibody staining solution per sample

15. Resuspend each sample with 75 μL of mastermix. Store samples at 4^{o}C overnight (protected from light). During this time, prepare 5 μg/mL PI (propidium iodide) solution in 1x PBS to stain you cells with. Depending on your cell pellet size or number of cells, you resuspend in a volume that can give you 300-1000 counts per second on the flow cytometer. Counts are the objects or cells detected by the cytometer. The more diluted your sample, the longer it will take to analyze at least 10,000 cells for analysis.

16. Next day, centrifuge cells at 2100 rpm for 2 min at 4^{o}C. Remove as much supernatant without disturbing pellet. Resuspend pellet with 5 μg/mL PI solution. Allow 20-30 minutes for staining to occur at room temperature in the dark.

17. Analyze all samples by flow cytometry using FACSCalibur Flow cytometer (BD Biosciences) at the UT Southwestern flow cytometry core facility located in north campus (NA7.300). Detect FITC at 530nm wavelength emission and PI at 670nm wavelength emission.

18. Use FlowJo software (Tree Star) at flow cytometry facility to analyze data.

APPENDIX I
Protocol: Apoptosis Analysis by Annexin V/PI Staining and Flow Cytometry

Reagents

- D10 media
- Trypsin
- 1x PBS (ice-cold)
- Annexin V-FITC Kit (Miltenyi Biotec – Catalog #130-092-052)
    - *(100x) Annexin V-FITC
    - (20x) Binding buffer stock solution
    - *(200x) PI solution at 100 μg/mL
- *FITC-Anti-BrdU-IgG (BD Biosciences – catalog #556028)
- 5mL Polystyrene Round-bottom FACS tube with cell-strainer cap (BD Falcon – catalog # 352235)
- Annexin V/PI staining solution
    - Dilute 20x Annexin V binding buffer to 1x in ddH2O
    - Add 100x Annexin V-FITC and 200x PI to 1x final. Mix well by vortexing briefly.
    - Prepare some buffer with no FITC nor PI or FITC only or PI only for controls and compensation adjustment.

  *Light-sensitive reagents.

Protocol

1. Plate cells in 12-well tissue culture plates in 1 mL D10 media per well overnight
    a. Plate triplicate well per condition being assayed. Include 3 additional wells for the following controls (no staining, Annexin V-FITC only, PI only)
    b. Plating density is determined empirically for each cell line. The longer time you will culture your cells, the fewer cells you should plate initially. The shorter time you culture your cells, the more cells you should plate. You need at least 10,000 cell counts by flow cytometry. For mouse MPNST cells, plate 20,000 cells per well if you will harvest cells 3-4 days later.
    c. For cell death analysis, your cells should be evenly distributed in the well. Clustered cells may respond different to drugs or different conditions.

2. Next day after cells have properly attached, and appear healthy, prepare your drug media. Aspirate all media from wells, and immediately replace with drug media by gently pipetting down on one side of well. Place back incubator.
    a. Note: If media is not replaced in less than 1 minute, the cells may dry up, leading to death of cells (false-positive result). Best to aspirate a few wells or for one drug media condition at a time.

3. When cells are ready for analysis of apoptosis, for each well, use 1mL pipetman to collect the floating cells into a 15mL conical tube.

4. Rinse well with 500 μL of 1x PBS, and then collect that PBS into the conical tube.

5. Add 180 μL of Trypsin, and incubate at 37^{o}C for 4min.Check to see if cells are dissociated and rounded.

6. Add 800 μL of DMEM with 5% FBS to neutralize the Trypsin.

7. Using 1mL pipetman, pipet cells up and down 6 times to further dissociate cells, and then transfer to conical tube.

8. Rinse the well with 500 μL of 1x PBS, and transfer to conical tube. Repeat this step once more.

9. Centrifuge at 2100 rpm for 5min at 4^{o}C.

10. Carefully aspirate supernatant. Avoid disturbing pellet. It is okay to leave 50 μL of supernatant.

11. Resuspend cell pellet in 300 μL of Annexin V/PI staining solution.

12. Pass cell solution through FACS tube with meshed/cell-strainer cap.
    a. Note, very clumpy or concentrated cells will be more difficult to pass through. For concentrated cells, if a problem, dilute slightly with further Annexin V/PI staining solution, and try again to pass through.

13. Keep tube on ice, and protect sample from light.

14. Analyze all samples by flow cytometry using FACSCalibur Flow cytometer (BD Biosciences) at the UT Southwestern flow cytometry core facility located in north campus (NA7.300). Detect FITC at 530nm wavelength emission and PI at 670nm wavelength emission.

15. Use FlowJo software (Tree Star) at flow cytometry facility to analyze data.

APPENDIX J
Protocol: Chromatin Immunoprecipitation (ChIP)-PCR

Reagents

- 16% methanol free-formaldehyde (Thermo Scientific – Catalog#28908)
- 100x Halt Protease Inhibitor Cocktail (Thermo Scientific – Catalog#87786)
- 100x Halt Phosphatase Inhibitor Cocktail (Thermo Scientific – Catalog#78420)
- ChIP-grade Protein A/G Plus Agarose beads (Thermo Scientific – Catalog#26159)
- RNaseA (10mg/mL in ddH_2O)
- Proteinase K (Research Products International Corp. – Catalog #39450-01-6)
- 2x iTaq Universal SYBR green supermix (Bio-Rad – Catalog#172-5124)
- *Hypotonic Lysis buffer (10mM Tris-HCl pH8, 10mM NaCl, 3mM MgCl2)
- *SDS Lysis buffer (50mM Tris-HCl pH8, 10mM EDTA, 10mM EGTA, 1% SDS)
- *IP Dilution buffer (20mM Tris-HCl pH 8, 150mM EDTA, 2mM EDTA pH 8, 1% Triton X-100)
- *Wash buffer (20mM Tris-HCl pH 8, 150mM NaCl, 2mM EDTA pH 8, 1% Triton X-100, 0.1% SDS)
- *Final Wash buffer (20mM Tris-HCl pH 8, 500mM NaCl, 2mM EDTA pH 8, 1% Triton X-100, 0.1% SDS)
- *Elution buffer (100mM $NaHCO_3$, 1% SDS)
  *All buffers should be supplemented with protease inhibitors and phosphatase inhibitors prior to use. Keep all buffers cold at 4^oC.

Protocol

1. (Evening) Plate cells to density of 4-5 x 10^6 sMPNST cells per 150mm tissue culture plate. 25 mL volume final volume per plate.

2. (Next Morning) Add vehicle or drug directly to media, and swirl well to mix evenly on to cells.
   a. Make sure cells are evenly dispersed on dishes.

3. (24 hours later) Incubate plates at room temperature for 30 min to equilibrate to room temperature.

4. Fix cells:
   a. Add 1.5 mL of fresh 16% formaldehyde (methanol-free) to each plate (per 25 mL volume) to yield 1% final.
   b. Mix by swirling plates on orbital shaker gently at RT for 10 min. (cover plates with foil since formaldehyde is light-sensitive).
   c. Immediately stop the fixing by quenching with 2.7 mL of 10X glycine (1.25 M) per plate to yield>125 mM glycine (final). Gently rotate on orbital shaker for 5 min at RT.

5. Harvest cells:
    a. Place all plates on ice.
    b. Aspirate media all media.
    c. Wash 2X with 15 mL cold-sterile 1x PBS. Remove all excess PBS.
    d. Add 5 mL of cold-PBS to plate. Scrape off cells to collect into PBS on one side. Pipet up and down to break cells in to single cell suspension. Transfer cells to 50 mL conical tube pre-chilled on ice.
    e. Add 10 mL PBS to plate, and transfer remainder into the first collection in 50 mL tube.
    f. Centrifuge for 8 min at 4^{o}C at 5000 x g. Aspirate sup carefully
    g. Resuspend in 1mL cold PBS, and transfer to 1.5 mL tube. Centrifuge for 5 min at 5000xg at 4^{o}C. Aspirate sup.

6. Lyse cells:
    a. Resuspend pellet in 800 μL of HLB (Hypotonic lysis buffer). Pipet up and down 20 times, and incubate on ice for 10min.
    b. Centrifuge for at 5000 x g for 5min at 4^{o}C. Aspirate sup.
    c. Resuspend nuclei pellet in 500 μL of SDS lysis buffer. Pipet up and down on ice 30 times. Incubate on ice for 10min. (over long period, 1% SDS in buffer will precipitate. May need to remove from ice, and pipet up and down a few time to re-dissolve SDS)
    d. Dilute each sample with 500 μL of IP dilution buffer. (This will reduce SDS percentage to prevent precipitation. High SDS percentage not suggested for IP).
    e. Mix, and collect 50 μL of each sample for unsonicated control.

7. Sonicate chromatin samples
    a. Experimentally determine optimal shearing conditions for downstream application.

8. Clear samples by centrifuging at 4^{o}C for 30sec at 8000 x g. Transfer sonicated chromatin supernatant to fresh 1.5mL tube on ice. Take 2 μL for analysis on NanoDrop spectrophotometer for DNA concentration. Store sample in -80^{o}C for up to month before use or continue with chromatin immunoprecipitation (ChIP).

9. Based on DNA concentration measured, calculate amount of chromatin equivalent to 25 μg DNA to use as input per immunoprecipitation (IP), and 10% of that for the 10% input control.

10. Thaw chromatin sample on ice. Mix well with pipetman gently. Aliquot 2 x 25 μg DNA equivalent chromatin and 2.5 μg DNA equivalent chromatin (your

10% input sample) to 1.5mL tubes. Save 10% input sample in minus -20°C for purification of DNA after IP.

11. Now the 25 μg DNA equivalent chromatin, dilute 1:10 with IP dilution buffer. Add 1 μg of negative control antibody. Incubate for 60 min at 4°C while rotating. Add 20 μL of protein A/G agarose beads. Incubate for 60 min at 4°C while rotating.

12. Centrifuge antibody-bead complex at 4°C for 2min at 2000 x g. Transfer pre-cleared chromatin sample to new 1.5mL tube (pre-chilled on ice). Add 1-10 μg of specific antibody or negative control antibody.

13. Incubate at 4°C for 2 hours while rotating. Add 30 mL of protein A/G beads per IP. Incubate at 4°C for 1 hour while rotating.

14. Centrifuge antibody-bead complex at 4°C for 2 min at 2000 x g. Remove as much supernatant without removing beads. Wash 3x with 1mL of Wash buffer. Centrifuge at 4°C for 2 min at 2000 x g between each wash.

15. Wash beads 1x with 1mL Final Wash buffer. Centrifuge beads at 4°C for 2 min at 2000 x g. Remove as much supernatant without removing beads.

16. Elute DNA by adding 120 μL of Elution buffer to the protein A/G beads, and rotate for 15 min at 30°C.

17. Centrifuge for 1 min at 2000 x g, and transfer supernatant to new 1.5mL tube. Store at supernatant at -20°C or continue with DNA purification.

18. Adjust IP and 10% input samples to 150 μL final volume with water. Add additional 300 μL of water.

19. For each sample, add 6 μL of 10 mg/mL RNaseA, and 18 μL of 5M NaCl. Mix and incubate at 37°C for 60min.

20. Add 6 μL of 20 mg/mL Proteinase K, mix and incubate 4 hours or overnight at 65°C while shaking. This step will digest proteins and help with reversing cross-links.

21. Purify DNA by phenol: chloroform extraction followed by ethanol precipitation, and resuspension of DNA in at least 100 μL of ddH_2O. Dilute 10% input DNA to 2.5 ng/μL. Use higher concentration DNA if necessary to achieve higher signal over background.

22. Setup qPCR reactions
    a. 3.75 μL nuclease free-water + 10 μL of 2x SYBR Green supermix + 1.25μL of 10 mM primer mix (forward + reverse) + 5 μL DNA sample.
    b. Analyze on CFX Connect Real-time PCR platform (Bio-Rad).
    c. Use % input method for data analysis (see http://www.lifetechnologies.com/us/en/home/life-science/epigenetics-noncoding-rna-research/chromatin-remodeling/chromatin-immunoprecipitation-chip/chip-analysis.html).

Antibodies used for ChIP

Manufacturer	Catalog #	Antibody	Amount Used per ChIP
Bethyl Labs	A301-985A100	BRD4 (mouse/human isoform A)	4 μg
Cell Signaling Technology	2729	Normal Rabbit IgG	4 μg

ChIP-qPCR primers used

Primer Name	Primer Sequence (5'-->3')
mCcnd1_-2670_F	TGA AAT CCG CTC AGG GTA AC
mCcnd1_-2670_R	GGA CTT GGC TGT TTC TGC TC
mCcnd1_-955_F	TCA CCT TAT CGG CTC ACA AGT
mCcnd1_-955_R	AGA CAC GAT AGG CTC CTT CC
mCcnd1_-585_F	CCA GCG AGG AGG AAT AGA TG
mCcnd1_-585_R	AGC GTC CCT GTC TTC TTT CA
mCcnd1_-98_F	CCC AGT TTG GAG AGA AGC AG
mCcnd1_-98_R	ACT CCC CTG TAG TCC GTG TG
mCcnd1_+1037_F	TGC CTG GCC CAG AGA AA
mCcnd1_+1037_R	CAG GTT CCT CCA AAT CCA GAA C

BIBLIOGRAPHY

Ahuja, D., Saenz-Robles, M.T., and Pipas, J.M. (2005). SV40 large T antigen targets multiple cellular pathways to elicit cellular transformation. Oncogene *24*, 7729-7745.

Albers, A.C., and Gutmann, D.H. (2009). Gliomas in patients with neurofibromatosis type 1. Expert Review of Neurotherapeutics *9*, 535-539.

Albritton, K., Rankin, C., Coffin, C., Ratner, N., Budd, G., Schuetze, S., Randall, R., Declue, J., and Borden, E. (2006). Phase II study of erlotinib in metastatic or unresectable malignant peripheral nerve sheath tumors (MPNST). Journal of Clinical Oncology *24*, 9518.

Alsarraj, J., Faraji, F., Geiger, T.R., Mattaini, K.R., Williams, M., Wu, J., Ha, N.-H., Merlino, T., Walker, R.C., Bosley, A.D.*, et al.* (2013). BRD4 Short Isoform Interacts with RRP1B, SIPA1 and Components of the LINC Complex at the Inner Face of the Nuclear Membrane. PLoS ONE *8*, e80746.

Alsarraj, J., Walker, R.C., Webster, J.D., Geiger, T.R., Crawford, N.P.S., Simpson, R.M., Ozato, K., and Hunter, K.W. (2011). Deletion of the Proline-Rich Region of the Murine Metastasis Susceptibility Gene Brd4 Promotes Epithelial-to-Mesenchymal Transition- and Stem Cell-Like Conversion. Cancer Research *71*, 3121-3131.

Altman, B.J., Wofford, J.A., Zhao, Y., Coloff, J.L., Ferguson, E.C., Wieman, H.L., Day, A.E., Ilkayeva, O., and Rathmell, J.C. (2009). Autophagy Provides Nutrients but Can Lead to Chop-dependent Induction of Bim to Sensitize Growth Factor–deprived Cells to Apoptosis. Molecular Biology of the Cell *20*, 1180-1191.

Anand, P., Brown, Jonathan D., Lin, Charles Y., Qi, J., Zhang, R., Artero, Pedro C., Alaiti, M.A., Bullard, J., Alazem, K., Margulies, Kenneth B.*, et al.* (2013). BET Bromodomains Mediate Transcriptional Pause Release in Heart Failure. Cell *154*, 569-582.

Anders, L., Guenther, M.G., Qi, J., Fan, Z.P., Marineau, J.J., Rahl, P.B., Loven, J., Sigova, A.A., Smith, W.B., Lee, T.I.*, et al.* (2014). Genome-wide localization of small molecules. Nat Biotech *32*, 92-96.

Asangani, I.A., Dommeti, V.L., Wang, X., Malik, R., Cieslik, M., Yang, R., Escara-Wilke, J., Wilder-Romans, K., Dhanireddy, S., Engelke, C.*, et al.* (2014). Therapeutic targeting of BET bromodomain proteins in castration-resistant prostate cancer. Nature *advance online publication*.

Bajenaru, M.L., Hernandez, M.R., Perry, A., Zhu, Y., Parada, L.F., Garbow, J.R., and Gutmann, D.H. (2003). Optic Nerve Glioma in Mice Requires Astrocyte Nf1 Gene Inactivation and Nf1 Brain Heterozygosity. Cancer Research *63*, 8573-8577.

Ballester, R., Marchuk, D., Boguski, M., Saulino, A., Letcher, R., Wigler, M., and Collins, F. (1990). The NF1 locus encodes a protein functionally related to mammalian GAP and yeast IRA proteins. Cell *63*, 851-859.

Basseri, S., and Austin, R.C. (2012). Endoplasmic Reticulum Stress and Lipid Metabolism: Mechanisms and Therapeutic Potential. Biochemistry Research International *2012*, 13.

Bean, G.R., Ganesan, Y.T., Dong, Y., Takeda, S., Liu, H., Chan, P.M., Huang, Y., Chodosh, L.A., Zambetti, G.P., Hsieh, J.J.-D.*, et al.* (2013). PUMA and BIM Are Required for Oncogene Inactivation-Induced Apoptosis. Sci Signal *6*, ra20-.
Beck, D., Niessner, H., Smalley, K.S.M., Flaherty, K., Paraiso, K.H.T., Busch, C., Sinnberg, T., Vasseur, S., Iovanna, J.L., Driessen, S.*, et al.* (2013). Vemurafenib Potently Induces Endoplasmic Reticulum Stress-Mediated Apoptosis in BRAFV600E Melanoma Cells. Sci Signal *6*, ra7-.
Belkina, A.C., and Denis, G.V. (2012). BET domain co-regulators in obesity, inflammation and cancer. Nat Rev Cancer *12*, 465-477.
Belkina, A.C., Nikolajczyk, B.S., and Denis, G.V. (2013). BET Protein Function Is Required for Inflammation: Brd2 Genetic Disruption and BET Inhibitor JQ1 Impair Mouse Macrophage Inflammatory Responses. The Journal of Immunology.
Bhadury, J., Nilsson, L.M., Veppil Muralidharan, S., Green, L.C., Li, Z., Gesner, E.M., Hansen, H.C., Keller, U.B., McLure, K.G., and Nilsson, J.A. (2014). BET and HDAC inhibitors induce similar genes and biological effects and synergize to kill in Myc-induced murine lymphoma. Proceedings of the National Academy of Sciences.
Biernaskie, J.A., McKenzie, I.A., Toma, J.G., and Miller, F.D. (2007). Isolation of skin-derived precursors (SKPs) and differentiation and enrichment of their Schwann cell progeny. Nat Protocols *1*, 2803-2812.
Brannan, C.I., Perkins, A.S., Vogel, K.S., Ratner, N., Nordlund, M.L., Reid, S.W., Buchberg, A.M., Jenkins, N.A., Parada, L.F., and Copeland, N.G. (1994). Targeted disruption of the neurofibromatosis type-1 gene leads to developmental abnormalities in heart and various neural crest-derived tissues. Genes & Development *8*, 1019-1029.
Burgess, M.R., Skaggs, B.J., Shah, N.P., Lee, F.Y., and Sawyers, C.L. (2005). Comparative analysis of two clinically active BCR-ABL kinase inhibitors reveals the role of conformation-specific binding in resistance. Proceedings of the National Academy of Sciences of the United States of America *102*, 3395-3400.
Campaner, S., Spreafico, F., Burgold, T., Doni, M., Rosato, U., Amati, B., and Testa, G. (2011). The Methyltransferase Set7/9 (Setd7) Is Dispensable for the p53-Mediated DNA Damage Response In Vivo. Molecular cell *43*, 681-688.
Chaidos, A., Caputo, V., Gouvedenou, K., Liu, B., Marigo, I., Chaudhry, M.S., Rotolo, A., Tough, D.F., Smithers, N.N., Bassil, A.K.*, et al.* (2014). Potent antimyeloma activity of the novel bromodomain inhibitors I-BET151 and I-BET762. Blood *123*, 697-705.
Chau, V., Lim, S.K., Mo, W., Liu, C., Patel, A.J., McKay, R.M., Wei, S., Posner, B.A., De Brabander, J.K., Williams, N.S.*, et al.* (2013a). Preclinical Therapeutic Efficacy of a Novel Pharmacologic Inducer of Apoptosis in Malignant Peripheral Nerve Sheath Tumors. Cancer Research.
Chau, V., Lim, S.K., Mo, W., Liu, C., Patel, A.J., McKay, R.M., Wei, S., Posner, B.A., De Brabander, J.K., Williams, N.S.*, et al.* (2013b). Preclinical therapeutic efficacy of a novel pharmacological inducer of apoptosis in malignant peripheral nerve sheath tumors. Cancer Research.
Cheng, E.H.Y.A., Wei, M.C., Weiler, S., Flavell, R.A., Mak, T.W., Lindsten, T., and Korsmeyer, S.J. (2001). BCL-2, BCL-XL Sequester BH3 Domain-Only Molecules

Preventing BAX- and BAK-Mediated Mitochondrial Apoptosis. Molecular cell *8*, 705-711.
Cheng, Z., Gong, Y., Ma, Y., Lu, K., Lu, X., Pierce, L.A., Thompson, R.C., Muller, S., Knapp, S., and Wang, J. (2013). Inhibition of BET Bromodomain Targets Genetically Diverse Glioblastoma. Clinical Cancer Research.
Christensen, J.B., and Imperiale, M.J. (1995). Inactivation of the retinoblastoma susceptibility protein is not sufficient for the transforming function of the conserved region 2-like domain of simian virus 40 large T antigen. Journal of Virology *69*, 3945-3948.
Chuikov, S., Kurash, J.K., Wilson, J.R., Xiao, B., Justin, N., Ivanov, G.S., McKinney, K., Tempst, P., Prives, C., Gamblin, S.J.*, et al.* (2004). Regulation of p53 activity through lysine methylation. Nature *432*, 353-360.
Cichowski, K., Shih, T.S., Schmitt, E., Santiago, S., Reilly, K., McLaughlin, M.E., Bronson, R.T., and Jacks, T. (1999). Mouse Models of Tumor Development in Neurofibromatosis Type 1. Science *286*, 2172-2176.
Clarke, Hanna J., Chambers, Joseph E., Liniker, E., and Marciniak, Stefan J. (2014). Endoplasmic Reticulum Stress in Malignancy. Cancer Cell *25*, 563-573.
Cleary, M.L., Smith, S.D., and Sklar, J. (1986). Cloning and structural analysis of cDNAs for bcl-2 and a hybrid bcl-2/immunoglobulin transcript resulting from the t(14;18) translocation. Cell *47*, 19-28.
Corcoran, Ryan B., Cheng, Katherine A., Hata, Aaron N., Faber, Anthony C., Ebi, H., Coffee, Erin M., Greninger, P., Brown, Ronald D., Godfrey, Jason T., Cohoon, Travis J.*, et al.* (2013). Synthetic Lethal Interaction of Combined BCL-XL and MEK Inhibition Promotes Tumor Regressions in KRAS Mutant Cancer Models. Cancer Cell *23*, 121-128.
Cui, Y., Costa, R.M., Murphy, G.G., Elgersma, Y., Zhu, Y., Gutmann, D.H., Parada, L.F., Mody, I., and Silva, A.J. (2008). Neurofibromin Regulation of ERK Signaling Modulates GABA Release and Learning. Cell *135*, 549-560.
Dasgupta, B., Yi, Y., Chen, D.Y., Weber, J.D., and Gutmann, D.H. (2005). Proteomic Analysis Reveals Hyperactivation of the Mammalian Target of Rapamycin Pathway in Neurofibromatosis 1–Associated Human and Mouse Brain Tumors. Cancer Research *65*, 2755-2760.
Dawson, M.A., Prinjha, R.K., Dittmann, A., Giotopoulos, G., Bantscheff, M., Chan, W.-I., Robson, S.C., Chung, C.-w., Hopf, C., Savitski, M.M.*, et al.* (2011). Inhibition of BET recruitment to chromatin as an effective treatment for MLL-fusion leukaemia. Nature *478*, 529-533.
De Raedt, T., Maertens, O., Chmara, M., Brems, H., Heyns, I., Sciot, R., Majounie, E., Upadhyaya, M., De Schepper, S., Speleman, F.*, et al.* (2006). Somatic loss of wild type NF1 allele in neurofibromas: Comparison of NF1 microdeletion and non-microdeletion patients. Genes, Chromosomes and Cancer *45*, 893-904.
Delmore, Jake E., Issa, Ghayas C., Lemieux, Madeleine E., Rahl, Peter B., Shi, J., Jacobs, Hannah M., Kastritis, E., Gilpatrick, T., Paranal, Ronald M., Qi, J.*, et al.* (2011). BET Bromodomain Inhibition as a Therapeutic Strategy to Target c-Myc. Cell *146*, 904-917.

Dey, A., Chitsaz, F., Abbasi, A., Misteli, T., and Ozato, K. (2003). The double bromodomain protein Brd4 binds to acetylated chromatin during interphase and mitosis. Proceedings of the National Academy of Sciences *100*, 8758-8763.
Donner, A.J., Ebmeier, C.C., Taatjes, D.J., and Espinosa, J.M. (2010). CDK8 is a positive regulator of transcriptional elongation within the serum response network. Nat Struct Mol Biol *17*, 194-201.
Duong, T., Sbidian, E., Valeyrie-Allanore, L., Vialette, C., Ferkal, S., Hadj-Rabia, S., Glorion, C., Lyonnet, S., Zerah, M., Kemlin, I.*, et al.* (2011). Mortality Associated with Neurofibromatosis 1: A Cohort Study of 1895 Patients in 1980-2006 in France. Orphanet Journal of Rare Diseases *6*, 18.
Endo, M., Kobayashi, C., Setsu, N., Takahashi, Y., Kohashi, K., Yamamoto, H., Tamiya, S., Matsuda, S., Iwamoto, Y., Tsuneyoshi, M.*, et al.* (2011). Prognostic Significance of p14ARF, p15INK4b, and p16INK4a Inactivation in Malignant Peripheral Nerve Sheath Tumors. Clinical Cancer Research *17*, 3771-3782.
Farina, A., Hattori, M., Qin, J., Nakatani, Y., Minato, N., and Ozato, K. (2004). Bromodomain Protein Brd4 Binds to GTPase-Activating SPA-1, Modulating Its Activity and Subcellular Localization. Molecular and Cellular Biology *24*, 9059-9069.
Fei, W., Wang, H., Fu, X., Bielby, C., and Yang, H. (2009). Conditions of endoplasmic reticulum stress stimulate lipid droplet formation in Saccharomyces cerevisiae. Biochemical Journal *424*, 61-67.
Fernandes, K.J.L., McKenzie, I.A., Mill, P., Smith, K.M., Akhavan, M., Barnabe-Heider, F., Biernaskie, J., Junek, A., Kobayashi, N.R., Toma, J.G.*, et al.* (2004). A dermal niche for multipotent adult skin-derived precursor cells. Nat Cell Biol *6*, 1082-1093.
Ferner, R.E., Huson, S.M., Thomas, N., Moss, C., Willshaw, H., Evans, D.G., Upadhyaya, M., Towers, R., Gleeson, M., Steiger, C.*, et al.* (2007). Guidelines for the diagnosis and management of individuals with neurofibromatosis 1. Journal of Medical Genetics *44*, 81-88.
Filippakopoulos, P., and Knapp, S. (2014). Targeting bromodomains: epigenetic readers of lysine acetylation. Nat Rev Drug Discov *13*, 337-356.
Filippakopoulos, P., Qi, J., Picaud, S., Shen, Y., Smith, W.B., Fedorov, O., Morse, E.M., Keates, T., Hickman, T.T., Felletar, I.*, et al.* (2010). Selective inhibition of BET bromodomains. Nature *468*, 1067-1073.
Firestein, R., Bass, A.J., Kim, S.Y., Dunn, I.F., Silver, S.J., Guney, I., Freed, E., Ligon, A.H., Vena, N., Ogino, S.*, et al.* (2008). CDK8 is a colorectal cancer oncogene that regulates [bgr]-catenin activity. Nature *455*, 547-551.
Fiskus, W., Sharma, S., Qi, J., Valenta, J.A., Schaub, L.J., Shah, B., Peth, K., Portier, B.P., Rodriguez, M., Devaraj, S.G.T.*, et al.* (2014). Highly Active Combination of BRD4 Antagonist and Histone Deacetylase Inhibitor against Human Acute Myelogenous Leukemia Cells. Molecular Cancer Therapeutics *13*, 1142-1154.
Floyd, S.R., Pacold, M.E., Huang, Q., Clarke, S.M., Lam, F.C., Cannell, I.G., Bryson, B.D., Rameseder, J., Lee, M.J., Blake, E.J.*, et al.* (2013). The bromodomain protein Brd4 insulates chromatin from DNA damage signalling. Nature *498*, 246-250.
Frahm, S., Mautner, V.-F., Brems, H., Legius, E., Debiec-Rychter, M., Friedrich, R.E., Knöfel, W.T., Peiper, M., and Kluwe, L. (2004). Genetic and phenotypic characterization

of tumor cells derived from malignant peripheral nerve sheath tumors of neurofibromatosis type 1 patients. Neurobiology of Disease *16*, 85-91.
Gallagher, S.J., Mijatov, B., Gunatilake, D., Tiffen, J.C., Gowrishankar, K., Jin, L., Pupo, G.M., Cullinane, C., Prinjha, R.K., Smithers, N.*, et al.* (2014). The Epigenetic Regulator I-BET151 Induces BIM-Dependent Apoptosis and Cell Cycle Arrest of Human Melanoma Cells. J Invest Dermatol.
Gregorian, C., Nakashima, J., Dry, S.M., Nghiemphu, P.L., Smith, K.B., Ao, Y., Dang, J., Lawson, G., Mellinghoff, I.K., Mischel, P.S.*, et al.* (2009). PTEN dosage is essential for neurofibroma development and malignant transformation. Proceedings of the National Academy of Sciences *106*, 19479-19484.
Gröschel, S., Sanders, Mathijs A., Hoogenboezem, R., de Wit, E., Bouwman, Britta A.M., Erpelinck, C., van der Velden, Vincent H.J., Havermans, M., Avellino, R., van Lom, K.*, et al.* (2014). A Single Oncogenic Enhancer Rearrangement Causes Concomitant EVI1 and GATA2 Deregulation in Leukemia. Cell *157*, 369-381.
Heyer, J., Kwong, L.N., Lowe, S.W., and Chin, L. (2010). Non-germline genetically engineered mouse models for translational cancer research. Nat Rev Cancer *10*, 470-480.
Hnisz, D., Abraham, Brian J., Lee, Tong I., Lau, A., Saint-André, V., Sigova, Alla A., Hoke, Heather A., and Young, Richard A. (2013). Super-Enhancers in the Control of Cell Identity and Disease. Cell *155*, 934-947.
Houzelstein, D., Bullock, S.L., Lynch, D.E., Grigorieva, E.F., Wilson, V.A., and Beddington, R.S.P. (2002). Growth and Early Postimplantation Defects in Mice Deficient for the Bromodomain-Containing Protein Brd4†. Molecular and Cellular Biology *22*, 3794-3802.
Huijbregts, R.P.H., Roth, K.A., Schmidt, R.E., and Carroll, S.L. (2003). Hypertrophic Neuropathies and Malignant Peripheral Nerve Sheath Tumors in Transgenic Mice Overexpressing Glial Growth Factor β3 in Myelinating Schwann Cells. The Journal of Neuroscience *23*, 7269-7280.
Ismat, F.A., Xu, J., Lu, M.M., and Epstein, J.A. (2006). The neurofibromin GAP-related domain rescues endothelial but not neural crest development in Nf1–/– mice. The Journal of Clinical Investigation *116*, 2378-2384.
Jacks, T., Shih, T.S., Schmitt, E.M., Bronson, R.T., Bernards, A., and Weinberg, R.A. (1994). Tumour predisposition in mice heterozygous for a targeted mutation in Nf1. Nat Genet *7*, 353-361.
Jang, M.K., Mochizuki, K., Zhou, M., Jeong, H.-S., Brady, J.N., and Ozato, K. (2005). The Bromodomain Protein Brd4 Is a Positive Regulatory Component of P-TEFb and Stimulates RNA Polymerase II-Dependent Transcription. Molecular cell *19*, 523-534.
Jessen, K.R., and Mirsky, R. (2005). The origin and development of glial cells in peripheral nerves. Nat Rev Neurosci *6*, 671-682.
Jessen, W.J., Miller, S.J., Jousma, E., Wu, J., Rizvi, T.A., Brundage, M.E., Eaves, D., Widemann, B., Kim, M.-O., Dombi, E.*, et al.* (2013). MEK inhibition exhibits efficacy in human and mouse neurofibromatosis tumors. The Journal of Clinical Investigation *123*, 340-347.

Johannessen, C.M., Johnson, B.W., Williams, S.M.G., Chan, A.W., Reczek, E.E., Lynch, R.C., Rioth, M.J., McClatchey, A., Ryeom, S., and Cichowski, K. (2008). TORC1 Is Essential for NF1-Associated Malignancies. Current biology : CB *18*, 56-62.
Joseph, N.M., Mosher, J.T., Buchstaller, J., Snider, P., McKeever, P.E., Lim, M., Conway, S.J., Parada, L.F., Zhu, Y., and Morrison, S.J. (2008). The Loss of Nf1 Transiently Promotes Self-Renewal but Not Tumorigenesis by Neural Crest Stem Cells. Cancer Cell *13*, 129-140.
Karali, E., Bellou, S., Stellas, D., Klinakis, A., Murphy, C., and Fotsis, T. (2014). VEGF Signals through ATF6 and PERK to Promote Endothelial Cell Survival and Angiogenesis in the Absence of ER Stress. Molecular cell *54*, 559-572.
Keng, V.W., Rahrmann, E.P., Watson, A.L., Tschida, B.R., Moertel, C.L., Jessen, W.J., Rizvi, T.A., Collins, M.H., Ratner, N., and Largaespada, D.A. (2012). PTEN and NF1 Inactivation in Schwann Cells Produces a Severe Phenotype in the Peripheral Nervous System That Promotes the Development and Malignant Progression of Peripheral Nerve Sheath Tumors. Cancer Research *72*, 3405-3413.
King, A.A., Debaun, M.R., Riccardi, V.M., and Gutmann, D.H. (2000). Malignant peripheral nerve sheath tumors in neurofibromatosis 1. American Journal of Medical Genetics *93*, 388-392.
King, B., Trimarchi, T., Reavie, L., Xu, L., Mullenders, J., Ntziachristos, P., Aranda-Orgilles, B., Perez-Garcia, A., Shi, J., Vakoc, C.*, et al.* (2013). The Ubiquitin Ligase FBXW7 Modulates Leukemia-Initiating Cell Activity by Regulating MYC Stability. Cell *153*, 1552-1566.
Kurash, J.K., Lei, H., Shen, Q., Marston, W.L., Granda, B.W., Fan, H., Wall, D., Li, E., and Gaudet, F. (2008). Methylation of p53 by Set7/9 Mediates p53 Acetylation and Activity In Vivo. Molecular cell *29*, 392-400.
Lakkis, M.M., and Tennekoon, G.I. (2000). Neurofibromatosis type 1 I. General overview. Journal of Neuroscience Research *62*, 755-763.
Le, L.Q., Liu, C., Shipman, T., Chen, Z., Suter, U., and Parada, L.F. (2011). Susceptible Stages in Schwann Cells for NF1-Associated Plexiform Neurofibroma Development. Cancer Research *71*, 4686-4695.
Le, L.Q., and Parada, L.F. (2007). Tumor microenvironment and neurofibromatosis type I: connecting the GAPs. Oncogene *26*, 4609-4616.
Le, L.Q., Shipman, T., Burns, D.K., and Parada, L.F. (2009). Cell of Origin and Microenvironment Contribution for NF1-Associated Dermal Neurofibromas. Cell stem cell *4*, 453-463.
Lehnertz, B., Rogalski, Jason C., Schulze, Felix M., Yi, L., Lin, S., Kast, J., and Rossi, Fabio M.V. (2011). p53-Dependent Transcription and Tumor Suppression Are Not Affected in Set7/9-Deficient Mice. Molecular cell *43*, 673-680.
Lerner, Alana G., Upton, J.-P., Praveen, P.V.K., Ghosh, R., Nakagawa, Y., Igbaria, A., Shen, S., Nguyen, V., Backes, Bradley J., Heiman, M.*, et al.* (2012). IRE1α Induces Thioredoxin-Interacting Protein to Activate the NLRP3 Inflammasome and Promote Programmed Cell Death under Irremediable ER Stress. Cell Metabolism *16*, 250-264.

Letai, A., Bassik, M.C., Walensky, L.D., Sorcinelli, M.D., Weiler, S., and Korsmeyer, S.J. (2002). Distinct BH3 domains either sensitize or activate mitochondrial apoptosis, serving as prototype cancer therapeutics. Cancer Cell *2*, 183-192.
Li, W., Cui, Y., Kushner, S.A., Brown, R.A.M., Jentsch, J.D., Frankland, P.W., Cannon, T.D., and Silva, A.J. (2005). The HMG-CoA Reductase Inhibitor Lovastatin Reverses the Learning and Attention Deficits in a Mouse Model of Neurofibromatosis Type 1. Current Biology *15*, 1961-1967.
Li, Z., Guo, J., Wu, Y., and Zhou, Q. (2013). The BET bromodomain inhibitor JQ1 activates HIV latency through antagonizing Brd4 inhibition of Tat-transactivation. Nucleic Acids Research *41*, 277-287.
Ling, B.C., Wu, J., Miller, S.J., Monk, K.R., Shamekh, R., Rizvi, T.A., DeCourten-Myers, G., Vogel, K.S., DeClue, J.E., and Ratner, N. (2005). Role for the epidermal growth factor receptor in neurofibromatosis-related peripheral nerve tumorigenesis. Cancer Cell *7*, 65-75.
Linzer, D.I.H., and Levine, A.J. (1979). Characterization of a 54K Dalton cellular SV40 tumor antigen present in SV40-transformed cells and uninfected embryonal carcinoma cells. Cell *17*, 43-52.
Lovén, J., Hoke, Heather A., Lin, Charles Y., Lau, A., Orlando, David A., Vakoc, Christopher R., Bradner, James E., Lee, Tong I., and Young, Richard A. (2013). Selective Inhibition of Tumor Oncogenes by Disruption of Super-Enhancers. Cell *153*, 320-334.
Lu, M., Lawrence, D.A., Marsters, S., Acosta-Alvear, D., Kimmig, P., Mendez, A.S., Paton, A.W., Paton, J.C., Walter, P., and Ashkenazi, A. (2014). Opposing unfolded-protein-response signals converge on death receptor 5 to control apoptosis. Science *345*, 98-101.
Luo, H., Yang, Y., Duan, J., Wu, P., Jiang, Q., and Xu, C. (2013). PTEN-regulated AKT/FoxO3a/Bim signaling contributes to reactive oxygen species-mediated apoptosis in selenite-treated colorectal cancer cells. Cell Death Dis *4*, e481.
Malone, C.F., Fromm, J.A., Maertens, O., De Raedt, T., Ingraham, R., and Cichowski, K. (2014). Defining key signaling nodes and therapeutic biomarkers in NF1-mutant cancers. Cancer Discovery.
Marmorstein, R., and Berger, S.L. (2001). Structure and function of bromodomains in chromatin-regulating complexes. Gene *272*, 1-9.
Martin, G.A., Viskoohil, D., Bollag, G., McCabe, P.C., Crosier, W.J., Haubruck, H., Conroy, L., Clark, R., O'Connell, P., Cawthon, R.M*., et al.* (1990). The GAP-related domain of the neurofibromatosis type 1 gene product interacts with ras p21. Cell *63*, 843-849.
Mason, E.F., and Rathmell, J.C. (2011). Cell metabolism: An essential link between cell growth and apoptosis. Biochimica et Biophysica Acta (BBA) - Molecular Cell Research *1813*, 645-654.
Matzuk, M.M., McKeown, M.R., Filippakopoulos, P., Li, Q., Ma, L., Agno, J.E., Lemieux, M.E., Picaud, S., Yu, R.N., Qi, J*., et al.* (2012). Small-Molecule Inhibition of BRDT for Male Contraception. Cell *150*, 673-684.
Mayes, D.A., Rizvi, T.A., Cancelas, J.A., Kolasinski, N.T., Ciraolo, G.M., Stemmer-Rachamimov, A.O., and Ratner, N. (2011). Perinatal or Adult Nf1 Inactivation Using

Tamoxifen-Inducible PlpCre Each Cause Neurofibroma Formation. Cancer Research *71*, 4675-4685.
McDonnell, T.J., Deane, N., Platt, F.M., Nunez, G., Jaeger, U., McKearn, J.P., and Korsmeyer, S.J. (1989). bcl-2-Immunoglobulin transgenic mice demonstrate extended B cell survival and follicular lymphoproliferation. Cell *57*, 79-88.
McDonnell, T.J., and Korsmeyer, S.J. (1991). Progression from lymphoid hyperplasia to high-grade malignant lymphoma in mice transgenic for the t(14;18). Nature *349*, 254-256.
McLaughlin, M.E., and Jacks, T. (2002). Thinking beyond the tumor cell: Nf1 haploinsufficiency in the tumor environment. Cancer Cell *1*, 408-410.
Mertz, J.A., Conery, A.R., Bryant, B.M., Sandy, P., Balasubramanian, S., Mele, D.A., Bergeron, L., and Sims, R.J. (2011). Targeting MYC dependence in cancer by inhibiting BET bromodomains. Proceedings of the National Academy of Sciences.
Mo, W., Chen, J., Patel, A., Zhang, L., Chau, V., Li, Y., Cho, W., Lim, K., Xu, J., Lazar, Alexander J.*, et al.* (2013). CXCR4/CXCL12 Mediate Autocrine Cell- Cycle Progression in NF1-Associated Malignant Peripheral Nerve Sheath Tumors. Cell *152*, 1077-1090.
Mochizuki, K., Nishiyama, A., Jang, M.K., Dey, A., Ghosh, A., Tamura, T., Natsume, H., Yao, H., and Ozato, K. (2008). The Bromodomain Protein Brd4 Stimulates G1 Gene Transcription and Promotes Progression to S Phase. Journal of Biological Chemistry *283*, 9040-9048.
Muller, P.A.J., and Vousden, K.H. (2013). p53 mutations in cancer. Nat Cell Biol *15*, 2-8.
Mungrue, I.N., Pagnon, J., Kohannim, O., Gargalovic, P.S., and Lusis, A.J. (2009). CHAC1/MGC4504 Is a Novel Proapoptotic Component of the Unfolded Protein Response, Downstream of the ATF4-ATF3-CHOP Cascade. The Journal of Immunology *182*, 466-476.
Munro, S., Khaire, N., Inche, A., Carr, S., and La Thangue, N.B. (2010). Lysine methylation regulates the pRb tumour suppressor protein. Oncogene *29*, 2357-2367.
Nicodeme, E., Jeffrey, K.L., Schaefer, U., Beinke, S., Dewell, S., Chung, C.-w., Chandwani, R., Marazzi, I., Wilson, P., Coste, H.*, et al.* (2010). Suppression of inflammation by a synthetic histone mimic. Nature *468*, 1119-1123.
Nishioka, K., Chuikov, S., Sarma, K., Erdjument-Bromage, H., Allis, C.D., Tempst, P., and Reinberg, D. (2002). Set9, a novel histone H3 methyltransferase that facilitates transcription by precluding histone tail modifications required for heterochromatin formation. Genes & Development *16*, 479-489.
Oltersdorf, T., Elmore, S.W., Shoemaker, A.R., Armstrong, R.C., Augeri, D.J., Belli, B.A., Bruncko, M., Deckwerth, T.L., Dinges, J., Hajduk, P.J.*, et al.* (2005). An inhibitor of Bcl-2 family proteins induces regression of solid tumours. Nature *435*, 677-681.
Oslowski, C.M., and Urano, F. (2011). Chapter Four - Measuring ER Stress and the Unfolded Protein Response Using Mammalian Tissue Culture System. In Methods in Enzymology, P.M. Conn, ed. (Academic Press), pp. 71-92.
Oudhoff, Menno J., Freeman, Spencer A., Couzens, Amber L., Antignano, F., Kuznetsova, E., Min, Paul H., Northrop, Jeffrey P., Lehnertz, B., Barsyte-Lovejoy, D., Vedadi, M.*, et al.* Control of the Hippo Pathway by Set7-Dependent Methylation of Yap. Developmental Cell *26*, 188-194.

Parker, S.C.J., Stitzel, M.L., Taylor, D.L., Orozco, J.M., Erdos, M.R., Akiyama, J.A., van Bueren, K.L., Chines, P.S., Narisu, N., Program, N.C.S.*, et al.* (2013). Chromatin stretch enhancer states drive cell-specific gene regulation and harbor human disease risk variants. Proceedings of the National Academy of Sciences.
Patel, Amish J., Liao, C.-P., Chen, Z., Liu, C., Wang, Y., and Le, Lu Q. (2014). BET Bromodomain Inhibition Triggers Apoptosis of NF1-Associated Malignant Peripheral Nerve Sheath Tumors through Bim Induction. Cell Reports *6*, 81-92.
Patel, A.V., Eaves, D., Jessen, W.J., Rizvi, T.A., Ecsedy, J.A., Qian, M.G., Aronow, B.J., Perentesis, J.P., Serra, E., Cripe, T.P.*, et al.* (2012). Ras-Driven Transcriptome Analysis Identifies Aurora Kinase A as a Potential Malignant Peripheral Nerve Sheath Tumor Therapeutic Target. Clinical Cancer Research *18*, 5020-5030.
Patel, M.C., Debrosse, M., Smith, M., Dey, A., Huynh, W., Sarai, N., Heightman, T.D., Tamura, T., and Ozato, K. (2013). BRD4 coordinates recruitment of pause-release factor P-TEFb and the pausing complex NELF/DSIF to regulate transcription elongation of interferon stimulated genes. Molecular and Cellular Biology.
Perrone, F., Da Riva, L., Orsenigo, M., Losa, M., Jocollè, G., Millefanti, C., Pastore, E., Gronchi, A., Pierotti, M.A., and Pilotti, S. (2009). PDGFRA, PDGFRB, EGFR, and downstream signaling activation in malignant peripheral nerve sheath tumor. Neuro-Oncology *11*, 725-736.
PERRY, A., KUNZ, S.N., FULLER, C.E., BANERJEE, R., MARLEY, E.F., LIAPIS, H., WATSON, M.A., and GUTMANN, D.H. (2002). Differential NF1, p16, and EGFR Patterns by Interphase Cytogenetics (FISH) in Malignant Peripheral Nerve Sheath Tumor (MPNST) and Morphologically Similar Spindle Cell Neoplasms. Journal of Neuropathology & Experimental Neurology *61*, 702-709.
Pietenpol, J.A., and Stewart, Z.A. (2002). Cell cycle checkpoint signaling:: Cell cycle arrest versus apoptosis. Toxicology *181–182*, 475-481.
Puissant, A., Frumm, S.M., Alexe, G., Bassil, C.F., Qi, J., Chanthery, Y.H., Nekritz, E.A., Zeid, R., Gustafson, W.C., Greninger, P.*, et al.* (2013). Targeting MYCN in Neuroblastoma by BET Bromodomain Inhibition. Cancer Discovery *3*, 308-323.
Puthalakath, H., O'Reilly, L.A., Gunn, P., Lee, L., Kelly, P.N., Huntington, N.D., Hughes, P.D., Michalak, E.M., McKimm-Breschkin, J., Motoyama, N.*, et al.* (2007). ER Stress Triggers Apoptosis by Activating BH3-Only Protein Bim. Cell *129*, 1337-1349.
Rahman, S., Sowa, M.E., Ottinger, M., Smith, J.A., Shi, Y., Harper, J.W., and Howley, P.M. (2011). The Brd4 Extraterminal Domain Confers Transcription Activation Independent of pTEFb by Recruiting Multiple Proteins, Including NSD3. Molecular and Cellular Biology *31*, 2641-2652.
Ribeiro, S., Napoli, I., White, Ian J., Parrinello, S., Flanagan, Adrienne M., Suter, U., Parada, Luis F., and Lloyd, Alison C. (2013). Injury Signals Cooperate with Nf1 Loss to Relieve the Tumor-Suppressive Environment of Adult Peripheral Nerve. Cell Reports *5*, 126-136.
Shah, N.P., Nicoll, J.M., Nagar, B., Gorre, M.E., Paquette, R.L., Kuriyan, J., and Sawyers, C.L. (2002). Multiple BCR-ABL kinase domain mutations confer polyclonal resistance to the tyrosine kinase inhibitor imatinib (STI571) in chronic phase and blast crisis chronic myeloid leukemia. Cancer Cell *2*, 117-125.

Shannon, K., Watterson, J., Johnson, P., O'Connell, P., Lange, B., Shah, N., Steinherz, P., Kan, Y., and Priest, J. (1992). Monosomy 7 myeloproliferative disease in children with neurofibromatosis, type 1: epidemiology and molecular analysis. Blood *79*, 1311-1318.
Shi, J., and Vakoc, Christopher R. (2014). The Mechanisms behind the Therapeutic Activity of BET Bromodomain Inhibition. Molecular cell *54*, 728-736.
Shimamura, T., Chen, Z., Soucheray, M., Carretero, J., Kikuchi, E., Tchaicha, J.H., Gao, Y., Cheng, K.A., Cohoon, T.J., Qi, J.*, et al.* (2013). Efficacy of BET Bromodomain Inhibition in Kras-Mutant Non–Small Cell Lung Cancer. Clinical Cancer Research *19*, 6183-6192.
Spiltoir, J.I., Stratton, M.S., Cavasin, M.A., Demos-Davies, K., Reid, B.G., Qi, J., Bradner, J.E., and McKinsey, T.A. (2013). BET acetyl-lysine binding proteins control pathological cardiac hypertrophy. Journal of Molecular and Cellular Cardiology *63*, 175-179.
Spitz, J.L. (2005). Genodermatoses; a clinical guide to genetic skin disorders, 2d ed. Lippincott Williams & Wilkins, 400.
Stanlie, A., Yousif, Ashraf S., Akiyama, H., Honjo, T., and Begum, Nasim A. (2014). Chromatin Reader Brd4 Functions in Ig Class Switching as a Repair Complex Adaptor of Nonhomologous End-Joining. Molecular cell.
Sunters, A., Fernández de Mattos, S., Stahl, M., Brosens, J.J., Zoumpoulidou, G., Saunders, C.A., Coffer, P.J., Medema, R.H., Coombes, R.C., and Lam, E.W.-F. (2003). FoxO3a Transcriptional Regulation of Bim Controls Apoptosis in Paclitaxel-treated Breast Cancer Cell Lines. Journal of Biological Chemistry *278*, 49795-49805.
Tait, S.W.G., and Green, D.R. (2010). Mitochondria and cell death: outer membrane permeabilization and beyond. Nat Rev Mol Cell Biol *11*, 621-632.
Tamkun, J.W., Deuring, R., Scott, M.P., Kissinger, M., Pattatucci, A.M., Kaufman, T.C., and Kennison, J.A. (1992). brahma: A regulator of Drosophila homeotic genes structurally related to the yeast transcriptional activator SNF2SWI2. Cell *68*, 561-572.
Torres, K.E., Zhu, Q.-S., Bill, K., Lopez, G., Ghadimi, M.P., Xie, X., Young, E.D., Liu, J., Nguyen, T., Bolshakov, S.*, et al.* (2011). Activated MET Is a Molecular Prognosticator and Potential Therapeutic Target for Malignant Peripheral Nerve Sheath Tumors. Clinical Cancer Research *17*, 3943-3955.
Tsujimoto, Y., Finger, L., Yunis, J., Nowell, P., and Croce, C. (1984). Cloning of the chromosome breakpoint of neoplastic B cells with the t(14;18) chromosome translocation. Science *226*, 1097-1099.
Upadhyaya, M., Han, S., Consoli, C., Majounie, E., Horan, M., Thomas, N.S., Potts, C., Griffiths, S., Ruggieri, M., von Deimling, A.*, et al.* (2004). Characterization of the somatic mutational spectrum of the neurofibromatosis type 1 (NF1) gene in neurofibromatosis patients with benign and malignant tumors. Human Mutation *23*, 134-146.
van Galen, P., Kreso, A., Mbong, N., Kent, D.G., Fitzmaurice, T., Chambers, J.E., Xie, S., Laurenti, E., Hermans, K., Eppert, K.*, et al.* (2014). The unfolded protein response governs integrity of the haematopoietic stem-cell pool during stress. Nature *510*, 268-272.

Vogel, K.S., Klesse, L.J., Velasco-Miguel, S., Meyers, K., Rushing, E.J., and Parada, L.F. (1999). Mouse Tumor Model for Neurofibromatosis Type 1. Science *286*, 2176-2179.
Wallace, M., Marchuk, D., Andersen, L., Letcher, R., Odeh, H., Saulino, A., Fountain, J., Brereton, A., Nicholson, J., Mitchell, A.*, et al.* (1990). Type 1 neurofibromatosis gene: identification of a large transcript disrupted in three NF1 patients. Science *249*, 181-186.
Wang, F., Liu, H., Blanton, W.P., Belkina, A., Lebrasseur, N.K., and Denis, G.V. (2009). Brd2 disruption in mice causes severe obesity without Type 2 diabetes. Biochemical Journal *425*, 71-83.
Wang, H., Cao, R., Xia, L., Erdjument-Bromage, H., Borchers, C., Tempst, P., and Zhang, Y. (2001). Purification and Functional Characterization of a Histone H3-Lysine 4-Specific Methyltransferase. Molecular cell *8*, 1207-1217.
Wang, Y., Kim, E., Wang, X., Novitch, Bennett G., Yoshikawa, K., Chang, L.-S., and Zhu, Y. (2012). ERK Inhibition Rescues Defects in Fate Specification of Nf1-Deficient Neural Progenitors and Brain Abnormalities. Cell *150*, 816-830.
Wei, M.C., Zong, W.-X., Cheng, E.H.-Y., Lindsten, T., Panoutsakopoulou, V., Ross, A.J., Roth, K.A., MacGregor, G.R., Thompson, C.B., and Korsmeyer, S.J. (2001). Proapoptotic BAX and BAK: A Requisite Gateway to Mitochondrial Dysfunction and Death. Science *292*, 727-730.
Whyte, Warren A., Orlando, David A., Hnisz, D., Abraham, Brian J., Lin, Charles Y., Kagey, Michael H., Rahl, Peter B., Lee, Tong I., and Young, Richard A. (2013). Master Transcription Factors and Mediator Establish Super-Enhancers at Key Cell Identity Genes. Cell *153*, 307-319.
Wilson, T.R., Fridlyand, J., Yan, Y., Penuel, E., Burton, L., Chan, E., Peng, J., Lin, E., Wang, Y., Sosman, J.*, et al.* (2012). Widespread potential for growth-factor-driven resistance to anticancer kinase inhibitors. Nature *487*, 505-509.
Wu, J., Patmore, D.M., Jousma, E., Eaves, D.W., Breving, K., Patel, A.V., Schwartz, E.B., Fuchs, J.R., Cripe, T.P., Stemmer-Rachamimov, A.O.*, et al.* (2013a). EGFR-STAT3 signaling promotes formation of malignant peripheral nerve sheath tumors. Oncogene.
Wu, J., Williams, J.P., Rizvi, T.A., Kordich, J.J., Witte, D., Meijer, D., Stemmer-Rachamimov, A.O., Cancelas, J.A., and Ratner, N. (2008). Plexiform and Dermal Neurofibromas and Pigmentation Are Caused by Nf1 Loss in Desert Hedgehog-Expressing Cells. Cancer Cell *13*, 105-116.
Wu, S.-Y., and Chiang, C.-M. (2007). The Double Bromodomain-containing Chromatin Adaptor Brd4 and Transcriptional Regulation. Journal of Biological Chemistry *282*, 13141-13145.
Wu, S.-Y., Lee, A.Y., Lai, H.-T., Zhang, H., and Chiang, C.-M. (2013b). Phospho Switch Triggers Brd4 Chromatin Binding and Activator Recruitment for Gene-Specific Targeting. Molecular cell *49*, 843-857.
Xiang, H., Noonan, E.J., Wang, J., Duan, H., Ma, L., Michie, S., and Boxer, L.M. (2011). The immunoglobulin heavy chain gene 3[prime] enhancers induce Bcl2 deregulation and lymphomagenesis in murine B cells. Leukemia *25*, 1484-1493.

Xu, C., Bailly-Maitre, B., and Reed, J.C. (2005). Endoplasmic reticulum stress: cell life and death decisions. The Journal of Clinical Investigation *115*, 2656-2664.
Xu, G., Lin, B., Tanaka, K., Dunn, D., Wood, D., Gesteland, R., White, R., Weiss, R., and Tamanoi, F. (1990a). The catalytic domain of the neurofibromatosis type 1 gene product stimulates ras GTPase and complements ira mutants of S. cerevisiae. Cell *63*, 835-841.
Xu, G., O'Connell, P., Viskochil, D., Cawthon, R., Robertson, M., Culver, M., Dunn, D., Stevens, J., Gesteland, R., White, R.*, et al.* (1990b). The neurofibromatosis type 1 gene encodes a protein related to GAP. Cell *62*, 599-608.
Yamazaki, H., Suzuki, M., Otsuki, A., Shimizu, R., Bresnick, Emery H., Engel, James D., and Yamamoto, M. (2014). A Remote GATA2 Hematopoietic Enhancer Drives Leukemogenesis in inv(3)(q21;q26) by Activating EVI1 Expression. Cancer Cell *25*, 415-427.
Yang, Z., He, N., and Zhou, Q. (2008). Brd4 Recruits P-TEFb to Chromosomes at Late Mitosis To Promote G1 Gene Expression and Cell Cycle Progression. Molecular and Cellular Biology *28*, 967-976.
Yang, Z., Yik, J.H.N., Chen, R., He, N., Jang, M.K., Ozato, K., and Zhou, Q. (2005). Recruitment of P-TEFb for Stimulation of Transcriptional Elongation by the Bromodomain Protein Brd4. Molecular cell *19*, 535-545.
Yauch, R.L., Dijkgraaf, G.J.P., Alicke, B., Januario, T., Ahn, C.P., Holcomb, T., Pujara, K., Stinson, J., Callahan, C.A., Tang, T.*, et al.* (2009). Smoothened Mutation Confers Resistance to a Hedgehog Pathway Inhibitor in Medulloblastoma. Science *326*, 572-574.
You, H., Pellegrini, M., Tsuchihara, K., Yamamoto, K., Hacker, G., Erlacher, M., Villunger, A., and Mak, T.W. (2006). FOXO3a-dependent regulation of Puma in response to cytokine/growth factor withdrawal. The Journal of Experimental Medicine *203*, 1657-1663.
Youle, R.J., and Strasser, A. (2008). The BCL-2 protein family: opposing activities that mediate cell death. Nat Rev Mol Cell Biol *9*, 47-59.
Zhang, Xiang H.F., Jin, X., Malladi, S., Zou, Y., Wen, Yong H., Brogi, E., Smid, M., Foekens, J.A., and Massagué, J. (2013). Selection of Bone Metastasis Seeds by Mesenchymal Signals in the Primary Tumor Stroma. Cell *154*, 1060-1073.
Zheng, H., Chang, L., Patel, N., Yang, J., Lowe, L., Burns, D.K., and Zhu, Y. (2008). Induction of Abnormal Proliferation by Nonmyelinating Schwann Cells Triggers Neurofibroma Formation. Cancer Cell *13*, 117-128.
Zhu, J., Gaiha, Gaurav D., John, Sinu P., Pertel, T., Chin, Christopher R., Gao, G., Qu, H., Walker, Bruce D., Elledge, Stephen J., and Brass, Abraham L. (2012). Reactivation of Latent HIV-1 by Inhibition of BRD4. Cell Reports *2*, 807-816.
Zhu, Y., Ghosh, P., Charnay, P., Burns, D.K., and Parada, L.F. (2002). Neurofibromas in NF1: Schwann Cell Origin and Role of Tumor Environment. Science *296*, 920-922.
Zou, C., Smith, K.D., Liu, J., Lahat, G., Myers, S., Wang, W.-L., Zhang, W., McCutcheon, I.E., Slopis, J.M., Lazar, A.J.*, et al.* (2009). Clinical, Pathological, and Molecular Variables Predictive of Malignant Peripheral Nerve Sheath Tumor Outcome. Annals of Surgery *249*, 1014-1022 1010.1097/SLA.1010b1013e3181a1077e1019a.

Zuber, J., Shi, J., Wang, E., Rappaport, A.R., Herrmann, H., Sison, E.A., Magoon, D., Qi, J., Blatt, K., Wunderlich, M.*, et al.* (2011). RNAi screen identifies Brd4 as a therapeutic target in acute myeloid leukaemia. Nature *478*, 524-528.